The Molecular Toolbox: Dendrimer Decorated Biomaterials for Musculoskeletal Regeneration

Ryan Seelbach

Tesi Doctoral

Programa de Doctorat en Nanociències

The Molecular Toolbox:

Dendrimer Decorated Biomaterials for Musculoskeletal Regeneration

Presentada per,

Ryan Seelbach

Per optar el grau de doctor

Treball dirigit pel Dr. David Eglin

i Dr. Alvaro Mata

Amb el tutor Dr. Amilcar Labarta

Departament de Física Fonamental, Facultat de Física

i Institut de Nanociència i Nanotecnologia

Universitat de Barcelona

Barcelona, Febrero 2015

To my family,

for your love and support,

that gave me the courage,

to follow my dreams.

I believe in aristocracy, though – if that is the right word, and if a democrat may use it. Not an aristocracy of power, based upon rank and influence, but an aristocracy of the sensitive, the considerate and the plucky. Its members are to be found in all nations and classes, and all through the ages, and there is a secret understanding between them when they meet. They represent the true human tradition, the one permanent victory of our queer race over cruelty and chaos. Thousands of them perish in obscurity, a few are great names. They are sensitive for others as well as themselves, they are considerate without being fussy, their pluck is not swankiness but power to endure, and they can take a joke.

– E.M. Forster, Two Cheers for Democracy

Acknowledgements

Much can be said of a great many people in my life that I owe great thanks, and I no doubt owe a couple of rounds, for their guidance and good words along my way. First, and above all, the greatest figure in my life is my father. My foundation and silent spirit that always saw the potential inside of me. To my mother, to whom a son owes all, you gave me life. You gave me spirit. You taught me to work hard from the very beginning. To my grandfather, who gave me a home when the world was falling down around me. You are the lion of our family. To my late grandmother, not a day goes by without thinking of you. Perhaps you were the one to instill the first trappings of wisdom within my young, feeble mind.

To my mentors throughout the years, thank you. Teachers are such a strong influence in a student's life, and many times for me they went above and beyond. Mrs. Johnson, my eighth grade English teacher that was a shining presence during some of my darkest hours. Coach Hughes, my wrestling coach, that wrestling "room" above the bleachers has engendered more fortitude within me than any other stage. Up there, I learned to believe in myself again. Nothing seems nearly as hard as what I proved to myself on those mats, with sweat, blood, and not to forget a broken wrist. I think about those moments every day. Your pedagogic approached has provided many young athletes with the platform to achieve, if they chose to take advantage of it. And I believe most did. Dr. J. Patrick Polley, my undergraduate physics advisor at Beloit College, within your classrooms I witnessed the brilliance and beauty of physics nurtured many, many times from the dusty, black chalkboards. Class was never dull with you. To weekly view your humor and your spirit and your wit was one of the great pleasures of my young life.

To my Ph.D. mentors Dr. David Eglin, Dr. Mauro Alini, and Dr. Alvaro Mata. Alvaro, thank you for giving me the opportunity to undertake this Ph.D. David, I find it difficult to enunciate the words that would adequately express what I would like to say but I will try. Thank you. You stepped into a role that basically fell at your feet, you have been a phenomenal mentor to me. Capable of being strong when you needed to be, at a distance when necessary, but never lacking the ability to slide in the quick witted humor that left me with a good laugh and sometimes great optimism.

To the people I met along the way, my Beloit crew, the Davosers, las amigas mías de la Plataforma de Nanotecnología, and my friends back home. Often these days the distance of oceans may be between us, but ever near you are all to me. I hope that I may pass on the greatness humanity that each of you has once upon a time engendered in me.

Finally to my wife, thank you. We had wonderful times in Switzerland and Spain, getting to know the best of each other and making many lasting memories. We have already been on many adventures in the four years we have known each other. The one by your side is the best.

Glossary of Abbreviations

- % (w/v) = weight per volume percent
- ^{1}H NMR = Proton nuclear magnetic resonance
- 3D = three dimensional
- AIBN = Azobisisobutyronitrile
- α-MEM = Alpha modified Eagle's medium
- ANOVA = The analysis of variance statistical model
- Basal = Osteogenic permissive media for cell culture
- BCP = 1-bromo-3-chloro-propane
- bFGF-2 = Basic fibroblast growth factor type 2
- BMP-2 = Recombinant human bone morphogenetic protein type 2
- cDNA = Complementary deoxyribonucleic acid
- $CuBr(PPh_3)_3$ = Bromotris(triphenylphosphine) copper(I)
- $CuSO_4 \bullet 5H_2O$ = Copper sulphate pentahydrate
- D = Asp, Aspartic acid
- DCM = Dichloromethane
- DEPC = Diethyl pyrocarbonate
- DG = Degree of grafting
- DIEA = *N*,*N*-diisopropylethylamine
- DIPCDI = *N*,*N*'-diisopropylcarbodiimide
- DMEM = Dulbecco's modified Eagle medium
- DMF = *N*-dimethylformamide
- DMSO = *N*-dimethylsulfoxide
- DTPA = diethylene triamine pentaacetic acid
- EDC = *N*-(3-dimethylaminopropyl)-*N'*-ethylcarbodiimide hydrochloride
- EDTA = Ethylenediaminetetraacetic acid disodium salt
- EPHP = *N*-ethylpiperidine hypophosphite
- FBS-Hyclone = Human MSC qualified fetal bovine serum FCS = Fetal calf serum
- G = Gly, Glycine
- H = His, Histidine

- hALP = Human alkaline phosphatase
- hCOL2 = Human type II collagen
- hGAPDH = Human glyceraldehyde 3-phosphate dehydrogenase
- hMSC = Human mesenchymal stem cells, also referred to as mesenchymal stromal cells
- hRUNx2 = Human runt-related transcription factor type 2
- hSOX9 = Human (sex determining region Y)-box 9
- Hyal = Bicomponent hydrogel containing Hyal-pN (13 % (w/v)) and Hyal-pa (2 % (w/v))
- Hyal-LPL = Hyaluronic acid modified with (human) TGF-β1 binding epitope dendrimers
- Hyal-pN = Poly(*N*-isopropylacrylamide) grafted hyaluronic acid brush copolymer
- Hyal-pa = Propargylamide modified hyaluronic acid
- Hyal-RGDS = Hyaluronic acid modified with RGDS functionalized dendrimers
- Hyal-RSGD = Hyaluronic acid modified with RSGD functionalized dendrimers
- Hyal-YPV = Hyaluronic acid modified with (human) BMP-2 binding epitope dendrimers
- ICP-SFMS = Inductively coupled plasma – sector field mass spectrometry
- L = Leu, Leucine
- LCST = lower critical solution temperature
- MeOH = Methanol
- mol% = molar percent, additionally referred to as the molar fraction
- N = Asn, Asparagine
- NaAsc = Ascorbic acid sodium salt
- NaBr = Sodium bromide
- NaHA = Hyaluronic acid sodium salt
- NaN_3 = Sodium azide
- $NaNO_3$ = Sodium nitrate
- NEAA = Non-essential amino acids
- NHS = *N*-hydroxysuccinimide
- NIPAM *N*-isopropylacrylamide
- ODM = Osteogenic differentiation media for cell culture
- OEG = *O*-(2-Aminoethyl)-*O*'-(2-azidoethyl)pentaethylene glycol
- OxymaPure = Ethyl(hydroxyimino)cyanoacetate

- P = Pro, Proline
- PCR = Polymerase chain reaction
- pN = poly(*N*-isopropylacrylamide)
- PyBOP = Benzotriazol-1-yl-oxytripyrrolidinophosphonium hexafluorophosphate
- qRT-PCR = Quantitative reverse transcription polymerase chain reaction
- R= Arg, Arginine
- RGDS = Bicomponent hydrogel containing Hyal-pN (13 % (w/v)) and Hyal-RGDS (2 % (w/v))
- RNA = Ribonucleic acid
- RSGD = Bicomponent hydrogel containing Hyal-pN (13 % (w/v)) and Hyal-RSGD (2 % (w/v))
- S = Ser, Serine
- TBAF = Tetrabutylammonium fluoride trihydrate
- TBAHA = Hyaluronic acid tetrabutylammonium salt
- TFA = Trifluoroacetic acid
- TGF-β1 = Recombinant human transforming growth factor beta 1
- T = Thr, Threonine
- V = Val, Valine
- vol% = the percentage by volume of a solute mixed with a solvent (generally water)
- Y = Tyr, Tyrosine

Table of Contents

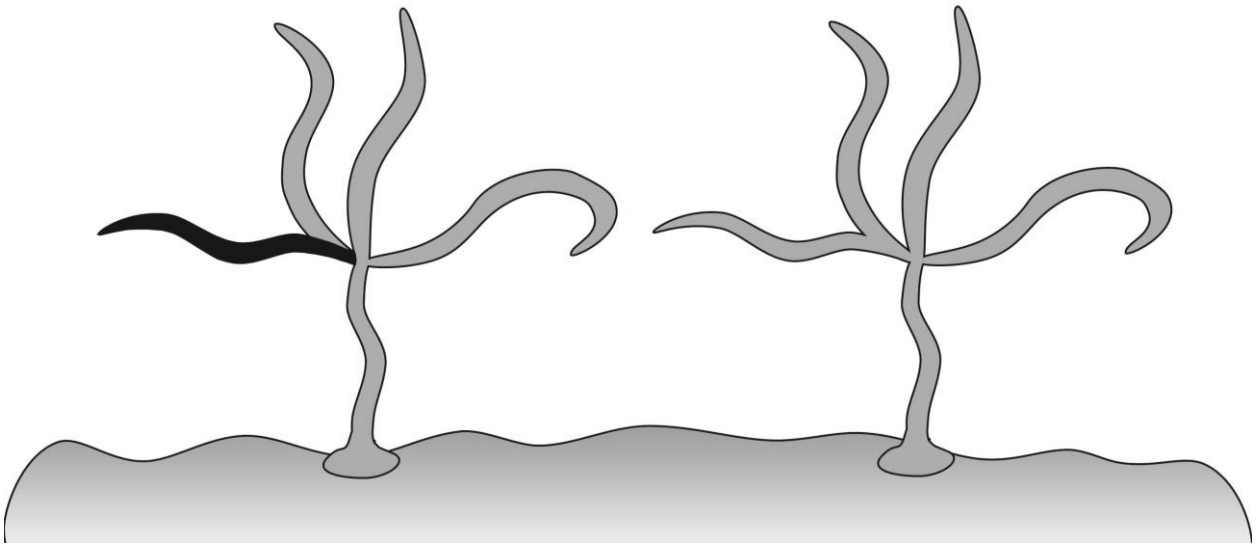

Chapter 1 – Introduction

1.1. Smart biomaterials for regenerative medicine applications

The body alone cannot heal all wounds. For example, complex non-union fractures or osteosarcomas yield bone defects that require surgical intervention in order for the body to sufficiently heal. Every year millions of Americans are inflicted with musculoskeletal injury, which incur hundreds of billions of dollars of medical costs by the way of surgery, physical rehabilitation, and lost wages [1, 2]. Patients also run risks from surgery due to infection and implant rejection which often lead to secondary revisions and extended patient morbidity. Therefore, the need for clinically relevant advanced medical therapies is evident.

Regenerative medicine takes multifaceted approaches towards healing complex injury and restoring normal tissue function by combining biomaterials with cells and drugs [3]. Biomaterials

are synthetic or naturally inspired polymer-based, ceramic, or composite systems that support the body's healing process by providing an environment for cellular growth and development [4]. Polymer-based materials can be swelled in aqueous solutions and reacted *in situ* to form hydrogels. Generally speaking, these materials require surgery for implantation. A newer class of biomaterials can be laproscopically introduced by injection as a liquid which undergo a change of state upon exposure to their new environment. So-called "smart" biomaterials have great potential in clinically relevant applications.

Recently, naturally occurring polymers found in the human body have inspired biomaterials that play active roles in the regenerative process. One polymer, hyaluronic acid, has ubiquitous roles in the human body, and is an important component to tissue development and healing. These materials are proving to be more capable to the complex tasks of guiding tissue regeneration; however, the search continues for laboratory inspired solutions to help guide the regeneration process. We need to be able to control the presentation of bioactive agents in the microenvironment which is the level at which cells operate. Some researchers have attempted to augment the scaffold biochemistry by controlling the spatial presentation of bioactive molecules by playing with clustering peptide sequences, but they do not have a high control over the nanoscale aspect. For the problem of controlling the molecular architecture of the biomaterial microenvironment, nanotechnology has a solution. Dendrimers are synthetic branched macromolecules which are symmetric, monodisperse, and globular in shape. Most importantly however, is that their inherent structure maintains strict presentation of terminal groups. Up to this point, never before have dendrimers been covalently mixed with biomaterials to provide strict control over the presentation of biomolecules in the scaffold microenvironment. This novel technology poses a new biomaterials niche for guiding bone regeneration.

The motivation of the thesis is to contribute to the development of intelligent biomaterial platforms by combining peptide epitope binding dendrimers with a thermoreversible biomaterial platform based on hyaluronic acid in the hope to advance bone regeneration.

1.2 Objectives of the thesis

The objectives of the thesis are:

a. Synthesize and characterize a thermoreversible hyaluronic acid based hydrogel carrier that is modified with peptide epitope terminated multivalent dendrimers.
b. Characterize the *in vitro* capacity of this novel smart biomaterial as a drug delivery system able to locally deliver potent bioactive drugs such as growth factors.
c. Characterize the *in vitro* capacity of the dendrimer decorated smart biomaterial as a system to dually transport cells and provide them with an enhanced microenvironment designed to guide osteogenic behavior.
d. Carry out a pilot study that characterizes the *in vivo* efficacy of the thermoreversible hyaluronic acid in delivering BMP-2 and human mesenchymal stromal cells for bone repair.

1.3 Contributions of the thesis

This thesis has been constructed based upon four publications that either have been published or are currently being drafted for publication. The contributions of this thesis are;

a. The first contribution elaborated the methodology key to the synthesis of the smart biomaterial platform. Two copper based catalysts were tested for their efficiency in an azide-alkyne cycloaddition reaction, popularly known as a "click" reaction. Within these experiments, the covalent grafting of azide terminated poly(*N*-isopropylacrylamide (N_3-pN) to a propargylamine modified hyaluronic acid (Hyal-pa) backbone in different aqueous solvents were characterized. This set of experiments was published in a manuscript entitled, *Copper catalyst efficiency for the CuAAC synthesis of a* poly(*N-isopropylacrylamide) conjugated hyaluronan* (*Seelbach et al., Clinical Hemorheology and Microcirculation, 2015. In Press.).*
b. The second contribution covered the *in vitro* characterization of the capacity of the biomaterial as a drug delivery system. The copper catalyzed azide-alkyne cycloaddition (CuAAC) reaction was translated to synthesize Hyal-pa covalently modified with dendrimers that were designed to bind to recombinant human bone morphogenetic protein type 2 (BMP-2) or recombinant human transforming growth factor beta 1 (TGF-

β1) which was subsequently combined with the thermoreversible hyaluronan copolymer (Hyal-pN). An in vitro release study was carried out over one week to profile the release mechanics of the dendrimer modified biomaterial loaded with BMP-2 or TGF-β1. This work has been written into a manuscript entitled, *Peptide binding dendrimer decorated injectable hyaluronan hydrogels modulate the controlled release of BMP-2 and TGF-β1*, and has been submitted to the Journal of Controlled Release.

c. The third contribution examines the potential of Hyal-pN combined with integrin binding dendrimers as a suitable scaffold for the *in vitro* osteogenic culture of human mesenchymal stem cells (hMSCs). The cell-scaffold constructs were analyzed for cellular viability and morphology, osteogenic marker expression, and tissue development. The capacity of the biomaterial to guide osteogenesis was published as a manuscript entitled, *Multivalent Dendrimers Presenting Spatially Controlled Clusters of Binding Epitopes in Thermoresponsive Hyaluronan Hydrogels* [5].

d. The fourth contribution examines the *in vivo* efficacy of the biomaterial in a mouse animal model. The Hyal-pN biomaterial, which was synthesized by an improved method that eliminated the necessity of the copper catalyst, was loaded with hMSCs and BMP-2 then subcutaneously injected into the skin folds of mice. The condition of the animals and implant sites were observed postoperatively over a 1 month period. The implants were excised after the animals were sacrificed and ectopic bone formation was measured via x-ray scanning. This compilation of this work is planned to be published in 2015.

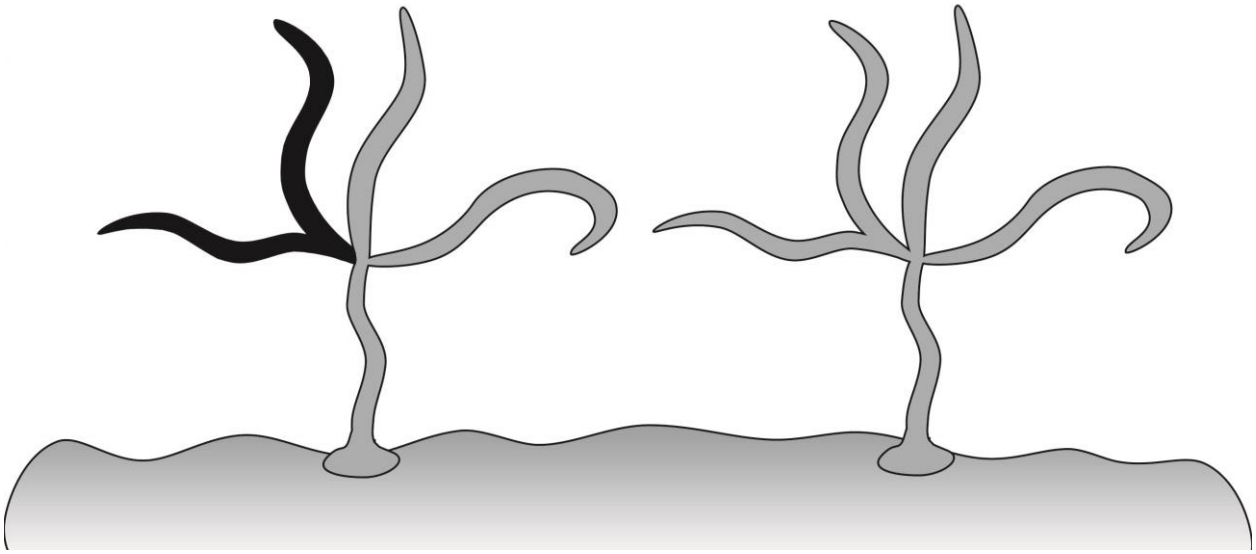

Chapter 2 - State of the Art

Research has come a long way since the 1960s when poly(hydroxyl ethyl methacrylate) (pHEMA) hydrogels became the first "soft" biomaterial for surgical implantation [6]. Hydrogels, including pHEMA, are hydrated polymeric networks that are swelled with water and can pose viable three-dimensional (3D) structures for cell viability. They are constructed from natural or synthetic hydrophilic polymers, have weak mechanical stability, and maintain well-defined chemical and physical characteristics. Through often facile chemical modification, polymer scaffolds can be tuned to exhibit an effective porosity, viscoelasticity, osmolarity, wettability, or virtually any other desired characteristic optimal for the delivery of cells and drugs or to drive tissue healing [7-10]. Hydrogels inspired by naturally occurring polymers such as hyaluronic acid have been investigated for its efficacy in musculoskeletal regeneration [4, 11, 12]. For instance,

photocrosslinking methacrylated hyaluronic acid has been shown to influence cellular retention and modulate the dispersion of extracellular matrix (ECM) produced by terminally differentiated human mesenchymal stem cells (hMSC) [13].

New forms of hydrogels that dually serve as polymer carriers as well as stable scaffolds capable of supporting cellular growth and development are being classified as "intelligent" biomaterials [14]. Smart hydrogels are generally liquid yet undergo a transitional change of state *in situ* due to an environmental stimulus such as temperature, pH, or salinity usually enacted upon exposure to the physiological conditions inside the body. These materials are unique for their utility as delivery systems for cells or drugs. Furthermore due to their inherent properties, these materials can be potentially inserted laproscopically in contrast to more invasive surgical methods for implantation. The growing class of smart biomaterials must be able to satisfy a few requirements in order to be efficacious for clinical therapies [14].

1. They must be reversible. They must exhibit the transitional change of state from liquid to viscoelastic solid with a mild stimulus in a timely manner.
2. They must be injectable. Hence the materials must be a shear-thinning solution inside of the operating theater. Upon injection into the targeted site, the material must stabilize into a hydrogel.
3. They must be an effective carrier for drugs or cells or both. The materials must be able to protect cells which are sensitive to shearing forces and localize potent agents such as growth factors at the delivery site.
4. They must provide a stable depot in which the cells may survive and the drugs preserve their bioactivity.
5. The must be biocompatible. They cannot invoke an adverse host immune response that counteracts the healing process.
6. They must be biodegradable. The optimum period of biodegradability would be the direct inverse of time it takes for new healthy tissue to regrow.
7. They must be mechanically stable. A seminal paper by Discher *et al.* highlighted the importance of matching the mechanical character of the biomaterial to the targeted tissue [15]. Currently, most hydrogels do not match the profile of stronger tissues such as tendon or bone.

One polymer platform that satisfies most of these requirements is the poly(*N*-isopropylacrylamide) grafted hyaluronan (Hyal-pN) brush copolymer [16]. Hyal-pN exists as an injectable solution at room temperature making it an ideal vehicle to transport growth factors and cells. The brush copolymer forms hydrogen bonds with water molecules until an increase in temperature causes an entropy driven collapse of the pN and the water is expelled [17]. Above this lower critical solution temperature (LCST) the polymers act as a hydrogel. The process is reversible if the temperature is again lowered below the LCST. This hydrogel is capable of forming a stable scaffold to nurture the cellular growth and development important for tissue regeneration. And since it is based on hyaluronic acid, it is biodegradable.

2.1. Injectable hydrogel carrier systems from thermoresponsive hyaluronan

Hyaluronic acid and its analogs are extensively used in the pharmaceutical and medical fields largely due to the multitude of roles it holds within the human body, especially in tissue repair [18]. Hyaluronic acid derivatives are prepared by chemical modification at either the hydroxyl group on the C6 position of the *N*-acetylglucosamine or at the carboxylic acid of the *D*-glucuronic acid [11, 12]. The obtained conjugates have a wide range of properties which span from enhanced rheological features to gel-like properties that can be triggered by external stimuli [19, 20]. Hyaluronan derivatives demonstrating gelling ability by the application of chemical and physical stimuli, triggering covalent or non-covalent crosslinking, have been subject to extensive research for applications in drug and cellular delivery [3, 4, 21].

Among them, temperature responsive poly(*N*-isopropylacrylamide) conjugated hyaluronic acid are polymeric materials soluble at room temperature in aqueous solutions, yet experience a sol-gel transition upon a temperature increase (Fig. 1). These polymers could exploit a marketable niche as drug or cell vehicles for biomedical applications [22-27].

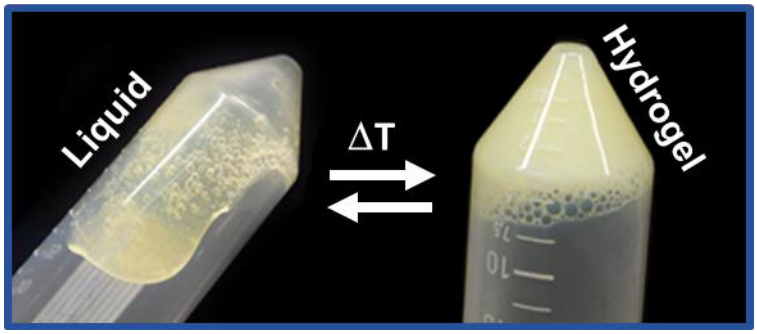

Fig. 1. Visual representation of the temperature responsive hyaluronan hydrogel platform which is an injectable solution at ambient temperature, but will undergo a sol-gel temperature induced transition into a hydrogel due to the hydrophobic collapse of poly(*N*-isopropylacrylamide).

These thermoresponsive derivatives exhibit a brush-like architecture comprising linear poly(*N*-isopropylacrylamide) (pN) grafted onto a core hyaluronan backbone. Synthetic pathways including direct polymerization of pN from the hyaluronan and amidation reactions coupling preformed amino-terminated pN onto hyaluronan have been proposed [28-30]. The main difficulty of the former "growing from" strategy is to form adequate hyaluronan macro-initiators to govern pN chain growth [23]. The latter "coupling onto" approach often lacks control because amino-terminated pN is synthesized by radical polymerization which often yields a polydispersity index above 1.2 [29].

Mortisen *et al.* described the preparation of azido terminated poly(*N*-isopropylacrylamide) (N_3-pN) synthesized by reversible addition-fragmentation chain transfer polymerization (RAFT) which was subsequently grafted via the 1,3-dipolar cycloaddition reaction (CuAAC) onto the glycosaminoglycan backbone displaying alkyne moieties [16]. This "coupling onto" method was employed for its high efficiency. Moreover, this approach theoretically provided strong control over the macromolecular architecture and mechanical properties.

The CuAAC reaction in aqueous conditions is frequently carried out in the presence of the copper-ascorbate (CuAsc) catalytic ion system generated by the combination of copper sulfate and ascorbic acid in water [31, 32]. Despite the reported high efficiency of CuAsc in CuAAC [32], the presence of either compound in a hyaluronan solution can lead to the catalytic degradation of the

polysaccharide chain, specifically at the β-1,4 glycosidic bond [33-35]. Thus if the catalyst is not removed efficiently, the controlled architecture of the copolymers and subsequent rheological features of the thermally responsive solutions is lost due to random cleavage of the disaccharide chains. Moreover, traces of copper ions in the final products could be potentially cytotoxic, thereby blocking the application of viable products in the medical field [36]. Therefore the efficiency of the two different CuAAC catalysts CuAsc and $CuBr(PPh_3)_3$, a cuprous salt containing a phosphorous ligand designed to stabilize the oxidative state of the Cu^{+1} ion [37], was compared for their ability to catalyze the reaction of an azide terminated poly(*N*-isopropylacrylamide) onto alkyne modified hyaluronan in different solvent conditions. The synthesized products were characterized by chromatography, infra-red spectroscopy, and proton nuclear magnetic resonance (^{1}H NMR). The rheological properties of the thermoresponsive derivative of hyaluronan compositions in solution were compared. Finally, the amount of copper in the final products was measured by inductively coupled plasma mass spectrometry.

2.2. Thermoreversible hydrogel vehicles combining peptide epitope binding dendrimers for drug delivery applications

The momentum of research towards ideal biomaterials that deliver growth factors (GFs) foreshadows the roles they will play in the coming future for clinical applications [38, 39]. Two cytokines, bone morphogenetic protein type 2 (BMP-2) and transforming growth factor beta 1 (TGF-β1), regulate a variety of processes in the body including tissue growth and development, immune system regulation, and homeostasis [40, 41]. However, there is much conversation among peers regarding the risks of these drugs, [42-45] illustrating the necessity to regiment how they are delivered in the body. The controlled and sustained release of GFs can be administered with biomaterials, for example, by exploiting the ability of a polymeric matrix to physically entrap the proteins, or by taking advantage of intrinsic electrostatic affinities of a biocompatible ceramic and the drug [2, 46, 47].

Polymer networks swelled in water, or hydrogels, can be loaded with GFs and will serve as depots that deliver a localized and sustained release of the therapeutic agent. Depending on the nature of the chemical structures of the polymers, the timed drug release profile, which is governed by gradient diffusion, will be parametrized by electrostatic interaction and the overall porosity of the scaffold [48-52]. More advanced hydrogel biomaterials feature dynamic

functionalities that effect a transitional change-of-state from liquid to hydrogel upon small environmental perturbations [53-58]. These so-called "smart" biomaterials can be administered laparoscopically as a solution, take on the additional role of carrier system, and can serve as vehicles to transport drugs or cells directly to an injury site in a minimally invasive way. Peptide amphiphile solutions that form networks *in situ* have been shown not only to provide a sustained release of loaded growth factors, but also to preserve their bioactivity [53, 54]. Further reports have supported these findings and shown an improved efficacy of BMP-2 for *in vivo* bone formation [59].

The ability of drug delivery systems to tune the temporal release of potent drugs such as BMP-2 and TGF-β1 has generated a clinically relevant niche for musculoskeletal regeneration therapies. Within this class of delivery systems is a thermosensitive polymer consisting of poly(*N*-isopropylacrylamide) grafted hyaluronic acid brush copolymers [16, 21, 24]. This polymer platform is exemplary for its shear-thinning property, injectablility, and capacity to form hydrogels with a temperature stimulus, proving its utility to facilitate a sustained drug release [21]. This polysaccharide has been frequently utilized to administer a sustained release of BMP-2 which has been shown to positively influence bone formation [49, 50, 60]. Hydrogels modified with peptide sequences with selective binding affinity to individual growth factors have been shown to extend the release profiles of loaded depots [53, 61].

Tools of nanotechnology can be employed to control the presentation of protein binding domains down to nanoscale precision. Interestingly, highly specialized branched macromolecules called dendrimers are singular in size and globular in shape and have been recently described as effective tools for applications in nanomedicine [62]. Moreover dendrimers, because they are synthetic, can be readily modified with versatile terminal sequences to target specific biochemical functions. These macromolecules have already been exhibited as highly advanced tools in the fight against cancer. Generation 2 PAMAM were synthesized as vectors for doxorubicin and were successfully able to target tumors via the alpha-fetoprotein receptor exhibiting high toxicity even in resistant cell lines [63].

Recently, orthogonal synthesis techniques have been used to synthesize disubstituted dendrimers exhibiting one functionality useful for covalent conjugation while the other four terminal sequences are modified with terminal peptide epitope sequences [62, 64, 65]. This

groundbreaking synthesis technique paved the way for using dendrimers to decorate biomaterials with clusters of peptide epitopes, effectively controlling the molecular architecture of the scaffold microenvironment with nanoscale precision. In chapter 4 section 2, disubstituted dendrimers bearing one azide functionality and four binding peptides, presenting the *Tyr-Pro-Val-His-Ser-Thr* (YPVHST) or *Leu-Pro-Leu-Gly-Asn-Ser-His* (LPLGNSH) sequences to target BMP-2 or TGF-β1 protein binding respectively, were synthesized and characterized. These unique macromolecules were then covalently conjugated to hyaluronic acid using a copper catalyzed azide-alkyne cycloaddition reaction, mixed with multiple batches of poly(*N*-isopropylacrylamide) of different lengths grafted to hyaluronic acid, then loaded with BMP-2 or TGF-β1. The influence of the dendrimers and the size of the pN on the *in vitro* release of loaded BMP-2 and TGF-β1 from the depots were quantified by sandwich enzyme-linked immunosorbent assay (Fig. 2). Furthermore, the degree of grafting and peptide contents of the polymers was assessed along with the viscoelastic characterization of aqueous formulations of the thermoreversible hydrogel with dendrimers around a physiological range of temperatures.

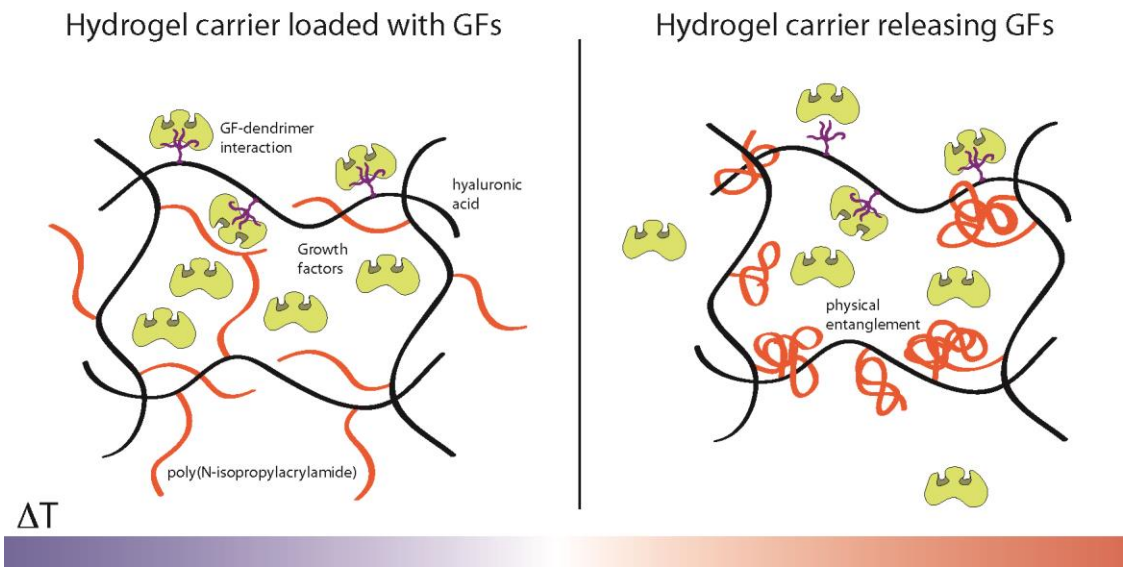

Fig. 2. Schematic representation of the BMP-2/TGF-β1 binding thermoreversible hydrogel platform releasing the loaded growth factors *in vitro*.

2.3. Injectable hyaluronan-based hydrogels decorated with integrin binding dendrimers utilized as a cell carrier-scaffold

Engineered microenvironments can provide a better understanding of normal and pathologic cellular behavior and expand therapeutic tissue repair solutions [64, 66]. Indeed, the ability to control in great detail the two-dimensional (2D) and three-dimensional (3D) microenvironments in which cells are encapsulated allow for deciphering the influence of chemical and mechanical cues in defined conditions, and potentially design instructive mimicking matrices [67].

Recent advances in the field of nanobiotechnology have allowed the development of small-molecule-based materials that are bioactive, biomimetic, multifunctional, and biodegradable [68]. Among these are dendrimers. These molecules are branched polymer nanostructures with a globular shape and well-defined molecular weight imparting a high degree of spatial control over selected biofunctionalities as a result of their architecture. While the application of dendrimers to biomaterials has only recently been explored, these well-defined nanostructures have been widely used in a variety of therapeutic applications, such as agents to deliver drugs, DNA, or other bioactive compounds [69]. For example dendrimers synthesized from polyesters, polyester-polyamide or diethylenetriaminepentaacetic acid cores have limited immunogenicity, and are biodegradable with low protein denaturation and blood clotting properties [62, 65, 70-72].

Recent works have also demonstrated their potential for incorporation within biomaterials resulting in targeted biological effects [73] and to promote osteogenic differentiation in vitro [74, 75]. However, there are no reports on their use to tailor hydrogel microenvironments. Of particular interest, hyaluronic acid hydrogel compositions have been shown to form relevant developmental microenvironments for stimulating neotissue growth and differentiation of human embryonic stem cells [76], allow for spatially controlled non-viral delivery of DNA *in vivo* [77], and improve the release kinetics of bone morphogenetic protein 2 (BMP-2) when compared to collagen sponges [78].

Hyaluronic acid, also commonly referred to as hyaluronan, is a shear thinning biopolymer with many biological roles that has been modified to create chemically and physically crosslinkable hydrogels that may also serve as injectable cell carriers [16, 79, 80]. Photocrosslinking methacrylated hyaluronic acid has been shown to influence cellular retention and modulate the dispersion of extracellular matrix (ECM) produced by terminally differentiated human

mesenchymal stem cells (hMSCs) [13]. Thermoresponsive hydrogels based on hyaluronan were also recently proposed as carriers for cell delivery [22] and an encapsulation matrix for both in vitro 3D cell culture [16] and organ culture systems [26, 27]. The thermoresponsive hydrogel is composed of copolymers based on a hyaluronic acid backbone and poly(*N*-isopropylacrylamide) brushes. The latter component is synthesized by RAFT polymerization and grafted onto hyaluronan bearing alkyne functions via a copper catalyzed azide-alkyne cycloaddition reaction [16] This copolymer system in solution forms thermoreversible hydrogels above a lower critical solution temperature (LCST). The hydrogel stiffness and swelling properties were controlled by the length and grafting density of the pN segment.

Interestingly, a report describing hyaluronic acid modified with *Arg-Gly-Asp-Ser* (RGDS) integrin binding epitope functionalized poly(*N*-isopropylacrylamide) was used to deliver human retinal pigment epithelial cells into mice subcutaneous implants. However, the lack of a reported cellular response caused by the biomaterial probably owed to the positioning of the peptide on the pN segment, which is responsible for the mechanism of the gelation of the biomaterial [22]. However chemically crosslinked hyaluronan hydrogels loaded with a clustered RGDS peptides at concentrations of 0.01, 0.1 and 1 mM did in fact illicit a strong influence in murine MSC spreading [81]. The latter demonstrated that a clustering effect of the RGDS increased the cellular response in the hyaluronan hydrogel, which lacked reversibility of crosslinks and a decoupled control over the mechanics and functionality of the macromolecular network. Based on these previous studies we concluded that within our system it is a) important that the RGDS peptide is grafted to the hyaluronic acid backbone to optimize the cellular recognition of the binding epitope and b) the optimal arrangement of lower concentrations of RGDS (~10μM) is a clustered presentation. Hence we considered that the use of RGDS functionalized dendrimers as reported herein to be a suitable test bed for the concept of controlled clustering via dendrimeric macromolecules to be compared to previous published reports.

In this study, we report on the development of a disubstituted dendrimer nanostructure with a singular molecular weight that is employed in an injectable, hyaluronan matrix to present spatially controlled clusters of bioactive binding epitopes for stem cell therapies. These dendrimers are true highly branched macromolecules that display a precise architecture and can present several designed functionalities at their terminal ends [62, 64]. We hypothesized that by

augmenting the thermoreversible hydrogel microenvironment with the multivalent RGDS dendrimers onto hyaluronic acid, the clusters of RGDS would, in concert with soluble osteogenic induction factors, boost the hMSC response towards an osteogenic lineage in our bicomponent hydrogel system. Furthermore, the dendrimers could effectively create microenvironments featuring clusters of binding epitopes which, when combined with thermoreversible hyaluronan brushes, yield a bicomponent polymer system with the capacity to deliver cells, form a hydrogel upon an increase in temperature, and localize the milieu to the delivery site (Fig. 3).We tested and demonstrated by rheological measurement that the temperature induced gelation and moduli were not affected by a biologically relevant amount of dendrimer conjugates. Bone marrow derived hMSCs were encapsulated into bicomponent hydrogel beads containing (or not) dendrimers and incubated in either osteogenic or basal culture media for a 21 day period. Cell viability, morphology, and gene expression were assessed, demonstrating the ability to tailor the biofunctionality of this 3D thermoreversible hyaluronic acid-based microenvironment. We believe this is the first body of work that describes the novelty of utilizing multivalent dendrimers to tailor the biofunctionality of a hyaluronan hydrogel.

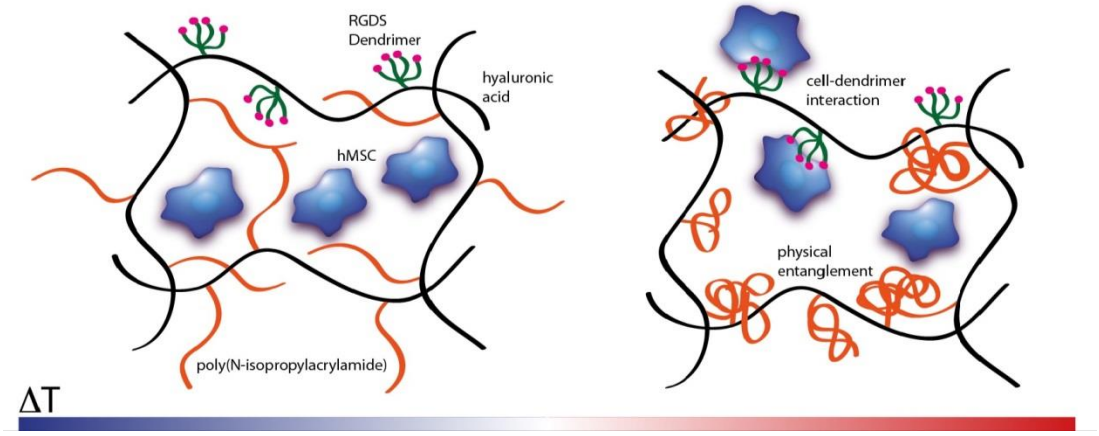

Fig. 3. Schematic representation of the hMSC encapsulation within the integrin binding dendrimer decorated hydrogel platform. The interaction between the intramembranous cellular integrin with the RGDS dendrimers is highlighted along with temperature responsive property of the hydrogel.

2.4. In vivo evaluation of the thermoresponsive hydrogel loaded with BMP-2 and hMSCs to induce ectopic bone formation in a mouse animal model

Hyaluronic acid based hydrogels are widely used in *in vivo* research that is focused on healing bone defects [39]. Previously a study by Kim *et al.* described the efficacy of an acrylated hyaluronic acid with sulfated PEG in both a subcutaneous implant and calvarial defect in a rat animal model [82]. The authors found that synergistic approach combining the biomaterial with BMP-2 and hMSCs showed good bone growth via histological analysis. Also the combination of hydrogel and BMP-2 was effective albeit less so to make new bone. This study illustrated the fundamental importance of a multifaceted approach toward the regeneration of bone defects by combining the biomaterial carrier with autologous cells, and pertinent bioactive agents such as growth factors.

The RGDS dendrimer decorated thermoreversible hydrogel has been shown to be an effective vehicle for cytokine and cellular delivery *in vitro*. Furthermore, the incorporation of dendrimers can alter the molecular architecture of the scaffold and mimic an optimal microenvironment for musculoskeletal regeneration. Therefore, in this *in vivo* study we examined the feasibility of this biomaterial alone (without peptide modified dendrimers) loaded with hMSCs and BMP-2 to stimulate ectopic bone formation in subcutaneous implants in a mouse animal model.

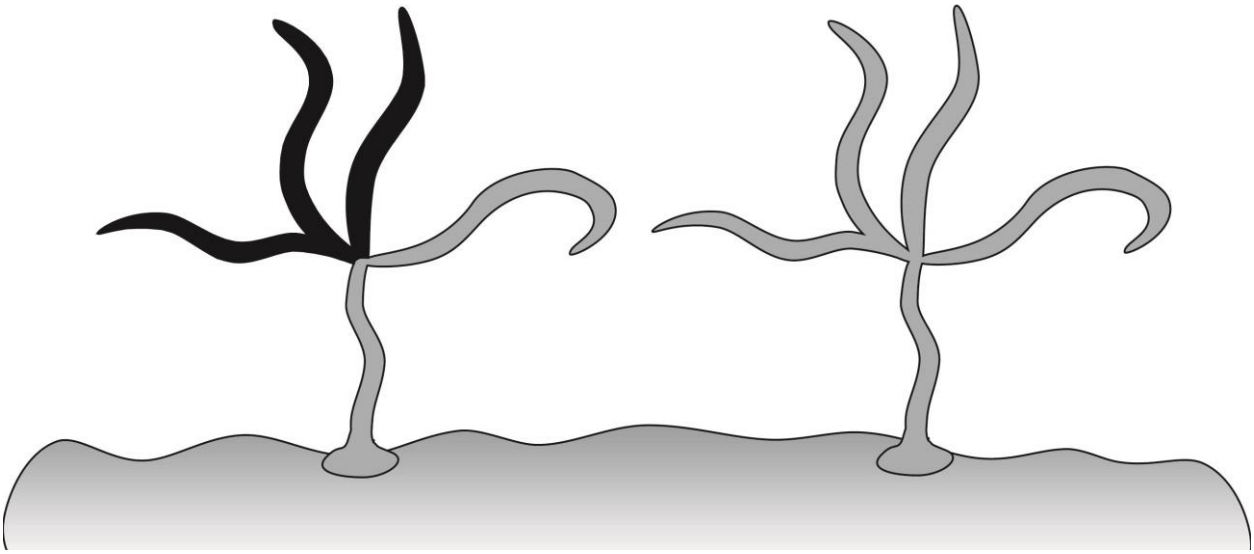

Chapter 3: Materials and Methods

3.1 Procedures employed in the comparative synthesis of Hyal-pN using $CuBr(PPh_3)_3$ and CuAsc catalyst systems

3.1.1. Materials used in this study

Hyaluronic acid sodium salt (HANa) from *Streptococcus equi* was purchased from Contipro Biotech s.r.o. (Czech Republic) (M_w = 293 kDa and M_w/M_n = 1.86 as assessed by size exclusion chromatography (SEC)). Tetrabutylammonium fluoride trihydrate (TBAF), *N*-(3-dimethylaminopropyl)-*N'*-ethylcarbodiimide hydrochloride (EDC), *N*-hydroxysuccinimide (NHS), propargylamine, sodium azide (NaN_3), *N*-dimethylsulfoxide (DMSO), sodium chloride, sodium azide, ascorbic acid sodium salt (NaAsc), copper sulphate pentahydrate ($CuSO_4 \bullet 5H_2O$),

bromotris(triphenylphosphine) copper(I) ($CuBr(PPh_3)_3$), ethylenediaminetetraacetic acid disodium salt (EDTA), *N*-ethylpiperidine hypophosphite (EPHP), *N*-isopropylacrylamide (NIPAM), azobisisobutyronitrile (AIBN), *N*-dimethylformamide (DMF), sodium nitrate ($NaNO_3$), sodium bromide (NaBr) Dowex 50X8 cation exchange resin (H Type) and phosphate buffered saline tablets were purchased from Sigma-Aldrich and were of the purest grade. Spectra/Por regenerated cellulose dialysis tubing (molecular weight cut-off MWCO =12-14 kDa, and 50 kDa) was purchased from Spectrum laboratories.

3.1.2 Synthesis of a propargylamide hyaluronan derivative

Hyaluronic acid propargylamide was prepared using a procedure already reported elsewhere [16, 83]. Briefly, NaHA was dissolved in deionized water (1 % (wt/vol)). The solution was added to a Dowex 50W-X8 cation exchange resin (H Type) loaded with tetrabutylammonium fluoride for ion exchange. After removal of the resin, the hyaluronic acid tetrabutylammonium salt (TBAHA) solution was lyophilized. TBAHA was then dissolved in DMSO at 1 % (wt/vol) and 3.3 molar equivalents of EDC, 6.3 molar equivalents NHS and 1.1 molar equivalents of propargylamine with respect to the disaccharide repeating units were added into the solution and left at room temperature for 5 days. The yielded Hyal-pa solution was dialyzed (MWCO = 12-14 kDa), lyophilized, and stored dry before characterization. The absence of significant amounts of tetrabutylammonium in the Hyal-pa was assessed by ^{1}H NMR and the presence of a signal at δ = 1.0 ppm attributed to the six methyl protons of the isopropyl group of the pN repeating monomer units.

3.1.3. Synthesis of azido terminated poly(N-isopropylacrylamide)

Reversible addition-fragmentation chain transfer polymerization of poly(N-isopropylacrylamide) with a single azido functional group was performed as already reported [16]. S-1-dodecyl-S'-(α,α'-dimethyl-α"-acetic acid) trithiocarbonate was prepared and modified with an azido group as described elsewhere and used as the chain transfer agent for the RAFT polymerization [84, 85]. The N_3-pN RAFT polymerization was performed as follows [86]; NIPAM (20 g, 0.18 mol), CTA (346 mg, 0.77 mmol), AIBN (6.3 mg, 0.04 mmol), and 1,4-dioxane (50 mL) were added in a round bottom flask, degassed by repetitive freeze-thawing under N_2, and heated at 70 ºC for 15 h under N_2. The polymerization was stopped by reducing the temperature and adding a small quantity of ethanol. Then 1,4-dioxane was added into the reaction to replenish the

evaporated solution followed by precipitation into diethyl ether, drying under vacuum, and characterization. The ratio NIPAM/CTA/AIBN was calculated to obtain N_3-pN with a M_w of 30 x 10^3 g·mol^{-1}. The experimental M_w measured using a multi-detector chromatographic system was 27.5 x 10^3 g·mol^{-1} with a polydispersity index of 1.18.

3.1.4. Poly(N-isopropylacrylamide) hyaluronan derivatives via CuAAC reactions

The coupling of N_3-pN onto Hyal-pa was performed via the CuAAC reaction under strict Schlenk conditions using the $CuSO_4$•$5H_2O$ /ascorbic acid (CuAsc) catalyst or the $CuBr(PPh_3)_3$. Two different concentrations of copper were optimized and chosen to drive the reactions based on the experimental parameters of previous studies which utilized a 1:1 molar eq. CuAsc [16] or 0.5 mol% $CuBr(PPh_3)_3$ [37]. Moreover, in order to quench the CuAsc driven reactions, a solution of EDTA was used as previously reported by Mortisen *et al.* [16]. Lal and Díez-Gonzaléz showed that in the presence of NaBr, the $CuBr(PPh_3)_3$ driven reaction rates dropped precipitously and therefore was employed to arrest this set of reactions [37]. Thus, the reactions were carried out as follows. Briefly, Hyal-pa was dissolved in pure water (18.2 MΩ) or a ratio of DMSO to water (3:2 vol/vol) which was defined by the solubility characteristics of the $CuBr(PPh_3)_3$ in the solvent mixture at 0.5 % (wt/vol). Then, N_3-pN corresponding to a 0.04 molar equivalent (or 4 mol%) of the total disaccharides was added. A CuAsc catalyst solution was prepared by the dropwise addition of 0.047 g (2 x 10^{-5} mol) of $CuSO_4$•$5H_2O$ dissolved in 1 ml of water into 1 ml of water containing 0.37 g (2 x 10^{-4} mol) of NaAsc. The catalyst solution was added dropwise to the reactants solution (800 µl in 8 ml of reactant solution). The CuAAC proceeded for 4 hours at room temperature under stirring, at which point 0.37 g (10^{-3} mol) of EDTA solid was added directly to the reaction in order to chelate the copper ions, thereby halting the reaction.

A second catalyst solution was prepared by dissolving 0.0047 g (5 x 10^{-6} mol) of $CuBr(PPh_3)_3$ in 2 ml of water. DMSO was added dropwise until dissolution of the salt. The solution was added to the reactants solution (400 µl in 8.4 ml of reactant solution). The CuAAC proceeded overnight at room temperature under stirring. Then the reaction was stopped with the addition of 10 ml of 0.1 M NaBr. Finally a third catalyst solution was prepared by dissolving 4.7 mg (5 x 10^{-6} mol) $CuBr(PPh_3)_3$ in 2 ml of DMSO. The catalyst solution was added to the reactants (400 µl in 8.4 ml of reactant which were dissolved in 3:2 DMSO/H_2O) and allowed to react for 12 hours before quenching with 10 ml of 0.1 M NaBr. All products were dialyzed

against 0.1 M NaBr and water (MWCO = 12-14 kDa) for 5 days, then lyophilized and stored dry until further characterization.

3.1.5 Chromatographic characterization of polymer molecular weight distributions

The average molecular weight (M_w) of hyaluronic acid was obtained using a modular multi-detector size exclusion chromatography system consisting of an Alliance 2695 separation module (Waters, USA) equipped with two on-line detectors: a multi angle light scattering (MALS) Dawn DSP-F photometer (Wyatt, USA) and a 2414 differential refractometer (DRI) from Waters that was used as a concentration detector. Chromatographic specifications: two Shodex OHpak columns (KB806-KB805) from Showa Denko; mobile phase: 0.20 M NaCl; flow rate: 0.5 mL/min; temperature: 35 ºC; injection volume: 150 µL; sample concentration: 0.2 or 0.8 mg/mL depending on the M_w of the sample. The specific refractive index increment, dn/dc, with respect to the mobile phase was measured by a Chromatix KMX-16 differential refractometer. The M_w of N_3-pN was obtained by an integrated multi-detector GPCV 2000 chromatographic system from Waters (USA). The GPCV 2000 system was equipped with three online detectors: (1) a differential viscometer (DV), (2) a differential refractometer (DRI) as a concentration detector and (3) an additional MALS Dawn DSP-F photometer (Wyatt, USA). Chromatographic specifications: two PLgel Mixed C columns from Polymer Laboratories (UK); mobile phase: *N*,*N*-dimethylformamide (DMF) + 0.1 M LiCl; flow rate: 0.8 mL/min; temperature: 50 ◦C; injection volume: 218.5 µL; sample concentration = 2 mg/mL. Derivatives of hyaluronan and Hyal-pN, could not be analyzed accurately and with confidence using chromatography due to non-solubility at the operating temperature.

3.1.6 Attenuated total reflectance Fourier transform infra-red spectrophotometry (ATR-FTIR)

ATR-FTIR analysis was performed on a Bruker Tensor 27 spectrophotometer equipped with a single reflection diamond attenuated total reflection accessory. Dry Hyal-pa or the as-received NaHA powder was placed directly on the accessory. Spectra were acquired between 4000 and 500 cm^{-1} (average of 32 scans), and processed with the Opus software (version 6.5, Bruker Optik GmbH, Ettlingen, Germany, www.bruker.com).

3.1.7 Proton nuclear magnetic resonance spectroscopy (^{1}H NMR)

All ^{1}H NMR analysis was performed on a Bruker Avance AV-500 NMR spectrometer using deuterium oxide as solvent and processed with Mestrenova software (version 6.0.2, Mestrelab Research S.L., Santiago de Compostela, Spain, www.mestrelab.com).

The degree of grafting (DG mol%) of propargylamide onto Hyal-pa was determined by first performing the CuAAC reaction with CuAsc and an excess of 2.2 molar NaN_3 compared to calculated hyaluronan disaccharides as described and secondly collecting the ^{1}H NMR spectra and calculating the integration of the triazole proton signal (δ= 7.88 ppm) to the integration of the acetyl proton signal (δ= 2.00 ppm) ratio [16]. The pN degree of grafting (DG mol%) onto Hyal-pa was determined by comparing the ratios of integration of the signals from 3.00 to 3.77 ppm (corresponding to 9 protons of the hyaluronan disaccharide) and the singlet at 1.14 ppm (corresponding to the 6 protons of the pN isopropyl group) [29].

3.1.8. Rheological characterization of Hyal-pN derivatives

Rheological measurements were performed with an Anton Paar Instruments MCR 302 rheometer (Anton Paar GmbH, Graz, Austria) equipped with a Peltier plate temperature control and a steel cone geometry, Ø = 25 mm, 1°. Samples at room temperature were spread onto the Peltier plate pre-set at 15 °C. Additionally, low viscosity silicon oil was applied along the border of the cone after sample placement in order to avoid evaporation at the solution-atmosphere interface. The synthesized products were dissolved in PBS at 15 % (wt/vol). Storage modulus (G') and loss modulus (G") were measured as a function of the temperature increase at 1 °C/min from 20 to 40 °C with 0.1% oscillatory strain at 1 Hz. The linear viscoelastic range was evaluated at 20 °C and 35 °C by increasing the deformation from 0.01%-100% strain. Duplicate analysis was performed for each sample.

3.1.9. Inductively coupled plasma mass spectrometry (ICP-SFMS)

A sector-field inductively coupled plasma mass spectrometer (Element 2, Thermo Scientific, Germany) was used to assess the copper content in an aqueous solution of prepared polymer compositions following a standardized methodology (USEPA 200.8).

3.2. *In vitro evaluation of BMP-2 and TGF-β1 loaded hydrogel carrier for drug delivery*

3.2.1. Materials used in this study

Hyaluronic acid sodium salt from *Streptococcus equi* was purchased from Contipro Biotech s.r.o. (Czech Republic) (Mw = 293 kDa and PD = 1.86). Tetrabutylammonium fluoride trihydrat, *N*-(3-dimethylaminopropyl)-*N'*-ethylcarbodiimide hydrochloride, *N*-hydroxysuccinimide, propargylamine, *N*-dimethylsulfoxide, sodium chloride, sodium azide, ascorbic acid sodium salt, copper sulphate pentahydrate, ethylenediaminetetraacetic acid disodium salt, *N*-ethylpiperidine hypophosphite, *N*-isopropylacrylamide, azobisisobutyronitrile, *N*-dimethylformamide, sodium nitrate ($NaNO_3$), Dowex 50X8 cation exchange resin (H Type), *N,N'*-diisopropylcarbodiimide (DIPCDI), Trifluoroacetic acid (TFA), *N,N*'-diisopropylethylamine (DIEA), Triisopropylsilane (TIS), Di-*tert*-butyl dianhydride, Zinc, 10% wt Pd/C, and phosphate buffered saline tablets were purchased from Sigma-Aldrich and were of the purest grade. Spectra/Por regenerated cellulose dialysis tubing (MWCO=12-14 kDa) was purchased from Spectrum laboratories. NH4Cl was purchased from Pancreac. *O*-(2-Aminoethyl)-*O'*-(2-azidoethyl)pentaethylene glycol (OEG), Benzotriazol-1-yl-oxytripyrrolidinophosphonium hexafluorophosphate (PyBOP), and amino acids used for synthesizing the peptide binding sequences were purchased from Iris Biotech. Hexane, DCM, MeOH, and *tert*-butyl methyl ether were purchased from Solvents Documentation Synthesis. Ethyl (hydroxyimino)cyanoacetate (OxymaPure) was purchased from Luxembourg Industries. Recombinant BMP-2 and TGF-β1 and were obtained from Medtronic Inc. and Fitzgerald Industries respectively.

3.2.2. Synthesis of the DTPA derivative core unit: Bn-G1-4Boc

A bifunctional diethylene triamine pentaacetic acid (DTPA)-based core unit **1** was synthesized as described in the literature (Fig. 4) [62]. Molecule **1** (330 mg, 0.47 mmol) was dissolved in 30 mL of 4 M HCl in dioxane and left overnight. The next day the dioxane was evaporated to yield the unprotected DTPA. The unprotected core was dissolved in 250 mL of DCM/DMF (7:3) and PyBOP (1066 mg, 2.05 mmol) together with BocNH-PEG-NH2 (873 mg, 2.05 mmol) were added. The basicity of the reaction mixture was adjusted to pH 8 by the addition of DIEA. The reaction was allowed to stir for 2 hours after which the solvent was concentrated under reduced pressure. After evaporation of the organic phase, the crude product

containing residual DMF was dissolved in 50 ml of DCM and washed three times with 5% $NaHCO_3$ (50 mL). Another 20 ml of DCM was evaporated after the washing. The crude product redissolved again in 10 mL of DCM and transferred to a 50 ml falcon tube then precipitated in 40 ml of hexane followed by vigorous shaking and centrifugation. The supernatant was discarded and the precipitated pellet was purified with flash chromatography over basis alumina oxide with 1% MeOH in DCM as the eluent to yield the desired dendron (**2**, 619 mg, 63%). ^{1}H NMR (400 Mhz, CDCl3): δ = 2.65 (m, 4 H), 2.71 (m, 4 H), 3.19 (s, 8 H), 3.25 (m, 8 H), 3.38 (m, 8 H), 3.42 (s, 2 H9, 3.48 (m, 16 H),3.52-3.62 (m, 80 H), 5.08 (s, 2 H), 7.30 (m, 5 H), and 7.70 (bs, NH). ^{13}C NMR (100 MHz, CDCl3): δ = 2.65 28.36, 52.30, 53.05, 54.97, 58.64, 66.43, 69.61, 69.99, 70.16, 70.40, 78.98, 128.34, 128.39, 128.58, 135.43, 155.98, and 170.80. HPLC: 5→100% acetonitrile in water over 8 min (SunFire™ C18), t_R= 5.98 min. MS: Theoretical mass for $[C_{97}H_{181}N_{113}O_{38}]^{+}$: 2108.2569. Experimental mass detected by LC-MS: 1056.60 (M+2)/2. Experimental mass detected by HRMS: 2108.2588.

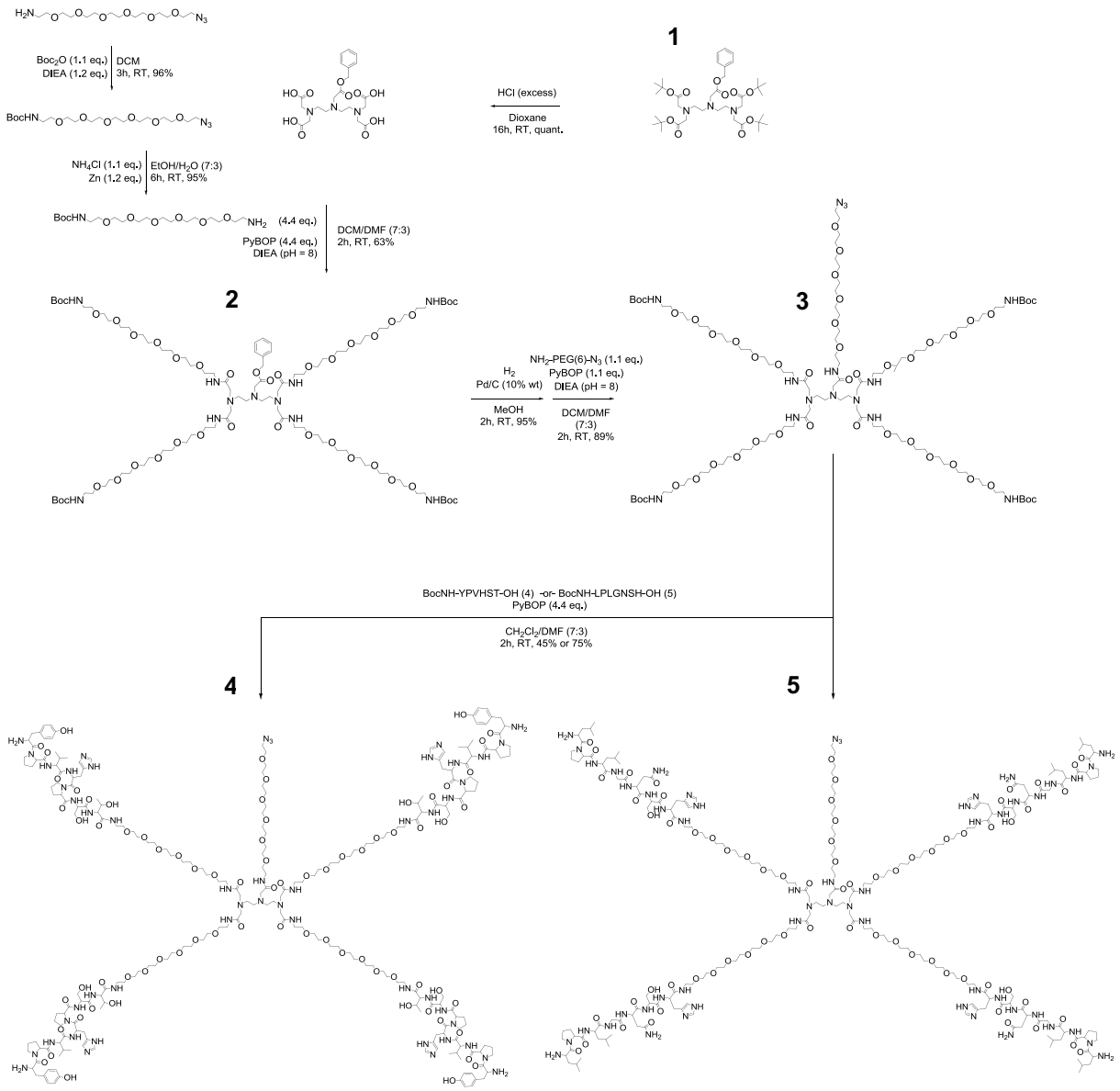

Fig. 4. The schematic workflow of the synthesis of the multivalent dendrimers starting with the DTPA-based core **1**, intermediate dendron molecules **2** and **3**, and finally the purified dendrimer-peptide conjugates functionalized with one terminal azide moiety and either BMP-2 (**4**) or TGF-β1 (**5**) binding epitopes. The reaction schematic was drawn with ChemDraw Ultra version 11.0 (Perkin Elmer, Inc., Waltham, MA, USA, www.cambridgesoft.com, 2014).

3.2.3. Chemical coupling of the dendron with an azide terminated branch: G1-4Boc-1N_3

The purified dendron (Bn-G1-4Boc, **2**) (800 mg, 0.38 mmol) was dissolved in 20 mL MeOH after which a heterogenous catalyst 10% wt Pd/C was added (80 mg). The contents were kept under nitrogen and a positive pressure was maintained on the reaction flask using an H_2 filled balloon. The reaction was stirred for two hours after which the flask was purged again with N_2. The catalyst was removed by filtration over cellite and the filter cake was washed several times with ethyl acetate. The organic phase consisting of MeOH and ethyl acetate was evaporated to yield yellow hued oil. The oil was dissolved in a mixture (7:3) of DCM/DMF (200 mL) and PyBOP (218 mg, 0.42 mmol) together with N_3-PEG-NH_2 (155 mg, 0.42 mmol) were added. The basicity of the reaction mixture was adjusted to pH 8 by the addition of DIEA. The reaction was allowed to stir for 2 hours after which the solvent was concentrated under reduced pressure. After evaporation of the organic phase, the crude product containing residual DMF was dissolved in 50 ml of DCM and washed three times with 5% $NaHCO_3$ (50 mL). Another 20 ml of DCM was evaporated after the washing. The crude product was redissolved in 10 mL of DCM and transferred to a 50 ml falcon tube then precipitated in 40 ml of hexane followed by vigorous shaking and centrifugation. The supernatant was discarded and the precipitated pellet corresponded to the crude product. The product G1-4Boc-1N_3, **3**, was purified with flash chromatography over basis alumina oxide and was eluted with 1% MeOH in DCM as the eluent to yield the desired dendron 3 (795 mg, 89%). ^{1}H NMR (400 Mhz, $CDCl_3$): δ = 1.44 (s, 36 H), 2.62 (bs, 4 H), 2.69 (bs, 4 H), 3.11 (s, 2 H), 3.21 (s, 10 H), 3.28-3.33 (m, 8 H), 3.39 (t, J = 4.96, 2 H), 3.41-3.47 (m, 10 H), 3.50-3.58 (m, 20 H), 3.58-3.67 (m, 100 H), and 7.57 (bs, NH). ^{13}C NMR (100 MHz, $CDCl_3$): δ = 28.41, 38.93, 40.34, 50.65, 53.19, 58.85, 58.64, 69.61, 70.00, 70.09, 70.20, 70.49, 155.89, and 170.79. HPLC: 5→100% acetonitrile in water over 8 min (SunFire™ C_{18}), t_R= 5.68 min. MS: Theoretical mass for $[C_{104}H_{203}N_{15}O_{43}]^+$: 2350.4159. Experimental mass detected by LC-MS: 1177.74 (M+2)/2. Experimental mass detected by HRMS: 2350.4182.

2.4 Solid phase peptide synthesis of BocNH-Tyr-Pro-Val-His-Ser-Thr-OH and BocNH-Leu-Pro-Leu-Gly-Asn-Ser-His-OH

Two peptide sequences *Tyr-Pro-Val-His-Ser-Thr* (YPVHST) and *Leu-Pro-Leu-Gly-Asn-Ser-His* (LPLGNSH) were synthesized by solid phase peptide synthesis on a 2-chlorotrityl resin using the Fmoc strategy yielding BocNH-YPVHST-OH and BocNH-LPLGNSH-OH. In both cases the C-terminal amino acid was introduced onto the solid support by addition of 4 eq. of DIEA onto the resin. The remaining three amino acids were coupled one after the other using OxymaPure and DIPCDI as the coupling reagents using HBTU as the coupling agent and HOBt as the additive in the presence of DIEA and in DMF. After coupling the final amino acid, the N-terminal amino group was capped with the Boc protecting group by reacting with di-*tert*-butyl dicarbonate and DIEA. The peptides were then cleaved from the resin using mild acidic conditions consisting of short washes with 1% TFA in DCM in order to keep the side chain protecting groups intact. The cleaved peptides were characterized by HPLC and LC-MS and were found to be 99% pure.

3.2.5. BMP-2 binding peptide biofunctionalization of the dendrimer platform: G1-1N_3-4NH_2YPVHPST

Dendron **3** (60 mg, 0.025 mmol) was dissolved in 5 mL TFA/H_2O (95:5) and stirred for 1h. Subsequently, the TFA was evaporated and the product was precipitated in methyl *tert*-butyl ether. After decanting the methyl *tert*-butyl ether, the pellet containing the deprotected dendrimer was dissolved in a mixture (7:3) of DCM/DMF (50 mL) and PyBOP (57 mg, 0.11 mmol) together with BocNH-YPVHST-OH (140 mg, 0.11 mmol) were added. The pH was adjusted to 8 by the addition of DIEA. After 2 hours, the solvent was concentrated under reduced pressure. After evaporation of the organic phase, the crude product was dissolved in 50 ml of DCM and washed three times with 5% $NaHCO_3$ (50 mL). Another 20 ml of DCM was evaporated after the washing. The crude product was dissolved again in 10 mL of DCM and then precipitated in 40 ml of hexane. The pellet corresponded to the crude product with the side chain protecting groups of the peptide still intact. The protecting groups were removed by dissolving the pellet in 10 mL of TFA/H_2O/TIS (95:2.5:2.5). After 1 hour, the TFA was removed and the compound was precipitated in cold *tert*-butyl methyl ether to give the crude peptide-dendron conjugate. The crude was then dialyzed overnight using a membrane with MWCO 1 kDa to yield the pure

dendron-peptide conjugate (**4)** (57 mg, 45%). HPLC: 0→100% acetonitrile in water over 8 min (SunFire™ C_{18}), t_R= 3.80 min. MS: Theoretical mass for $[C_{232}H_{375}N_{51}O_{75}]^+$: 5075.7098. Experimental mass detected by LC-MS: 1272.04 (M+4)/4; 1014.04 (M+5)/5; 848.25 (M+6)/6. Experimental mass detected by HRMS: 5075.7092.

3.2.6 TGF-β1 binding peptide biofunctionalization of the dendrimer platform: G1-1N$_3$-4NH$_2$LPLGNSH

Following the protocol for dendron-peptide conjugate **4**, dendron **3** (90 mg, 0.036 mmol) was deprotected and dissolved in a mixture (7:3) of DCM/DMF (50 mL) and PyBOP (82 mg, 0.158 mmol) together with BocNH-LPLGNSH-OH (215 mg, 0.158 mmol). The synthesized dendron-peptide conjugate **5** (130 mg, 75%) was then purified and characterized as described. HPLC: 0→100% acetonitrile in water over 8 min (SunFire™ C_{18}), t_R= 3.92 min. MS: Theoretical mass for $[C_{212}H_{371}N_{55}O_{71}]^+$: 4823.7111. Experimental mass detected by LC-MS: 1206.64 (M+4)/4; 967.07 (M+5)/5; 806.01 (M+6)/6; 691.08 (M+7)/7. Experimental mass detected by HRMS: 4823.7106.

3.2.7. Synthesis of dendrimer decorated hyaluronic acid

Hydrosoluble hyaluronic acid propargylamide was synthesized based on already established procedures [16]. Dendrimer **4** or **5** and Hyal-pa (0.5 % (wt/vol)) were solubilized in degassed MilliQ water such that the theoretical peptide content was 2 mm, hence 0.5 mm azide concentration. The CuAAC reaction was initiated by the addition of a solution of $CuSO_4$ pentahydrate salt and sodium ascorbic acid to the polymer solution such that the final copper to azide molar ratio was equivalent. The reaction was maintained under Schlenk parameters and stirred for 5 hours at room temperature while protected from light. The reaction was quenched by the addition of 0.5 g of EDTA disodium salt dehydrate. The yielded polymer products were then dialyzed with 0.1 m NaBr and water and lyophilized until dry. The products were verified by ^{1}H NMR and the peptide content was quantified by amino acid analysis. The reaction yield of Hyal-pa modified with dendrimer **4** (Hyal-YPV) was 33.7 ± 5.7 %, and with dendrimer **5** (Hyal-LPL) was 38.9 ± 1.5 %.

3.2.8. Synthesis of the thermoresponsive poly(N-isopropylacrylamide) derivative of hyaluronic acid

The synthesis of four different sizes of azido terminated poly(*N*-isopropylacrylamide) with M_n equal to 9.3, 16.3, 21.2, and 27.5 x 10^3 g•mol^{-1} was performed by RAFT homopolymerization using *S*-1-dodecyl-*S'*-(*α,α'*-dimethyl-*α"*-acetic acid) trithiocarbonate as reported [85-87]. The molecular weight distributions for N_3-pN were obtained as previously reported [16]. Hyal-pN was synthesized via CuAAC under Schlenk conditions by adding N_3-pN (9.3, 16.3, 21.2, or 27.5 x 10^3 g•mol^{-1}) to 0.5% (wt/vol) Hyal-pa in degassed MilliQ water. The N_3-pN were added to the Hyal-pa solutions such that the final degree of grafting would be 4 mol% of the total calculated disaccharides. The degree of pN derivation of the hyaluronic acid was assessed via ^{1}H NMR spectroscopy (Bruker Avance AV-500 NMR spectrometer) using deuterium oxide as solvent without residual HOD peak suppression and processed with Mestrenova software as already reported [26].

3.2.9. Rheological characterization of prepared hydrogel compositions

Rheological measurements were performed with an Anton Paar Instruments MCR 302 rheometer equipped with a Peltier plate temperature control and a steel cone geometry, Ø = 25 mm, 1°. Samples at room temperature were spread with a spatula onto the Peltier plate pre-set at 15 °C. Additionally, low viscosity silicon oil was applied along the border of the cone after sample placement in order to avoid evaporation at the solution-atmosphere interface. The Hyal-pN batches synthesized with 9.3, 16.3, 21.2, and 27.5 kDa pN (HpN9, HpN16, HpN21, and HpN28 respectively) were solubilized in PBS at 13 % (wt/vol) along with the addition of 2% (wt/vol) Hyal-pa, Hyal-LPL, or Hyal-YPV (Table 1). Storage modulus (G') and loss modulus (G") were measured as a function of the temperature increase at 1 °C/min from 20 to 40 °C with 0.1% oscillatory strain at 1 Hz. The linear viscoelastic range was evaluated at 20 °C and 37 °C by increasing the deformation from 0.01%-100% strain. Triplicate analysis was performed on each sample.

3.2.10. In vitro release of TGF-β1 and BMP-2 from the hydrogels

All polymer compositions were prepared in PBS at 30% (wt/vol) and stored at 4 °C under gentle mixing until the materials were fully solubilized (Table 1). Prior to the experiment, 40 mg

of the concentrated polymer solutions were weighted in the lids of LoBind® Eppendorf tubes (Sigma Aldrich). Then 38 µl of a swelling medium which consisted of 1% BSA in 4 mM HCl (pH 6) was added to the polymer solution. A stock solution of either TGF-β1 or BMP-2 at 100 µg/ml was delivered into the mixture of solutions such that 200 ng of protein was added to each sample and were left overnight at 4 °C. The following morning the final depot weights were recorded then incubated at 37 °C for 30 min. Once the hydrogels were fully formed, and confirmed by a quick inversion test, 1 ml of release buffer consisting of 0.1% BSA in PBS was added to the vials. The experiment was carried out at 37 °C under static conditions. Samples were taken at 0.5h, 2h, 4h, 24h, 48h, 72h, 120h and 168h by fully removing the liquid sample, and replenishing it with fresh release buffer. At the end of the experiment, depot weights were again recorded after the complete removal of the buffer. The amount of released protein was analyzed with ELISA (R&D Systems, Inc.) following the manufacturer's protocol. In this study the influence of two factors on the release of proteins from the Hyal-pN compositions were assessed: 1) of pN chain length / constant polymer weight and 2) of the addition of dendrimer decorated hyaluronan derivatives featuring binding epitopes.

Table 1. Description of the HG compositions. All depots contained 13 % (wt/vol) of their corresponding Hyal-pN batches; additionally 2 % (wt/vol) of Hyal-pa, Hyal-YPV, or Hyal-LPL was also added to augment the protein binding capability of the biomaterials.

	pN size (kDa)	**Non-binding**	**BMP-2 binding**	**TGF-β1 binding**
HpN9	9.2	HpN9-H	HpN9-YPV	HpN9-LPL
HpN16	16.3	HpN16-H	HpN16-YPV	HpN16-LPL
HpN21	21.2	HpN21-H	HpN21-YPV	HpN21-LPL
HpN28	27.5	HpN28-H	HpN28-YPV	HpN28-LPL

3.2.11. Statistical analysis of the release profiles

A mixed-design analysis of variance (ANOVA) was selected as the most appropriate statistical model for analysis of the data. The study framework consisted of repeated

measurements taken from the hydrogel depots whilst comparing the effects of the amount of protein released based upon the type of protein, the type of dendrimer, and the length of pN chains. Studentized residuals generated from the ANOVA procedure were examined and three residuals with a magnitude greater than or equal to ± 3 standard deviations were determined to be outliers. Analysis of the Q-Q plots generated from the residuals revealed that the data was normally distributed. Statistical significance between groups was determined with the Tukey HSD post hoc test with the significance level set at $p<0.05$.

3.3 Materials and methods employed in the in vitro evaluation of hMSCs encapsulated in RGDS decorated Hyal-pN

3.3.1. Materials used in this study

Hyaluronic acid sodium salt from *Streptococcus equi* was purchased from Contipro Biotech s.r.o. (Czech Republic) (Mw = 1506 kDa and PD = 1.53). Tetrabutylammonium fluoride trihydrate, *N*-(3-dimethylaminopropyl)-*N*'-ethylcarbodiimide hydrochloride, *N*-hydroxysuccinimide, propargylamine, *N*-dimethylsulfoxide, sodium chloride, sodium azide, ascorbic acid sodium salt, copper sulphate pentahydrate, ethylenediaminetetraacetic acid disodium salt, *N*-ethylpiperidine hypophosphite, *N*-isopropylacrylamide, azobisisobutyronitrile, *N*-dimethylformamide, sodium nitrate, Dowex 50X8 cation exchange resin (H Type), *N*,*N*'-diisopropylcarbodiimide, trifluoroacetic acid, *N*,*N'*-diisopropylethylamine, Triisopropylsilane (TIS), Di-*tert*-butyl dianhydride, Zinc, 10% wt Pd/C, dexamethasone-water soluble, β-glycerophosphate disodium salt hydrate, sodium citrate, phosphate buffered saline, 1-bromo-3-chloro-propane (BCP), diethyl pyrocarbonate (DEPC), the QuantiPro™ BCA Assay Kit, and the PKH26 red fluorescent cell linker kit were purchased from Sigma-Aldrich and were of the purest grade. Spectra/Por regenerated cellulose dialysis tubing (MWCO=12-14 kDa) was purchased from Spectrum laboratories. L(+)-ascorbic acid sodium salt, sodium chloride, calcium chloride, isopentane, xylene, toluidine blue, and Eukitt® quick-hardening mounting medium were purchased from Fluka and were of the purest grade. Buffered 4% formalin was purchased from Formafix. NH_4Cl was purchased from Pancreac. *O*-(2-Aminoethyl)-*O'*-(2-azidoethyl)pentaethylene glycol, Benzotriazol-1-yl-oxytripyrrolidinophosphonium hexafluorophosphate, arginine (Arg), serine (Ser), aspartic acid (Asp) and glycine (Gly) were purchased from Iris Biotech. Dichloromethane, and Methanol (MeOH), were purchased from

Solvents Documentation Synthesis. Ethyl (hydroxyimino)cyanoacetate (OxymaPure) was purchased from Luxembourg Industries. Alpha modified Eagle's medium (α-MEM), Dulbecco's modified Eagle medium (DMEM, 4.5 g/L glucose), human MSC qualified fetal bovine serum (FBS-Hyclone), fetal calf serum (FCS), penicillin/streptomycin (P/S), non-essential amino acids (NEAA), Trypsin-EDTA, SuperScript® VILO™ cDNA synthesis kit, TaqMan® Universal PCR Master Mix 2x, human glyceraldehyde 3-phosphate dehydrogenase (hGAPDH) endogenous control primer + probe kit, Prolong® Gold antifade reagent with DAPI, and LIVE/DEAD® cell viability assay were purchased from Life Technologies. Basic fibroblast growth factor type 2 (bFGF-2) were purchased from Fitzgerald industries. Cell culture well inserts (2 cm^2, PET membrane, 0.4 μm pore size) and 24 well companion plates were purchased from BD Falcon. High salt precipitation solution, TRI Reagent and polyacryl carrier were purchased from Molecular Research Center. Tissue freezing medium was purchased from Leica Biosystems.

3.3.2. Synthesis of the multivalent dendrimer starting material

A bifunctional DTPA-based core unit was synthesized as described in the literature [62]. A NH_2-OEG-NHBoc chain was synthesized by reacting N_3-OEG-NH_2 (O-(2-Aminoethyl)-O′ -(2-azidoethyl)pentaethylene glycol) with di-*tert*-butyl dicarbonate and the base DIEA to protect the amine, followed by the reduction of the azide with zinc dust and NH_4Cl. The benzyl protecting group of the DTPA derivative was removed by catalytic hydrogenation with 10% wt Pd/C in MeOH. Then, N_3-OEG-NH_2 was conjugated using the PyBOP as the coupling agent in DCM/DMF (7:3). The pH of the reaction mixture was adjusted to 8 by the drop-wise addition of DIEA. After incorporation of the first OEG-chain, the *tert*-butyl groups of the DTPA-based core unit were removed with 4 M HCl in dioxane and the four other chains, NH_2-OEG-NHBoc, were conjugated using PyBOP and DIEA in DCM/DMF (7:3) (G1-4Boc-1N_3). After incorporation of both types of OEG-chains the dendron was purified by means of semi-prep reversed phase chromatography. ChemDraw Ultra (version 11.0, Advanced Chemistry Development, Inc., Canada) was used to create the dendrimer reaction schematic (Fig. 5). **DTPA core:** ^{1}H NMR (400 MHz, $CDCl_3$): δ = 1.44 (s, 36 H), 2.82 (s, 8 H), 3.42 (s, 8 H), 3.59 (s, 2 H), 5.12 (s, 2 H), and 7.35 (m, 5 H). ^{13}C NMR (100 MHz, $CDCl_3$): δ = 28.13, 52.25, 52.75, 54.87, 56.02, 65.92, 80.79, 128.17, 128.23, 128.47, 135.87, and 170.60. HPLC: 50→100% acetonitrile in water over 8 min (SunFire™ C_{18}), t_R= 4.41 min. MS: Theoretical mass for $[C_{31}H_{61}N_3O_{10}+H]^+$: 708.4430.

Experimental mass detected by LC-MS: 708.46 (M+1). Experimental mass detected by HRMS (ES^+): 708.4424. **G1-4Boc-1N$_3$:** ^{1}H NMR (400 MHz, $CDCl_3$): δ = 1.44 (s, 36 H), 2.62 (bs, 4 H), 2.69 (bs, 4 H), 3.11 (s, 2 H), 3.21 (s, 10 H), 3.28-3.33 (m, 8 H), 3.39 (t, J = 4.96, 2 H), 3.41-3.47 (m, 10 H), 3.50-3.58 (m, 20 H), 3.58-3.67 (m, 100 H), and 7.57 (bs, NH). ^{13}C NMR (100 MHz, $CDCl_3$): δ = 28.41, 38.93, 40.34, 50.65, 53.19, 58.85, 58.64, 69.61, 70.00, 70.09, 70.20, 70.49, 155.89, and 170.79. HPLC: 5→100% acetonitrile in water over 8 min (SunFire™ C_{18}), t_R= 5.68 min. MS: Theoretical mass for $[C_{104}H_{203}N_{15}O_{43}]^+$: 2350.4159. Experimental mass detected by LC-MS: 1177.74 (M+2)/2. Experimental mass detected by HRMS: 2350.4182.

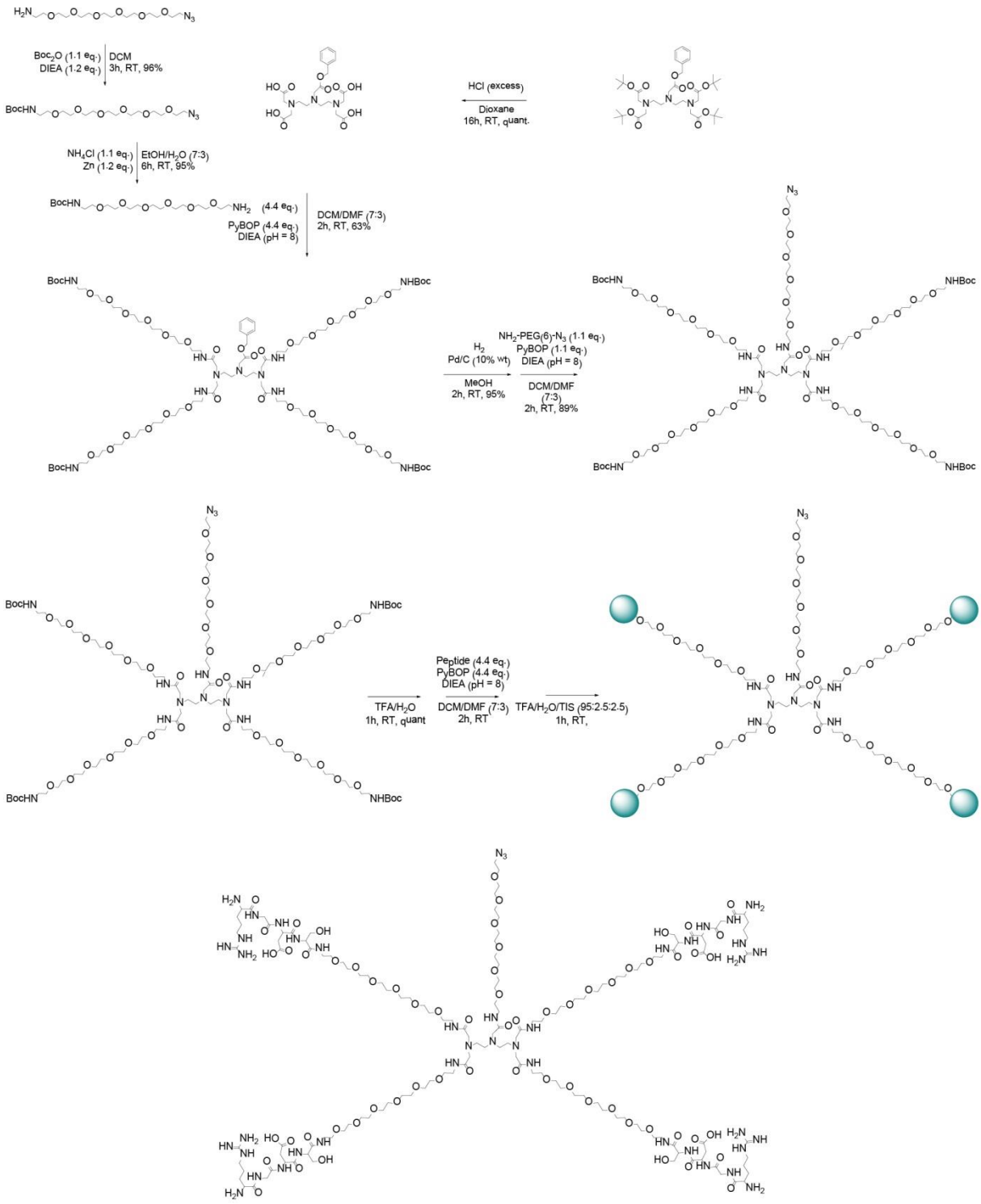

Fig. 5. The schematic workflow of the synthesis of the disubstituted dendrimer functionalized with four RGDS epitope branches and one terminal azide branch.

3.3.3 Solid phase synthesis NHBoc-Arg(Pbf)-Gly-Asp(tBu)-Ser(tBu)-COOH and NHBoc-Arg(Pbf)-Ser(tBu)-Gly-Asp(tBu)-COOH peptides

Two peptides; NHBoc-Arg(Pbf)-Gly-Asp(tBu)-Ser(tBu)-COOH (RGDS) and NHBoc-Arg(Pbf)-Ser(tBu)-Gly-Asp(tBu)- COOH (DGSR) sequences were synthesized by solid phase peptide synthesis on a 2-chlorotrityl resin using the Fmoc-strategy (Fig. 5). In both cases C-terminal amino acid was introduced on to the solid support by addition of 4 eq. of DIEA onto the resin, the remaining three amino acids were coupled one after the other using OxymaPure and DIPCDI as the coupling reagents. After coupling the fourth and final amino acid, the N-terminal amino group was capped with the Boc protecting group by reacting with di-*tert*-butyl dicarbonate and DIEA. The peptides were then cleaved from the resin using mild acidic conditions consisting of short washes with 1% TFA in DCM in order the keep the side chain protecting groups intact. The cleaved peptides were characterized by HPLC and LC-MS and the purity was found to be 99%. **Peptides:** Boc-NH-R(Pbf)GD(tBu)S(tBu)-OH: HPLC: 5→100% acetonitrile in water over 8 min (SunFire™ C_{18}), t_R= 7.53 min. MS: Theoretical mass for $[C_{41}H_{67}N_7O_{13}S]^+$: 897.4140. Experimental mass detected by HPLC-MS: 898.59. Boc-NH-D(tBu)GS(tBu)R(Pbf)-OH: HPLC: 0→100% acetonitrile in water over 8 min (SunFire™ C_{18}), t_R= 7.65 min. MS: Theoretical mass for $[C_{41}H_{67}N_7O_{13}S]^+$: 897.4099. Experimental mass detected by HPLC-MS: 898.52.

3.3.4. Synthesis of multivalent peptide dendrimers

The Boc-groups of the dendron branches were removed by treatment with TFA. Afterwards, the peptides were conjugated onto the dendron using PyBOP as the coupling agent in DCM/DMF (7:3) (Fig. 5). The conjugation was monitored by HPLC and LC-MS and after complete conjugation, the side chain protecting groups of the peptide-dendron conjugates were removed by TFA/H_2O/TIS (95:2.5:2.5). Then, the conjugates were precipitated in *tert*-butyl methyl ether and purified by means of dialysis using a membrane with MWCO 1 kDa. The peptide dendron conjugates were characterized by HPLC-MS and HRMS and the purity was 95%. **G1-1N_3-4NH_2RGDS**: HPLC: 0→100% acetonitrile in water over 8 min (SunFire™ C_{18}), t_R= 3.80 min. MS: Theoretical mass for $C_{144}H_{271}N_{43}O_{63}$: 3610.9324. Experimental mass detected by LC-MS: 724.06 (M+5)/5; 603.54 (M+6)/6; 517.51 (M+7). Experimental mass detected by HRMS: 3610.9268. **G1-1N_3-4NH_2DGSR** HPLC: 0→100% acetonitrile in water over 8 min

(SunFire™ C_{18}), t_R= 3.79 min. MS: Theoretical mass for $C_{144}H_{271}N_{43}O_{63}$: 3610.9324. Experimental mass detected by LC-MS: 1206.46 (M+3)/3; 905.07 (M+4)/4; 724.13 (M+5)/5. Experimental mass detected by HRMS: 3610. 9264

3.3.5. Synthesis of the thermoresponsive poly(N-isopropylacrylamide) derivative of hyaluronic acid

Hydrosoluble hyaluronic acid propargylamide was synthesized using an already established procedure [16]. The synthesis of azido terminated poly(*N*-isopropylacrylamide) with Mn equal to 28 x10^3 g•mol^{-1} (measured by SEC and correlated to MALDI-TOF as already reported [16]) was performed by RAFT homopolymerization using *S*-1-dodecyl-*S'*-(*α,α'*-dimethyl-*α"*-acetic acid) trithiocarbonate as reported [85-87]. Poly(*N*-isopropylacrylamide) grafted hyaluronic acid was obtained by copper catalyzed azide-alkyne cycloaddition under nitrogen/argon conditions by adding N_3-pN to 0.5% (wt/vol) Hyal-pa in degassed MilliQ water (18.2 MΩ). Careful measures were taken to maintain a positive pressure of argon on the reaction mixture before, during, and after the reaction in order to reduce oxidative degradation of the hyaluronic acid backbone. The N_3-pN was added to the Hyal-pa such that the molar amount corresponded to 53 mol% of the propargylamine modified disaccharides or 10 mol% of the total disaccharide units. Once solubilized the $CuSO_4$•$5H_20$ and NaAsc catalyst solution was prepared together as already reported [75]. After quenching of the catalyst with EDTA and dialysis against 0.1 M NaBr and water, the solutions were frozen at -80°C and lyophilized until dry. The degree of pN derivation of the hyaluronic acid was assessed via ^{1}H NMR spectroscopy (Bruker Avance AV-500 NMR spectrometer) using deuterium oxide as solvent without residual HOD peak suppression and processed with Mestrenova software as already reported [29].

3.3.6. Synthesis of RGDS dendrimer decorated hyaluronic acid

The method for grafting the disubstituted dendrimer to hyaluronic acid followed a protocol identical to the Hyal-pN. Briefly, dendrimer and Hyal-pa (0.5% (wt/vol)) were solubilized in degassed MilliQ water such that the theoretical peptide content was 2 mM, hence 0.5 mM azide concentration [88]. CuAAC was started by addition of $CuSO_4$•$5H_2O$ + NaAsc catalyst prepared in a ratio such that one Cu-Asc ion would facilitate one azide-alkyne reaction. The solution was stirred for 5 hours at room temperature and protected from light, at which point 0.5 g of EDTA disodium salt dehydrate was added to quench the reaction. The solution was then dialyzed with

0.1 M NaBr and water and lyophilized until dry. The grafting of the dendrimer onto hyaluronic acid was verified by ^{1}H NMR and quantified by amino acid analysis. We calculated a percent yield of 7.21 mol% and 8.85 mol% for the Hyal-RGDS and Hyal-DGSR respectively under the employed CuAAC reaction conditions.

3.3.7. Rheological characterization of prepared hydrogel compositions

Rheological measurements were performed with an Anton Paar Instruments MCR 302 rheometer equipped with a Peltier plate temperature control and a steel cone geometry, Ø = 25 mm, 1°. Samples at room temperature were spread with a spatula onto the Peltier plate pre-set at 15 °C. Additionally, low viscosity silicon oil was applied along the border of the cone after sample placement in order to avoid evaporation at the solution-atmosphere interface. The synthesized conjugates were dissolved in PBS at 13 % (wt/vol) Hyal-pN with addition of 2% (wt/vol) Hyal-pa, Hyal-RGDS, or Hyal-DGSR. Hyal-pN at 15% (wt/vol) in PBS was also measured (Table 2).

Table 2. List of materials tested with rheological measurement. All samples were dissolved in PBS (1x concentrated, pH 7.4).

Polymer Composition	**Hyal-pN + Hyal-RGDS**	**Hyal-pN + Hyal-DGSR**	**Hyal-pN + Hyal-pa**	**Hyal-pN**	**Hyal-pa + N_3-pN unreacted solution**
Total polymer weight (wt/vol)	15%	15%	15%	15%	15%
Hyal-pN (wt/vol)	13%	13%	13%	15%	0%
Decorated Hyal (wt/vol)	2%	2%	2%	0%	0%

Storage modulus (G') and loss modulus (G") were measured as a function of the temperature increase at 1 °C/min from 20 to 40 °C with 0.1% oscillatory strain at 1 Hz. The linear

viscoelastic range was evaluated at 20 °C and 35 °C by increasing the deformation from 0.01%-100% strain. Triplicate analysis was performed for each sample.

3.3.8. Subculture of bone marrow derived hMSCs

Fresh human bone marrow aspirates were obtained after full ethical approval (Zurich, Ref Nr. EK: KEK-ZH-NR: 2010-044/0) and informed patient consent. Bone marrow stromal cells were isolated from 3 donors (♂1970, ♂1952, ♀1994) by a standard density gradient procedure (Histopaque-1077) and selection by plastic adherence. The hMSCs were then cultured in polystyrene cell culture flasks at 37 °C, 5% CO_2, and 95% humidity in α-MEM, 10% FBS-Hyclone, 5 ng/mL bFGF-2, and 1% P/S. The cells were detached with Trypsin-EDTA at sub-confluence and seeded at 3000 cells/cm^2 into the required number of flasks. Thereafter, the medium was changed every 2-3 days. After the cells reached around 80% confluence, they were harvested and used for the experiment at passage 2-3. Each experiment was performed separately on each donor and the data was collated for statistics.

3.3.9. Preparation of the dendrimer decorated bicomponent, thermoreversible hyaluronan scaffolds seeding of hMSCs for cell culture experiments

Materials prepared in aseptic conditions were used without further sterilization. A Hyal-pN solution at 16.5% (wt/vol) in sterile PBS (1x concentrated, pH = 7.4) was prepared. Hyal-RGDS, Hyal-DGSR or Hyal-pa were solubilized in the Hyal-pN solution to make a theoretical dendrimer concentration of 0.04 mM/ml, 2% (wt/vol) polymer, approximately 19.1% (wt/vol) concentration of total material (Table 3).

Table 3. Selected Hyal-pN compositions used in this study. The final polymer concentration utilized was 15% (wt/vol) for all materials.

Hydrogel Name	Polymer Supplement	Description
RGDS	**Hyal-RGDS**, 2% (wt/vol), (0.16 mM) peptide	Integrin binding bicomponent hydrogel with the RGDS functionalized dendrimer
DGSR	**Hyal-DGSR**, 2% (wt/vol), (0.16 mM) peptide	Non-integrin binding bicomponent hydrogel with the DGSR scrambled control dendrimer
Hyal	**Hyal-pa**, 2% (wt/vol), No peptide	Non-integrin binding bicomponent hydrogel control without grafted dendrimers

On the day of seeding, the cells were trypsinized, counted with Trypan Blue, centrifuged and resuspended in DMEM, 10% FBS, and 1% P/S. The cells were added to cool (~4°C) polymer solutions such that the final concentrations were (1 x 10^6 cells/ml, 15% (wt/vol)) polymer, and 2 mM RGDS or DGSR peptide content or equivalent Hyal-pa) and very carefully resuspended to minimize shearing of the cells. Once the cells were satisfactorily suspended in the polymer solution, hydrogel beads were prepared by transferring the polymer over a cell culture well with a cell culture insert containing warm (~37 °C) media. The droplets were allowed to fall into the media which immediately formed beads upon exposure to the elevated temperature.

All beads were cultured in either osteogenic differentiation (ODM) or osteogenic permissive (basal) media. The bead sizes were controlled to 60-80 µl per bead and were consistent in all of the material groups due to the similar viscosity of the polymer solutions at room temperature. The ODM was prepared with 10% FCS, 1% NEAA, 1% P/S, 50 µm/ml L-ascorbic acid, 7 mM β-glycerol phosphate, and 100 nM dexamethasone and the basal medium omitted β-glycerophosphate and dexamethasone. In between measurements, the samples were cultured at 37 °C, 5% CO_2, and 95% humidity. Media was changed every 2-3 days for 21 days by replacing

the volumes both inside the cell insert and the culture well with prewarmed media. Samples were harvested at 7 and 21 days for cell viability quantification, gene expression and histology.

3.3.10. Determination of the viability of hMSCs encapsulated in the bicomponent dendrimer hydrogel

Cell viability was assessed by LIVE/DEAD® assay according to the manufacturer's instructions. The hMSCs were harvested from the thermoreversible hydrogels by removing 1-2 beads from the culture wells with a prewarmed spatula and placing them in a 1.5 ml Eppendorf tube before allowing them to momentarily cool for 5 minutes at 4°C before adding 100-200 µl of 4 °C DMEM. The polymer solution containing cells was gently resuspended while being careful to avoid aspirating the undissolved portions of the hydrogel in order to minimize mechanical shearing of the cells while in the viscous solution. If the material stayed out of solution after reasonable agitation, then the vial was replaced at 4 °C for another 5 minutes to aid the dissolution process. A LIVE/DEAD® solution (5-8 µM Calcein AM and 3 µM ethidium bromide homodimer 1 in DMEM) was added to the samples in a 1:1 ratio. Samples were imaged with a combined optical transmission/fluorescent microscope (Axiovert 200 M, Zeiss) coupled with 10x objective lens within 5-20 minutes after staining. Mean cell viability was quantified and normalized to the day 7 Hyal group according to the respective donor and media type.

3.3.11. Determination of the cellular morphology of hMSCs encapsulated in the bicomponent dendrimer hydrogel

Samples were harvested at 7 days in duplicate by transferring beads with a prewarmed spatula into boats containing prewarmed tissue freezing medium. The samples were then placed into a plastic weighting tray containing isopentane and subsequently floated on liquid nitrogen then stored at -20 °C. Cryosectioning was carried out using a Microm HM 500 OM Cryostat Microtome (Microm, Carl Zeiss) into 10 µm sections then adhered to a glass slide pretreated with either a positively charged or polysine coating. Cryosections were stained for 10 minutes with a working solution of PKH26 red fluorescent dye which was prepared according to the supplier protocol. The solution was gently wicked off the slide then stained with the Prolong® gold water-based mounting medium containing DAPI nuclear counterstain. All samples were imaged with a Zeiss Axioplan 2 microscope (Carl Zeiss Microscopy) equipped with a fluorescent

lamp containing the following filter set: Zeiss filter set # 25: exciter filter TBP 400/495/570, beam splitter FT 410/505/584, barrier filter TBP 460/530/610.

3.3.12. Histological characterization of toluidine blue stained hMSCs encapsulated in the bicomponent hydrogels

Cryosectioned samples were fixed with 70% ethanol for a minimum of 10 minutes. The fixed samples were then washed in a bath of dH_2O twice before placing them in a 0.1% toluidine blue staining solution for 6 minutes and again washed 2-3 times to remove excess dye then blotted and allowed to air dry for a minimum of 30 minutes. Once the samples were completely dry, they were washed in xylene for a minimum of 2 minutes before removing and mounting with Eukitt® mounting medium. After cryosectioning, 3-4 drops of Prolong® Gold antifade reagent with DAPI was placed upon a fresh, untreated slide, coverslipped, then immediately frozen at -20 °C until imaging. All samples were imaged with a Zeiss Axioplan 2 microscope (Carl Zeiss Microscopy).

3.3.13. Quantification of gene expression of osteogenic and chondrogenic markers of hMSCs cultured in the bicomponent hydrogels via quantified real time polymerase chain reaction

Samples were harvested at 7 and 21 days in triplicate by transferring beads to a 2 ml Eppendorf tube and adding 1 ml of TRI reagent and 5 µl of polyacryl carrier (Molecular Research Center). Samples were vigorously shaken for 15 seconds to allow the solvent to penetrate the cells and scaffolds and stored at -80 °C until RNA isolation. RNA was isolated according to the manufacturer's instructions. The RNA pellets were solubilized in DEPC water and assessed for concentration and purity with measured absorbance at 230 nm, 260 nm (nucleic acids), and 280 nm (proteins), using a NanoDrop ND 100 spectrometer (Witec). Reverse transcription (RT) was performed using the SuperScript® VILO™ cDNA synthesis kit according to the supplier protocol. Samples were prepared with 250 ng of mRNA then gently mixed and kept on ice until they were transferred to a Mastercycler Gradient (Eppendorf AG) which carried out a protocol as follows. The samples were incubated at 25 °C for 10 minutes, then at 42 °C for 60 minutes. The reaction was terminated by holding at 85 °C for 5 minutes. The machine was programmed to keep the temperature at 4 °C until the samples were collected. The cDNA samples were diluted to 100 µl with DEPC water containing Trizma base buffer and stored at -20

°C until further use. Quantitative reverse transcriptase polymerase chain reaction (qRT-PCR) was performed using an Applied Biosystems Real Time PCR System with the StepOnePlus™ Real-Time PCR Software v2.1 (Applied Biosystems). A stock solution for each gene was prepared by mixing 5 µl of TaqMan® Universal PCR Master Mix 2x, 0.2 µl forward primer 45 µM, 0.2 µl reverse primer 45 µl, 0.2 µl TaqMan probe 12.5 µM, and 2.4 µl DEPC water per reaction (Table 4). Assays-on-Demand were carried out by adding 5 µl of Master Mix, 0.5 µl of Primer+Probe Mix 20x, and 2.5 µl DEPC treated water per sample. After addition of the stock gene recognition solutions and cDNA, the plate was covered with a low absorbance adhesive cover, centrifuged briefly for 30 seconds (<1000 rpm) to release air bubbles from the bottom of the wells then transferred to the PCR instrument. Gene expression was quantified beginning with incubating the plate at 95 °C, then cycling the instrument 50 times for 15 seconds at 95 °C and 1 minute at 60 °C.

Table 4. Polymerase chain reaction oglionucleotides used as primers and probes in the analysis of mRNA expression.

Target gene	Primers sequence	Function
hRUNx2	5'-AGCAAGGTTCAACGATCTGAGAT-3'	Forward
	5'-TTTGTGAAGACGGTTATGGTCAA-3'	Reverse
	5'-TGAAACTCTTGCCTCGTCCACTCCG-3'	Probe
hALP	Ref. Sequence: NM_000478.3	Assay on Demand
hCOL2	5'- GGCAATAGCAGGTTCACGTACA-3'	Forward
	5'- GATAACAGTCTTGCCCCACTTACC-3'	Reverse
	5'-CCTGAAGGATGGCTGCACGAAACATAC-3'	Probe
hSOX9	Ref. Sequence: NM_000346.3	Assay on Demand
hGAPDH	Ref. Sequence: 4326317E	Primer + probe assay

Data analysis was calculated by determining ΔCt values of the specific target genes whereby the Ct values of the target gene is subtracted from the Ct value of the hGAPDH endogenous control (*e.g.* Ct(hSOX9) – Ct (hGAPDH) = ΔCt). The fold change in gene expression was calculated as ΔΔCt by normalizing the ΔCt of the target genes to the ΔCt of the hMSCs in monolayer culture at day 0 [89].

3.3.14. Statistical analysis of results

For the viability and mRNA expression results, hMSCs from 3 independent human donors were used and each experimental group was performed in duplicate or triplicate. Statistics were performed with SPSS v.21 software (IBM Inc.); p values <0.05 were considered to be statistically significant. A test for normality of distribution and variance of data was carried out with a Kolmogorov-Smirnov test with Lillefors significance correction. Thus the Kruskal-Wallis non-parametric test was compared pairwise over all material groups, media types, and time points.

3.4. Assessing the potential for ectopic bone growth in a murine model: in vivo evaluation of BMP-2 and hMSC loaded Hyal-pN in a subcutaneous implant

3.4.1. Materials used in this study

Hyaluronic acid sodium salt from *Streptococcus equi*. was purchased from Contipro Biotech s.r.o. (Czech Republic). Amino-terminated poly(*N*-isopropylacrylamide) of number-average molecular weight of 40 kDa was purchased from Polymer Source, Inc.. All other reagents not strictly specified were purchased from Sigma–Aldrich; chemicals were of analytical grade at least, and were used without further purification. Sera Plus fetal calf serum, α-MEM, penicillin/streptomycin, and Trypsin/EDTA were purchased from Gibco. Recombinant BMP-2 and bFGF-2 were obtained from Medtronic, Inc. and Fitzgerald Industries respectively.

3.4.2. Synthesis of Hyal-pN driven by the activation of hyaluronic acid with 4-(4,6-dimethoxy-1,3,5-triazin-2-yl)-4-methylmorpholinium

The protocol for the grafting of pN to Hyal was followed according to the report by D'Este *et al.* [29] 1.08 g of hyaluronic acid sodium salt was dissolved in 45 ml of water. The amino terminated poly(*N*-isopropylacrylamide) was dissolved in 45 ml of water. Solutions were

combined, and pH corrected to 6.5 with the addition of NaOH and HCl solutions. To this solution, 4-(4,6-dimethoxy-1,3,5-triazin-2-yl)-4-methylmorpholinium (DMTMM) in powder was added stoichiometrically equivalent to HA. The reaction was allowed to proceed at room temperature for 5 days. Hyal-pN derivatives were purified via dialysis with 50 kDa MWCO tubes for 5 days changing the water twice per day, followed by lyophilization of the co-polymers in sterile falcon tubes fitted with 0.1 μm glass filters to obtain a sterilized white spongy material.

3.4.3. ^{1}H NMR and rheological characterization of the Hyal-pN synthesized with the DMTMM activator

The degree of pN derivation of the hyaluronic acid was assessed via ^{1}H NMR spectroscopy (Bruker Avance AV-500 NMR spectrometer) using deuterium oxide as solvent without residual HOD peak suppression and processed with Mestrenova software as already reported [28, 29].

Rheological measurements were performed with an Anton Paar Instruments MCR 302 rheometer equipped with a Peltier plate temperature control and a steel cone geometry, Ø = 25 mm, 1°. Samples of Hyal-pN, previously solubilized at 10% (wt/vol), were spread with a spatula onto a Peltier plate pre-set at 15 °C. Additionally, low viscosity silicon oil was applied along the border of the cone after sample placement in order to avoid evaporation at the solution-atmosphere interface. Storage modulus and loss modulus were measured as a function of the temperature increase at 1 °C/min from 20 to 40 °C with 0.1% oscillatory strain at 1 Hz. The linear viscoelastic range was evaluated at 20 °C and 35 °C by increasing the deformation from 0.01%-100% strain. Triplicate analysis was performed.

3.4.4. Sterile preparation of the Hyal-pN for in vivo animal surgeries

The yielded lyophilized polymer was treated as sterile after lyophilization and only handled under a laminar flow hood. The dried Hyal-pN was weighted in sterile Eppendorf tubes, then solubilized with PBS to 20% (wt/vol). For selected vials, BMP-2 (Medtronic Inc.) was added to the polymer solutions such that the concentration was 10 μg/ml. These materials were allowed to solubilize and stored at 4 ^{o}C for no more than a week prior to use.

3.4.5. Inclusion criteria and preoperative care of the animal models

For the *in vivo* study, immunodeficient female CD-1 nude mice less than 9 weeks of age were provided by Charles River Laboratories International, Inc. Certificates of health were also provided by the breeder. The animals were checked by an experienced animal care taker for any abnormalities. Afterwards, they were housed in groups in individually ventilated cages. All handling was performed under a laminar flow system. The animals were allowed to acclimate for a minimum of two weeks before the surgeries were carried out.

3.4.6. Subculture of bone marrow derived hMSCs for hydrogel encapsulation

Fresh human bone marrow aspirates were obtained after full ethical approval (Zurich, Ref Nr. EK: KEK-ZH-NR: 2010-044/0) and informed patient consent. Bone marrow stromal cells were isolated from one patient (♂, 22 y/o) by a standard density gradient procedure (Histopaque-1077) and selection by plastic adherence. The hMSCs were then cultured in polystyrene cell culture flasks at 37 °C, 5% CO_2, and 95% humidity in α-MEM, 8-10% Sera Plus FCS, 5 ng/mL bFGF-2, and 1% P/S. The cells were detached with Trypsin-EDTA at sub-confluence and seeded at 3000 cells/cm^2 into the required number of flasks. Thereafter, the medium was changed every 2-3 days. After the cells reached around 80% confluence, they were harvested and used for the experiment at passage 2-3. Each experiment was performed separately on each donor and the data was collated for statistics.

3.4.7. Preparation of hMSC and BMP-2 loaded Hyal-pN

On the surgery day, the hMSCs were trypsinized, collected, counted and centrifuged. The cell pellet was resuspended in DMEM at $20x10^6$ cells/ml and seeded in a Hyal-pN solution reconstituted at 20% (wt/vol) to a final concentration of $10x10^6$ cells/ml. Due to the viscous nature of the polymer solution, the cells were mixed with the polymers by gentle agitation in between 5-10 minute periods of exposure to 4 ^oC. Once the solution had an homogenous appearance, it was loaded into a 1 ml syringe by aspirating 500 µl of the solution without a needle fixed to the tip. On the first surgery day two materials were prepared containing BMP-2 + hMSCs and BMP-2 only. (Table 9) On the second surgery day, the materials were prepared without BMP-2. Loaded syringes were stored in sterile sealed metal transport boxes that were

labeled with cells or without cells. The boxes were then loaded into a Styrofoam container packed with ice then transported to the preclinical facility.

3.4.8. Protocol for anesthesia and analgesia

On the day of surgery, each mouse was placed in an induction chamber and exposed to isoflurane (ca. 3 vol%, 1000 ml/min O_2) while the surgical area was prepared for aseptic surgical intervention. The animal was placed on top of a heat mat to prevent hypothermia and positioned in ventral recumbancy. Anesthesia was maintained with an isoflurane flow (ca. 1.52 vol%, 400 ml/min O_2) for the duration of the surgery. Prior to the subcutaneous injection of the biomaterials, local analgesia was administered transdermally with buprenorphin (1:10, 0.1 mg/kg). Immediately after the surgery, 1 ml of Ringer's solution was subcutaneously delivered to prevent dehydration. Postoperatively, the animals were given paracetamol in their drinking water (Dafalgan Sirup für Kinder®: 7ml + 100 ml water) for 2 days.

3.4.9. Surgical intervention

Two separate subcutaneous injections of approximately 0.2 ml of the selected biomaterials location, (Table 5) were injected to both sides of the thorax, right/ 0.5 cm behind the animal's neck and 0.5 cm lateral, or caudally, left/ 1 cm from tail base and 0.5 cm lateral. Caudal injections were primarily chosen; however, if there was a failure in bead formation within the primary site then a secondary bead was delivered in the thorax region. Only 2 thoracic beads were delivered of the 14 total injections. The temperature of the skin was taken before and after injection and documented on the surgery protocol.

Table 5: Overview of the material groups used per surgery.

Surgery Group	Left Implant	Right Implant	# of mice
1	Hydrogel alone	Hydrogel + BMSC	7
2	Hydrogel + BMP-2	Hydrogel + BMP-2 + BMSC	4

3.4.10. Postoperative care and in vivo analysis

The animals were once again group housed in the IVC cages. Any examination was performed under the laminar flow system. The animals were given analgesics for the first two days as described above. Each mouse was postoperatively assessed and scored twice a day for the first three days, followed by once a day between the fourth and seventh day, and once per week thereafter according a postoperative animal welfare assessment protocol (Table 6). The weights were recorded at 3, 7, 14 and 28 days post operation. Postoperative abruption criteria in which animals would be excluded from the experiment for non-surgical related illness were also followed according to Table 7.

Table 6. Example of postoperative animal welfare assessment sheet used to assess the conditional of the mice individually. These guidelines were strictly followed in order to ensure that quality care to every animal was provided.

Day post-op	-1
Behavior/ Overall Impression	
- Quiet and inattentative	0
- Inactive or hyperactive	2
- Apathetic (not responding to outer stimuli)	4
Appearance	
- Normal	0
- Slightly dirty, sticky, rough coat	1
- Really dirty, sticky, hair loss, red secretion around the eyes	3
Feces/Urine	
- Normal	0
- Abnormal (consistency, quantity, color)	2
Breathing	
- Normal	0
- Rapid frequency	2
- Very hard	3
Wound healing	
- Normal	0
- Inflammation (swelling, redness, high temperature)	1
- Infection (secretion)	3
Weight (Preoperative weight: kg)	
- 0-10% from preoperative weight	1
- Loss 11-20%	3
- Loss >20%	4
Total (0-19)	
Comments/ Measures	
Signature, Date	

Table 7. Example list of postoperative abruption criteria.

Total Score	Designated actions
0 to 3	No to moderate imparment/ distress
4 to 9	Mild pain/ distress-> inform veterinarian, shorten observation interval, administer analgesics
> or equal to 10	Strong pain: criteria for euthanasia
Animal facility: When score > 0, examine animal	
Postop on day 7:When score 1-3 return to facility	
On day 3, if an animal scores 6-19: criteria for euthanasia	

3.4.11. Euthanasia, post mortem evaluation, and sample excision

At 4 weeks post operation, the animals were euthanized and a macroscopic examination of the external body surface including all orifices and surgery sites was carried out. Following x-ray radiography, the skin area where the scaffold was injected was dissected from the mouse, including the injected material and surrounding skin.

3.4.12. Evaluation by X-ray radiography

After the post mortem evaluations, all animals were subjected to x-ray radiographies using a Philips Healthcare DigitalDiagnost (Philips Medical Systems).

3.4.13. Evaluation of tissue mineralization via μCT scan

The ectopic mineralization of tissue was quantified by a μCT scanner (Scanco Inc.). Microtomograph settings were fixed as follows: 177 μA, 45 kV, resolution = 12 microns; sigma = 0.8 - 1.0, threshold min = 200, and threshold max = 1000.

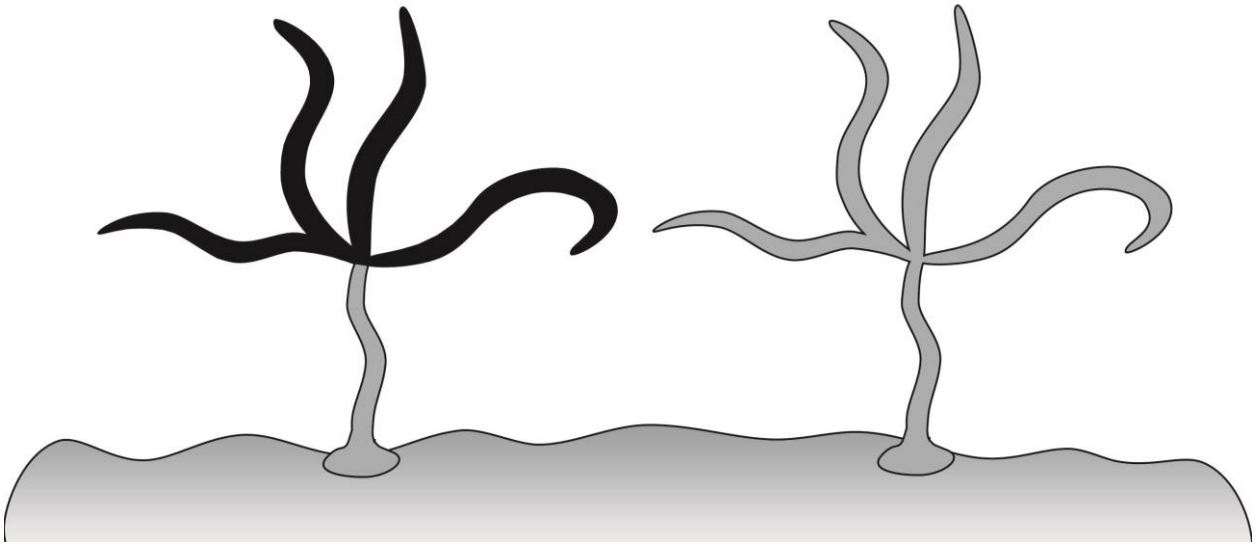

Chapter 4: Results

4.1 Results for the comparative synthesis of Hyal-pN using $CuBr(PPh_3)_3$ and CuAsc catalyst systems

The poly(*N*-isopropylacrylamide) derivatives of hyaluronan were prepared using a "coupling onto" approach (Fig. 6).

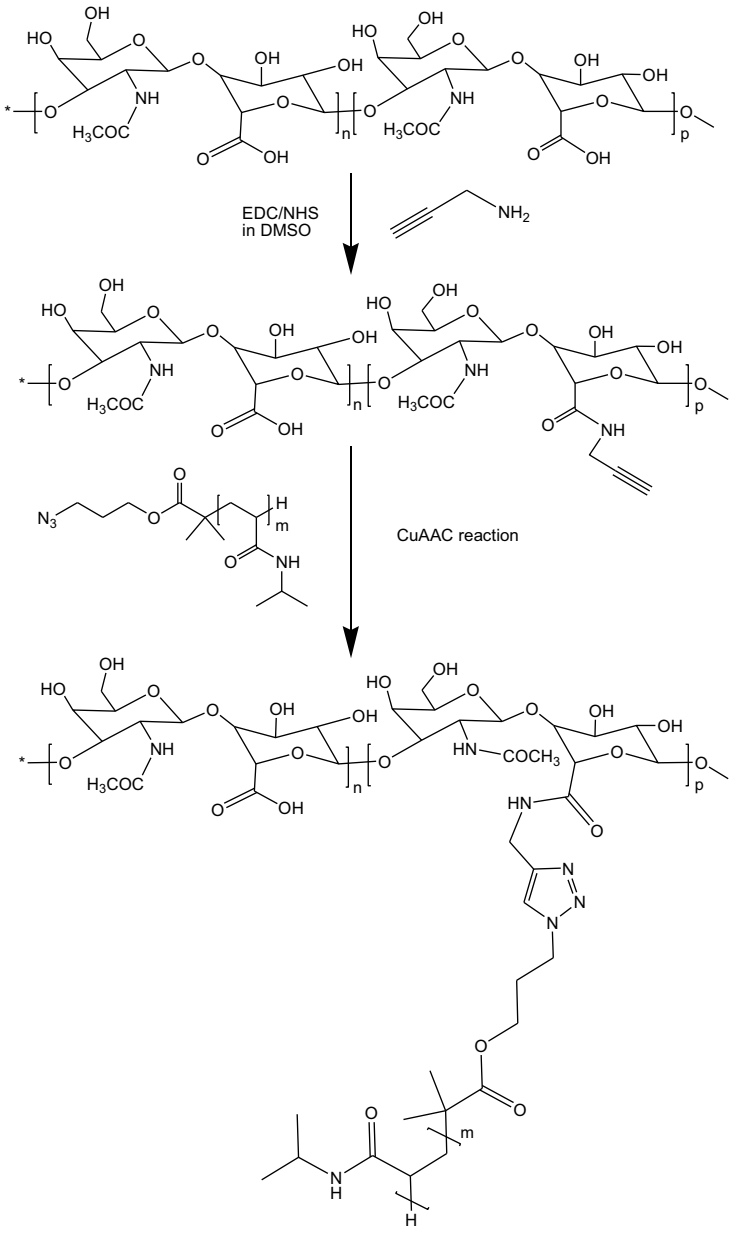

Fig. 6. Schematic of the CuAAC "coupling onto" preparation method for thermoresponsive derivatives of hyaluronic acid.

Propargylamide modified hyaluronan was first synthesized by an EDC/NHS amidation reaction and characterized. The CuAAC reaction was then carried out using RAFT polymerized N_3-pN to assess the efficiency of the catalysts and solvent conditions of the CuAAC reaction, and subsequent effects on the viscoelastic properties.

4.1.1. Propargylamide hyaluronan derivative

The grafting of the propargylamine on the hyaluronan was first qualitatively assessed by comparison to NaHA by ATR-FTIR (Fig. 7).

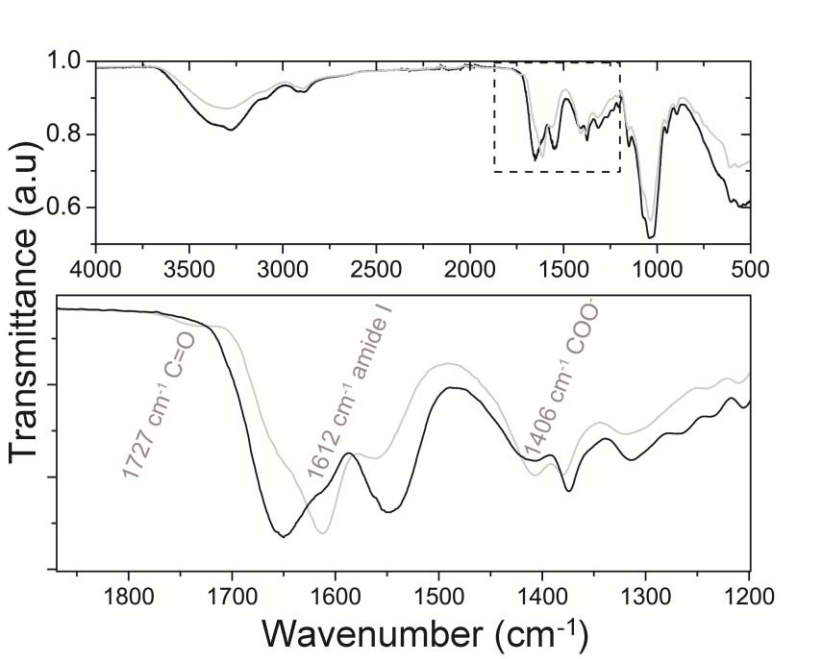

Fig. 7. ATR mid-IR spectra of NaHA (grey line) and Hyal-pa (black line) and close up for the 1875 to 1200 cm^{-1} regions.

The NaHA vibrational bands at 1727 cm^{-1} (C=O vibration of COOH), 1612 cm^{-1} (amide I), 1559 cm^{-1} (amide II) and 1406 cm^{-1} (COO^- symmetric) were strongly attenuated in the Hyal-pa infra-red spectrum [29]. Additional signals in the Hyal-pa IR spectra at 3280 cm^{-1} and 1650 cm^{-1} were observed suggesting the success of the amidation reaction. However an additional peak in the 2100-2200 cm^{-1} range, attributable to the vibrational band indicative of alkyne stretching, went undetected possibly due to a relatively low grafting. The ^1H NMR spectra (Fig. 8) did not allow confirmation of grafting of propargylamine onto hyaluronan due to signal overlap.

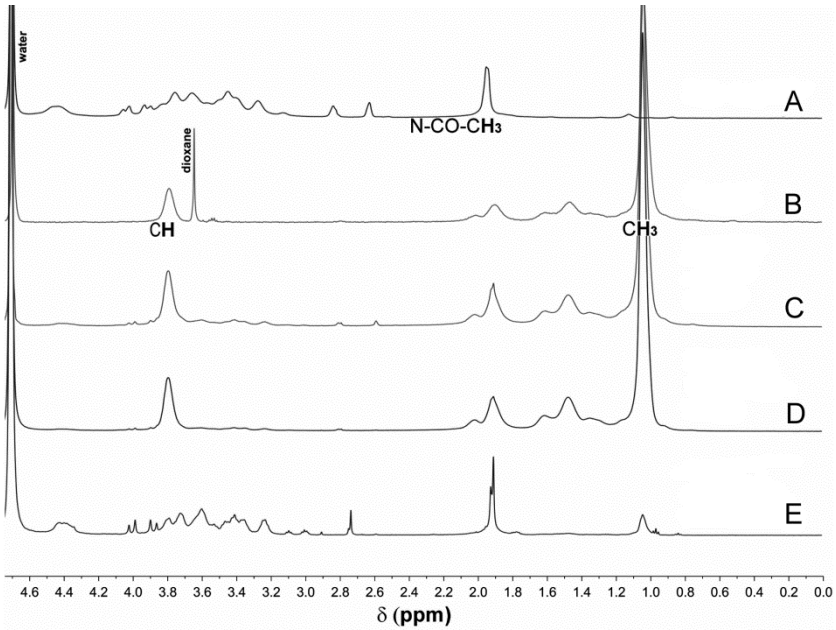

Fig. 8. ^{1}H NMR spectrum of (A) Hyal-pa, (B) N_3-pN, (C) Hyal-pa and N_3-pN reacted using CuAsc, (D) $CuBr(PPh_3)_3$ in water, and (E) $CuBr(PPh_3)_3$ in DMSO:water.

For this reason, the coupling was indirectly assessed by evaluating the reaction of NaN_3 to Hyal-pa using the CuAAC reaction with an aqueous solution of CuAsc. The appearance of a new signal at 7.8 ppm in the ^{1}H NMR spectrum of the reacted Hyal-pa compared to the initial spectrum was attributed to the single proton of the triazole ring formed during the reaction of the azide with the alkyne group on Hyal-pa (Fig. 9).

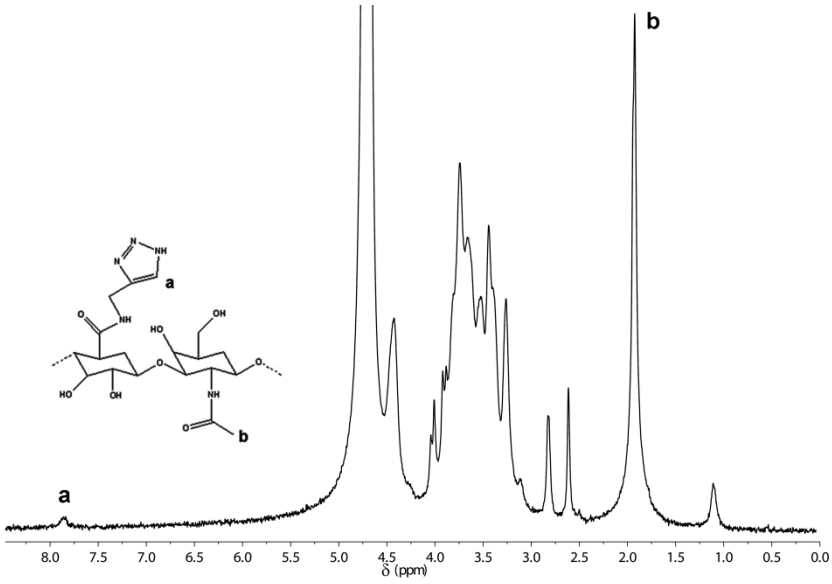

Fig. 9. ^{1}H NMR spectrum of Hyal-pa reacted with NaN_3 using CuAsc in water.

The amidation reaction efficiency was therefore calculated indirectly by the number of alkyne groups successfully reacted with NaN_3 to give a functional DG in mol% (Table 8).

Table 8. DG in mol% and recovered yield values of Hyal-pa and NaN_3 from the CuAAC reaction.

Catalyst	Solvent	DG (mol%)	Yield (wt %)
CuAsc	Water	5.3	82

4.1.2. Propargylamide hyaluronan derivative CuAAC reactions with N_3-pN

Having quantified the amount of reactive alkyne groups functionalized on the Hyal-pa polymer backbone using a model molecule (NaN_3), the thermoresponsive polymer N_3-pN was

grafted onto Hyal-pa with two different copper catalysts and solvent conditions. The products were characterized by ^{1}H NMR (Fig. 8) and quantified for DG in mol% (Table 9).

Table 9. DG mol%, recovered yield and copper content values of Hyal-pa reacted to N_3-pN under the aforementioned CuAAC conditions.

Catalyst	Solvent	Theoretical alkyne conversion (mol%)	Experimental alkyne conversion (mol%)[1]	Yield (wt %)	Cu (% total wt)[2]
CuAsc	Water	4	4.1	75	0.31
$CuBr(PPh_3)_3$	Water	4	4.6	98	0.36
$CuBr(PPh_3)_3$	3:2DMSO / Water	4	0.1	18	-

[1] calculated from ^{1}H NMR spectra, [2] measured by ICP-SFMS.

The yielded DG for the CuAsc and $CuBr(PPh_3)_3$ reactions in water was 4.1 mol% and 4.6 mol% respectively. It was found that the CuAAC reaction of Hyal-pa with N_3-pN using $CuBr(PPh_3)_3$ in DMSO:water led to a low DG of 0.1 mol% and low recovered weight of 18 % of the weight of initial reactant materials.

4.1.3. Rheological characterization of the CuAAC reacted hyaluronan derivatives

Rheological characterization of the Hyal-pN viscoelastic properties was carried out on 15 % (wt/vol) solutions of the synthesized polymers and Hyal-pa dissolved in PBS (pH 7.4). Temperature ramping experiments were conducted to exhibit the temperature dependent viscoelastic response and lower critical solution temperature (LCST) induction of sol-gel transitions of the Hyal-pN solutions (Fig. 10).

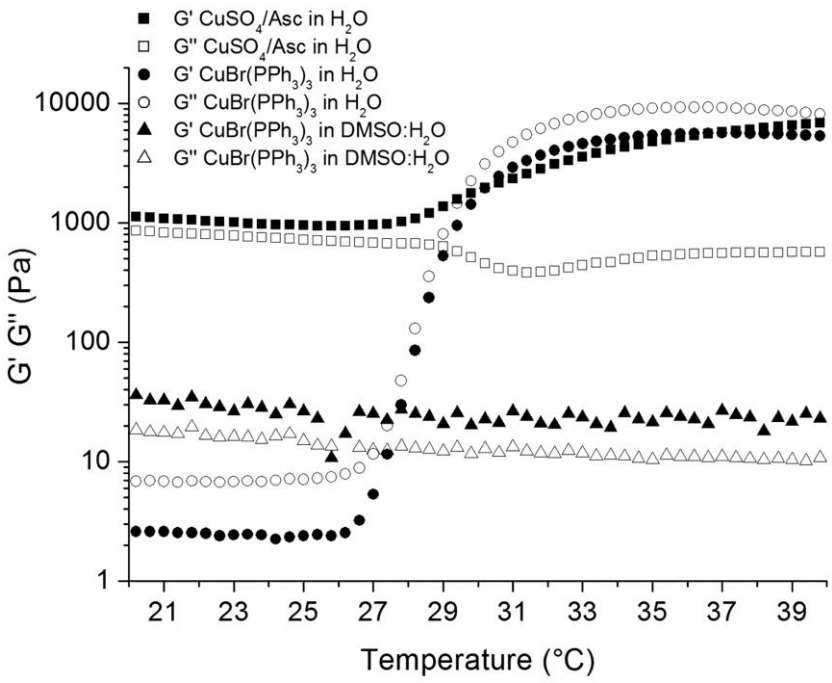

Fig. 10. Temperature ramping experiments of Hyal-pN synthesized with CuAsc in water (square), $CuBr(PPh_3)_3$ in water (circle), and $CuBr(PPh_3)_3$ in DMSO:water (triangle).

The Hyal-pa solution rheological profile did not exhibit a LCST and the G' and G" were respectively equal at 4.5 and 44.2 Pa at 20 ºC supporting a non-crosslinked state of the polymer in solution (data not shown). The rheological behavior of a physical mixture of Hyal-pa at 13 % (wt/vol) and N_3-pN at 2 % (wt/vol) as described in chapter 4 section 3, showed a clear LCST at 28.7 ºC, but no G', G" crossover indicative of gelation.

For the Hyal-pN reactions performed in water, a temperature dependent increase in storage modulus (G') was observed. This was not the case for the product reacted in DMSO:water as no LCST was observed at all. The LCST values measured for the CuAsc and $CuBr(PPh_3)_3$ catalyzed Hyal-pN reaction were 28.5 and 27.7 ºC respectively. Interestingly, the $CuBr(PPh_3)_3$ catalyzed Hyal-pN solution presented a threefold increase in moduli (G' and G") compared to a one fold increase of G' and near a constant G" for the CuAsc catalyzed Hyal-pN solution (Table 10).

Table 10. List of lower critical solution temperatures (LCST), elastic modulus (G') and viscous modulus (G") at 20 °C and 37 °C extrapolated from the rheological analysis of Hyal-pa reacted to N_3-pN under the aforementioned CuAAC conditions.

CuAAC conditions	LCST (°C)	G' (Pa) at 20 °C	G" (Pa) at 20 °C	G' (Pa) at 37 °C	G" (Pa) at 37 °C
CuAsc + Water	28.5	1130.0	855.0	5750.0	560.0
$CuBr(PPh_3)_3$ + Water	27.7	10.3	17.0	4810.0	5890.0
$CuBr(PPh_3)_3$ + 3:2 DMSO / Water	N/A	36.1	18.4	26.8	11.0

4.1.4. Copper residual in hyaluronan derivatives

Copper content in the Hyal-pN produced using the two catalyst systems in water was measured (Table 9). For the CuAsc, around 50% of the copper added (636 ppm) was removed down to a concentration of 310 ppm or 0.31 wt %. While for the $CuBr(PPh_3)_3$ the initial lower copper content used of 245 ppm still remained after dialysis 360 ppm or 0.36 wt %.

4.2. In vitro evaluation of BMP-2 and TGF-β1 loaded HGs

4.2.1. ^{1}H NMR Characterization

^{1}H NMR spectra confirmed the grafting of all the batches of N_3-pN to the Hyal-pN (Table 11). The DG ratios were calculated in mol% by attributing the ratio of the signal at δ = 1.14 ppm, corresponding to 6 protons of the N_3-pN isopropyl group to the shift at δ = 3.0-3.8 ppm, corresponding to 9 protons of the hyaluronic acid disaccharide ring. The calculated DGs of pN were all reported above the theoretical value. The higher than expected values can be attributed to the degradation of the hyaluronic acid during CuAAC which would subsequently change the observed ratios of N_3-pN to Hyal-pa. Direct characterization of the molecular size of the brush copolymers has yet to be made possible due to the difficulty of measuring Hyal-pN with HPLC methods; however, individually the Hyal-pa and N_3-pN were characterized with these methods.

We calculated the theoretical brush copolymer sizes based upon the Mw of the pN batches and the propargylamine substituted hyaluronic acid. Furthermore, the increasing ratio of poly(*N*-isopropylacrylamide) to hyaluronic acid signal is consistent with the grafting of higher molecular weight polymer chains to the polysaccharide backbone. A theoretical size of the brush copolymers was also calculated based upon the molecular weight distributions of the Hyal-pa and N_3-pN, assuming no degradation of the polysaccharide chain.

Table 11. Reported M_w of N_3-pN and DG and extrapolated size of the Hyal-pN determined by multi-detector HPLC and ^{1}H NMR methodologies.

Sample	Size of pN (kDa)[a]	% DG (theory)	% DG (actual)[b]	Calculated polymer brush size (kDa)
HpN9	9.2	4%	4.4%	561.0
HpN16	16.3	4%	4.4%	767.9
HpN21	21.2	4%	4.3%	896.6
HpN28	27.5	4%	4.2%	1057.8

[a] measured by multidetector HPLC; [b] calculated from ^{1}H NMR spectrum

The dendrimer grafted hyaluronic acid was synthesized based upon the same CuAAC reaction method. However, the theoretical molar ratio of grafted dendrimer to the Hyal-pa backbone was on the order of 10^{-5} moles which was too low for accurate quantification by ^{1}H NMR. Therefore, the experimental molar ratio was quantified by amino acid analysis.

4.2.2 Amino acid analysis of the dendrimer grafted hyaluronan

Amino acid analysis of the dendrimer-peptide conjugates grafted to Hyal-pa was employed in order to quantify the amount of peptides, and subsequently dendrimers, onto the polysaccharide backbone (Table 12). The reaction efficiency was 34% for the Hyal-YPV and 39% for the Hyal-LPL based upon the initial vs. the final calculated molar amounts of dendrimers to disaccharides.

Table 12. Reported quantities of peptides and dendrimers per hyaluronic acid disaccharides, extrapolated concentrations within the depots, and efficiency of the CuAAC reaction.

Sample	Ratio epitope to disaccharide (mmol/mg)[a]	Ratio dendrimer to disaccharide (mmol/mg)	Calculated epitope per hydrogel depot (mM)	Calculated yield of product (%)
Hyal-YPV	$6.5x10^{-6} \pm 1.1x10^{-6}$	$1.6x10^{-6} \pm 2.8x10^{-7}$	$3.4x10^{-2} \pm 4.1x10^{-3}$	33.7 ± 5.7 %
Hyal-LPL	$7.8x10^{-6} \pm 3.0x10^{-7}$	$1.9x10^{-6} \pm 7.6x10^{-8}$	$4.1x10^{-2} \pm 7.2x10^{-3}$	38.9 ± 1.5 %

[a] measured by a. a. analysis.

4.2.3 Rheological characterization of the bicomponent hydrogel biomaterials

All Hyal-pN batches showed the temperature sensitive response that is consistent with this polymer system [16, 22]. The concentrations of dendrimers employed in this study did not affect the mechanical properties of the hydrogels which agreed with our previous report (Fig. 11A).

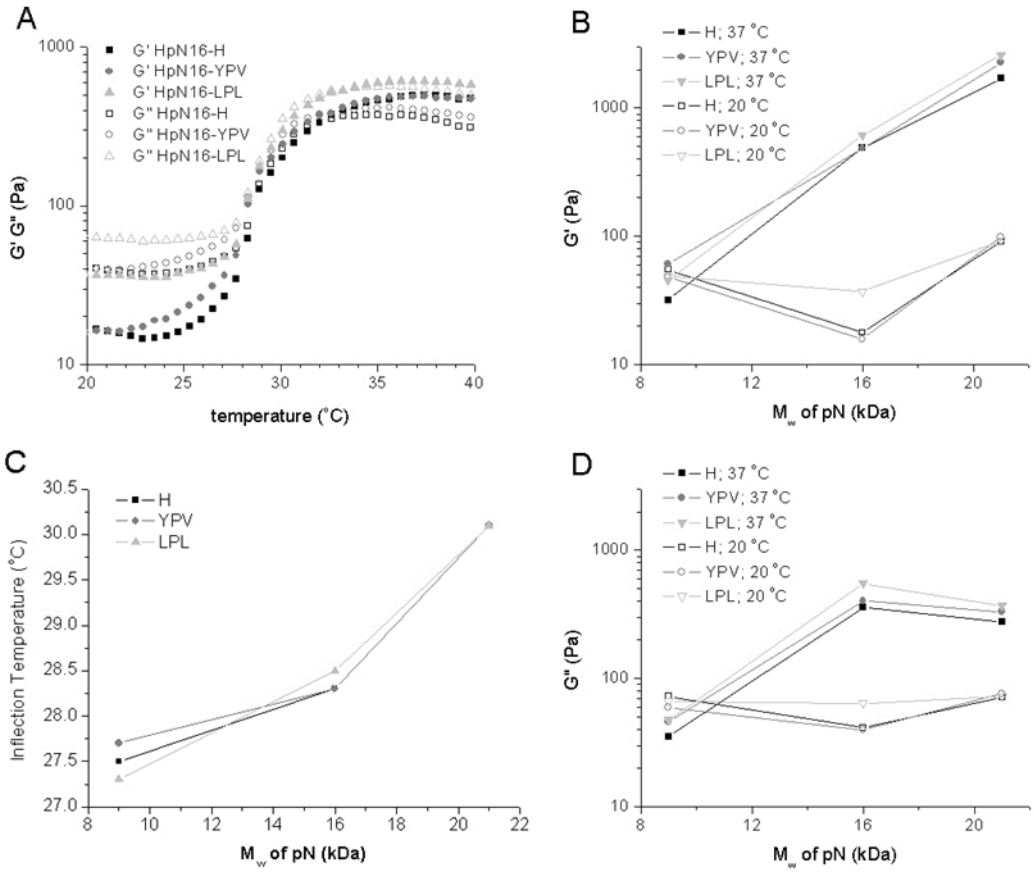

Fig. 11. Rheological characterization of the bicomponent hydrogels (13 % (wt/vol) in PBS) with (A) the influence of the dendrimer on G' and G" within HpN16, (B) the influence of pN size on the inflection temperature of the HGs, (C) the influence of pN size on G' at 37 °C and 20 ºC, (D) and G" at the same temperatures. The presence of dendrimers did not influence the mechanical properties in any hydrogels tested.

The inflection temperatures, the points at which the materials experienced an increase in viscoelasticity, increased along with the size of the pN chains and fell within the range of 27.3 to 30.1 °C (Fig. 11B). The influence of pN size over the viscoelastic moduli at 20 ºC and 37 ºC in Fig. 11B and 11D highlights the change in rheological properties for the different Hyal-pN batches. For HpN9, there was no temperature driven increase change in either G' or G" from 20 ºC to 37 ºC. Furthermore, the viscous modulus remained predominant over the storage modulus during the entire temperature sweep. In contrast, HpN16 experienced an increase in both viscous

and elastic character. The higher elastic modulus (G') value of 400 Pa compared to the viscous modulus (G'') value of 200 Pa at 37 ºC indicates the gel state of the aqueous formulation. Furthermore, HpN21 was also a stable hydrogel at 37 ºC exhibiting similar behavior to HpN16, albeit with an even stronger elastic character, with the G' at 2 kPa and the G" at 300 Pa.

4.2.4. In vitro release of BMP-2 and TGF-β1 loaded in binding epitope dendrimer containing hydrogels

During the release studies, the stability of the depots was observed. The appearance of cloudy release buffer was a clear sign that the depot was disassociating. The HpN9 hydrogel was not stable and disassociated after the first day of media changes. This data was consistent with results from the rheological experiments and the HpN9 was therefore not combined with the dendrimers for the release study. Although HpN16 also slightly disassociated during the first few media changes, most of the depot remained stable and did not further exhibit noticeable changes in volume over the release study period. HpN21 was stable, did not experience any noticeable loss of volume, nor was responsible for the presence of cloudy release media.

We first assessed the *in vitro* release of the growth factors from the three synthesized Hyal-pN batches, at 13% (wt/vol) in PBS, and supplemented with Hyal-pa, at 2% (wt/vol) in PBS (Fig. 12).

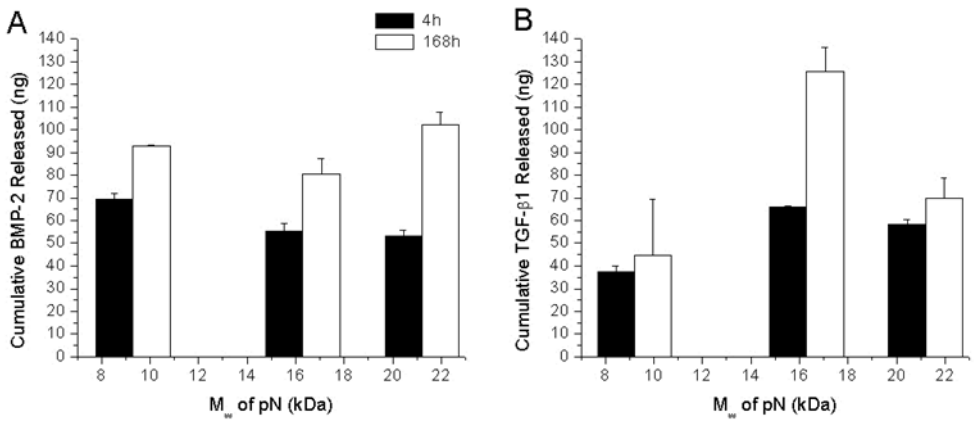

Fig. 12. Comparison of the cumulative release of (A) BMP-2 and (B) TGF-β1 at 4h (black) and 168h (white) from Hyal-pN hydrogels with three M_w of pN (kDa) and constant DG. The hydrogels were composed of 13% (wt/vol) Hyal-pN and 2% (wt/vol) Hyal-pa in PBS.

For HpN9, most of the measured protein was released within 4 h for both BMP-2 and TGF-β1 as values at 168 h were not significantly different. This is consistent with a soluble formulation rapidly releasing an entrapped molecule. The absolute amounts of growth factors released were always significantly lower than the loaded amount in all Hyal-pN, including HpN9. This pattern indicates that a significant amount of loaded BMP-2 and TGF-β1 interacted with the Hyal-pN macromolecules *in vitro*. Interestingly, while the amounts of BMP-2 not measured in the release media were consistent for the three Hyal-pN formulations, more variation are observed for TGF-β1, *e.g.* HpN16 at 168h. For the BMP-2 releasing HpN16 and HpN21 depots, the concentrations of BMP-2 released at 168 h were not significantly different to HpN9. A slightly less amount of BMP-2 was found in the release media at 4 h for HpN16 and HpN21 compared to HpN9. For the TGF-β1 releasing Hyal-pN, no significant trend in release was found with the pN M_w.

To assess the effect of the peptide binding dendrimers on the cytokine release, HpN16 and HpN21 were spiked with Hyal-pa, Hyal-YPV, or Hyal-LPL at 2 % (wt/vol) which corresponded to 0.034 mM and 0.041 mM concentrations of the BMP-2 and TGF-β1 binding epitopes per hydrogel depot respectively (Figs. 13 and 14).

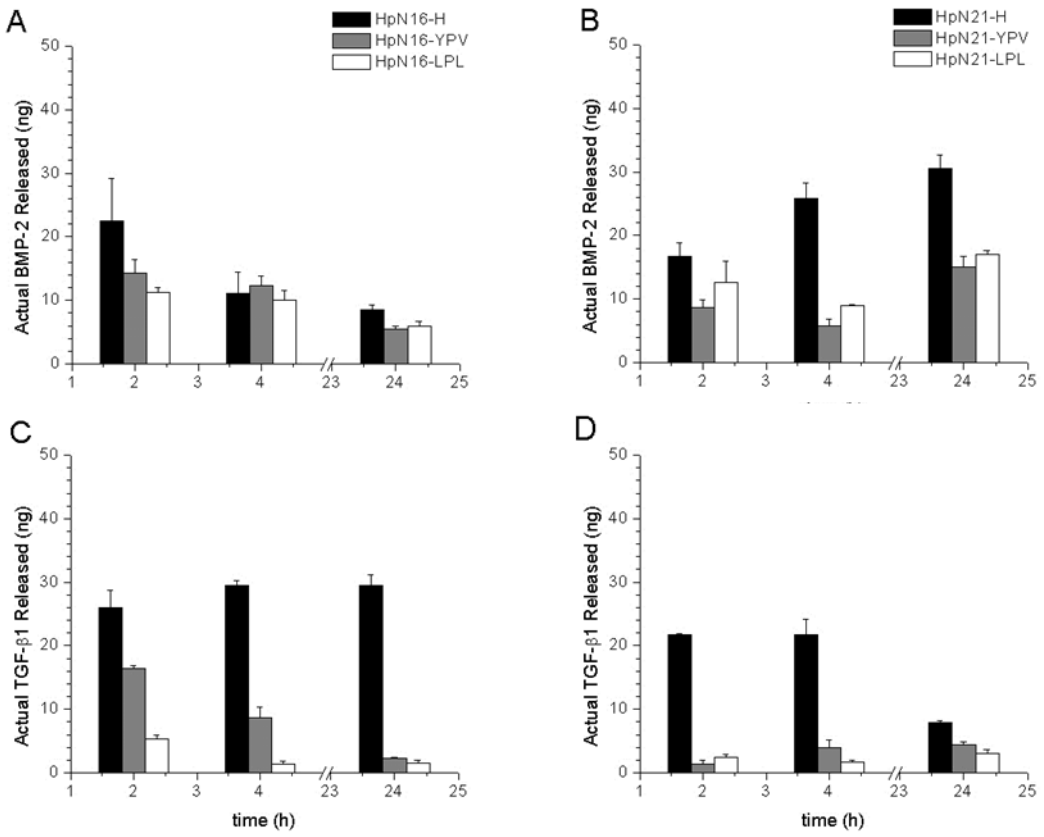

Fig. 13. Profiles of actual protein released at 2, 4 and 24 hours of (A and B) BMP-2 and (C and D) TGF-β1 from (A and C) HpN16 and (B and D) HpN21. Protein release data from the unmodified hydrogels are represented in black, whereas the BMP-2 and TGF-β1 binding hydrogels are represented in gray and white respectively.

The profiles of the first 24 hours of actual protein released were examined (Fig. 13). The difference in release profiles between the unmodified depots of HpN16 and HpN21 and the dendrimer modified hydrogels was statistically significant according to the Tukey HSD post hoc analysis ($p<0.0005$). A decrease of BMP-2 and TGF-β1 released in the media was observed when Hyal-YPV and Hyal-LPL were added in the Hyal-pN hydrogel formulation compared to Hyal-pa (no binding epitopes). Statistical analysis verified that the amount of drug released was significantly dependent on the presence of dendrimers and time, regardless of the hydrogel employed, $F(6,273) = 9.866$, $p<0.0005$, partial $\eta^2 = 0.178$. The peptide binding sequences employed in this study, however, were nonspecific to either protein binding affinity (i.e. TGF-β1

and BMP-2 have similar binding affinities with both LPLGNSH and YPVHST dendrimers). Furthermore, the release profiles between the dendrimer modified hydrogels statistically similar according to the Tukey's HSD post hoc analysis ($p = 0.892$).

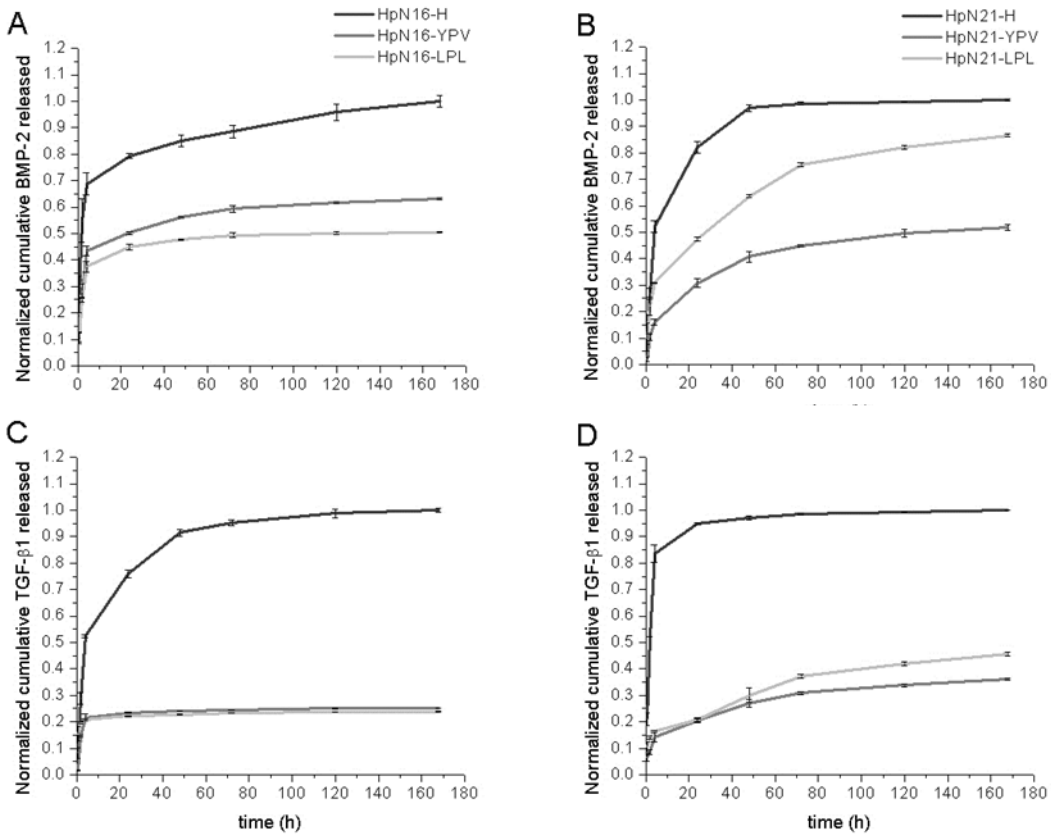

Fig. 14. Normalized cumulative protein release from loaded hydrogels showing the relative amounts of BMP-2 released from (A) HpN16 and (B) HpN21, and TGF-β1 released from (C) HpN16 and (D) HpN21. The results were normalized to the absolute amount of drug released by the unmodified hydrogels. Protein release data from normal hydrogels are represented as a dark gray line, whereas the BMP-2 and TGF-β1 binding hydrogels are represented as gray and light gray lines respectively.

The long-term cumulative release of growth factors from the different Hyal-pN formulations showed similar profiles irrespective of the pN and growth factor type (Fig. 14). In the absence of

binding epitopes presented via the dendrimers, an initial burst release is followed by a sustained release which reached a plateau after 100 h. The burst release was significantly decreased in the presence of dendrimers, irrespective of the binding epitope. For example, a relatively high amount of 126 ng of BMP-2 was released from the HpN16 hydrogel depot in absence of dendrimers was measured at1 week whereas only 31 and 29 ng were released within the same timeframe for the HpN16-YPV and HpN16-LPL dendrimer containing gels respectively. The presence of the LPL binding epitope bearing dendrimer resulted in a slightly higher BMP-2 retention in HpN16 compared to the YPV dendrimer, while the inverse was observed in the HpN21. Relatively low amounts of protein were detected (or released) for HpN21 as well as the dendrimer containing hydrogel counterparts (HpN21-YPV and HpN21-LPL). The LPL dendrimer displayed a higher BMP-2 binding affinity for HpN16 and was only marginally less effective at binding the protein in the case of HpN21.

4.3. Results obtained from the in vitro evaluation of hMSCs encapsulated in RGDS decorated Hyal-pN

4.3.1. Thermoresponsive hyaluronan derivative and dendrimer functionalized hyaluronan synthesized by "click" chemistry

Hyaluronic acid with a molecular weight of 1506 kDa was chosen as the macromolecular backbone of the bicomponent hydrogel composed of the thermoresponsive hyaluronan derivative and the dendrimer functionalized hyaluronan (Fig. 15).

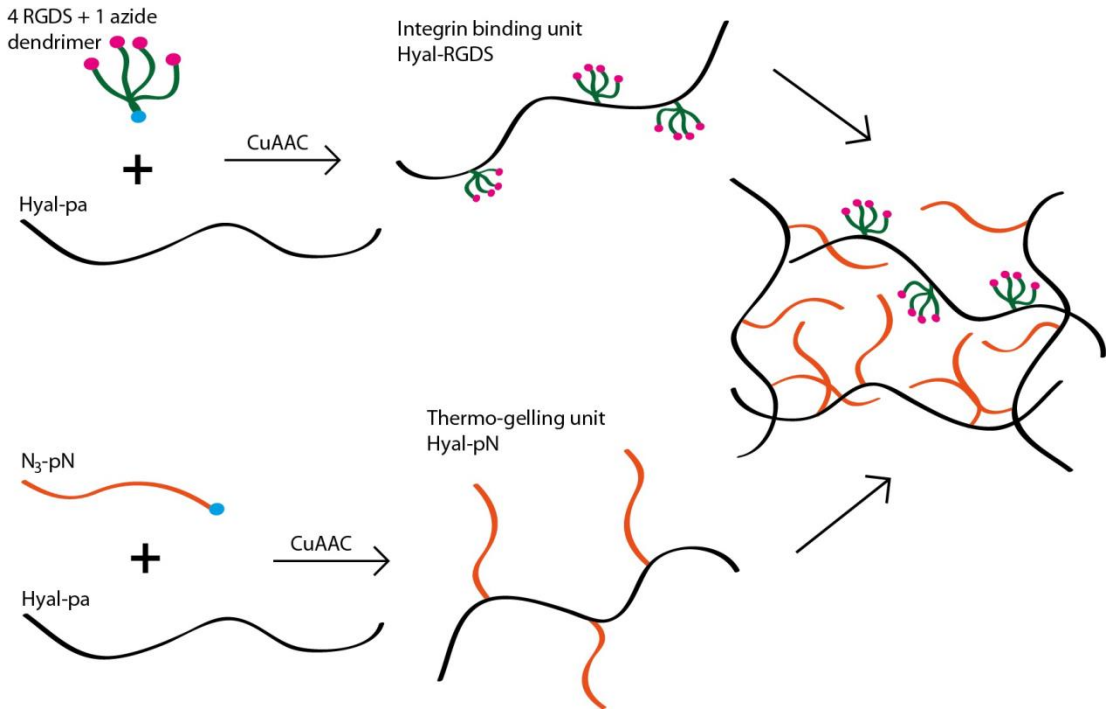

Fig. 15. Schematic layout of the bicomponent thermoreversible hydrogel platform which combines the RGDS dendrimer decorated hyaluronic acid with the thermoresponsive hyaluronic acid and was used as the cell carrier biomaterial in this study.

The DG was initially calculated from ^{1}H NMR by using methods previously reported (Fig. 16) [16, 29].

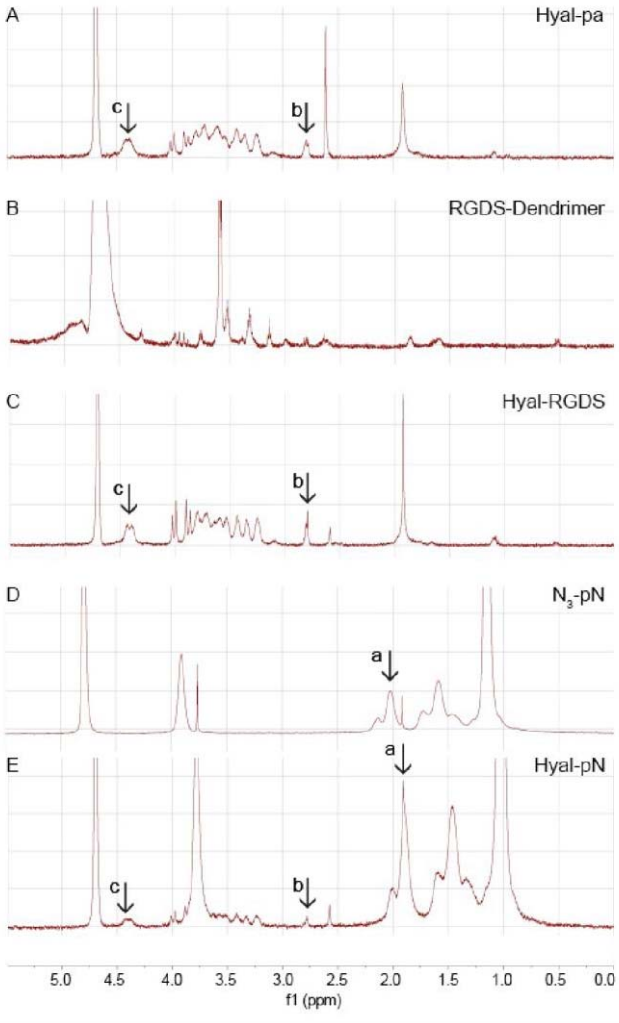

Fig. 16. ^{1}H NMR with spectra stacked from top to bottom exhibiting (A) Hyal-RGDS, (B) the RGDS dendrimer, (C) Hyal-pa, (D) N_3-pN, and (E) Hyal-pN. The peak at 1.91 ppm represents the sp^2 hybridized methyl group protons (a), the alkyne proton at 2.8 ppm (b), and the 3 and 4 position protons of the β–1,3 and β–1,4 glycosidic bonds of the modified hyaluronic acid backbone from 4.3 to 4.5 ppm (c).

The DG of the propargyl group on hyaluronan propargylamide was 18.6 mol%. Hyal-pa was further reacted with either azide-terminated poly(*N*-isopropylacrylamide) (N_3-pN) or the dendrimer via CuAAC. The experimental DG of pN on Hyal-pa was 9.9 mol% of the total initial carboxylic groups (the theoretical DG being 10 mol% of the total disaccharides or 53 mol% of the alkyne modified disaccharides) indicating a near complete coupling of the starting polymers.

A DG between 6 to 10 mol% of N_3-pN of the total disaccharides has been previously found optimal for the preparation of stable thermoreversible hydrogels [16]. The analysis of the dendrimer functionalized hyaluronan ^{1}H NMR spectra did not permit the quantification of the amount of grafted dendrimers due to the low theoretical grafting density (which was <5%). Thus, the amount of grafted dendrimers onto the hyaluronan backbone was indirectly measured by amino-acid quantification. An amount of 7.2 x 10^{-6} mmol Arg-Gly-Asp-Ser (RGDS) peptide and 8.11 x 10^{-6} mmol Arg-Ser-Gly-Asp (DGSR) peptide per mg of the hyaluronan conjugate was measured, leading to 1.80 x 10^{-6} mmol of the bioactive RGDS peptide dendrimer and 2.03 x 10^{-6} mmol of the DGSR dendrimer per mg of the hyaluronic acid derivative. The concentration of dendrimer in the reconstituted hydrogels was in the range of 0.04 mM, corresponding to a peptide concentration of approximately 0.16 mM. The use of a molecular modeling tool (Marvin 6.2.1, ChemAxon software package) permitted the 3D modeling of the RGDS dendrimer based on lowest energy conformations according to the DREIDING force field generator [90]. The four terminal peptide structures were found to be spaced ~ 0.5 nm from each other. To our best knowledge, this is the first report describing a controlled degree of spacing at the sub-nanometer scale for RGDS peptides.

4.3.2. Rheological characterization of the bicomponent hydrogel

The rheological properties of Hyal-pN and the mixture Hyal-pa with N_3-pN were characterized using temperature-ramping experiments (Table 13).

The mixture of Hyal-pa and N_3-pN showed a high increase of G' and G'' at 29 °C, but did not display a crossover of G' with G'', indicating that this composition continued to behave as a liquid above 29 °C (Fig. 17A). Hyal-pN presented a LCST and a crossover of G' with G'', indicating the formation of a hydrogel (Fig. 17). All compositions of the bicomponent hydrogels had shear-thinning character (Fig. 18).

Table 13. List of materials tested with rheological measurement. All samples were dissolved in PBS (1x concentrated, pH 7.4).

Polymer Composition	**Hyal-pN + Hyal-RGDS**	**Hyal-pN + Hyal-DGSR**	**Hyal-pN + Hyal-pa**	**Hyal-pN**	**Hyal-pa + N_3-pN unreacted solution**
Total polymer weight (wt/vol)	15%	15%	15%	15%	15%
Hyal-pN (wt/vol)	13%	13%	13%	15%	0%
Decorated Hyal (wt/vol)	2%	2%	2%	0%	0%

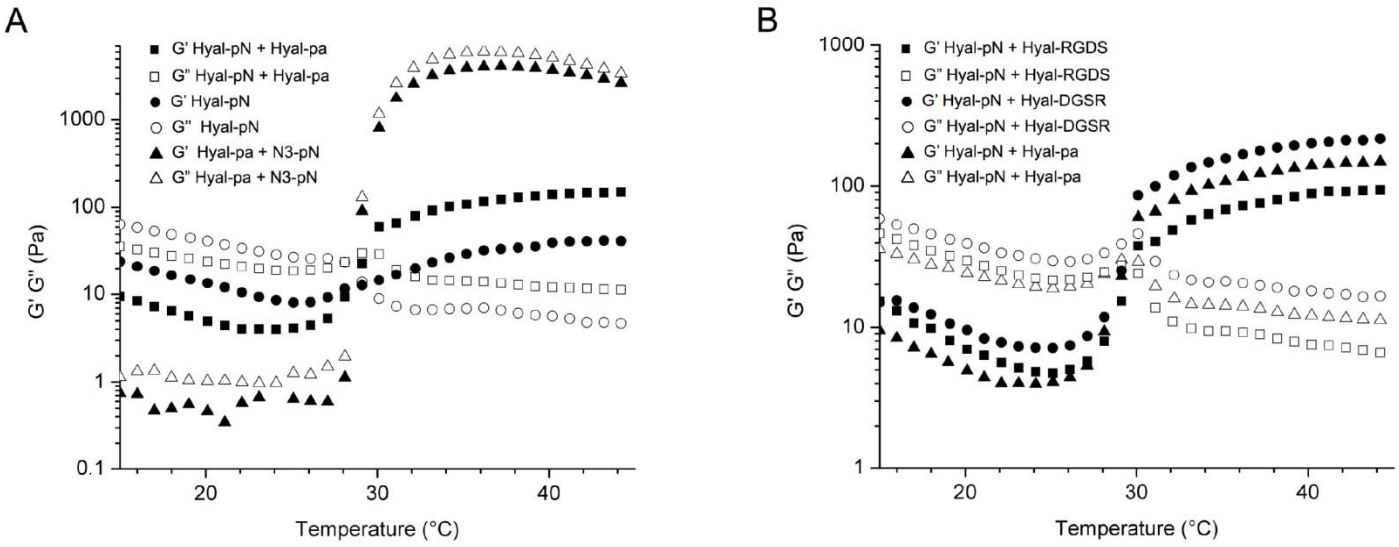

Fig. 17. Temperature ramping experiments illustrating the influence of the bicomponent hydrogel (A) and the dendrimer grafted bicomponent hydrogels (B) on the rheological character.

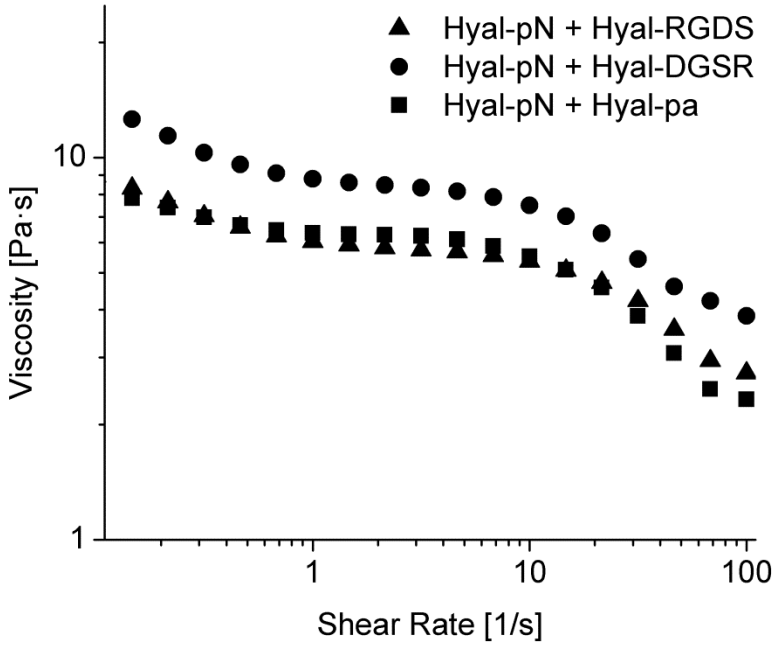

Fig. 18. Rotational shearing behavior of the bicomponent polymer compositions at 20°C.

The addition of Hyal-pa, Hyal-RDGS and Hyal-DGSR with Hyal-pN to constitute bicomponent polymer compositions were further characterized. Supplementing Hyal-pa, as an experimental control, (Fig. 17A) or the dendrimer conjugated hyaluronic acid (Fig. 17B) to the Hyal-pN did not impede hydrogel formation which showed a LSCT at 29.5 °C ± 0.7 °C. The G' and G" of the bicomponent hydrogel compositions at 37 °C were equal to 125 ± 41 Pa and 14 ± 5 Pa respectively. Incorporating the hyaluronic acid analogs increased the storage moduli by one order of magnitude whereas the LCST remained stable within a fraction of a degree. The viscosity of the bicomponent polymer solutions at 20°C was 16.3 ± 2.3 Pa*s (N=4).

4.3.3. Assessment of hMSC viability in the bicomponent hydrogels

In order to simplify the terminology, Hyal-pN supplemented with Hyal-pa, Hyal-RGDS, or Hyal-DGSR are henceforth referred to as the "Hyal group," "RGDS group," and "DGSR group" respectively (Table 14).

Table 14. Chart of selected Hyal-pN compositions used in this study. The final polymer concentration utilized was 15% (wt/vol) for all materials.

Hydrogel Name	Polymer Supplement	Description
RGDS	**Hyal-RGDS**, 2% (wt/vol), (0.16 mM) peptide	Integrin binding bicomponent hydrogel with the RGDS functionalized dendrimer
DGSR	**Hyal-DGSR**, 2% (wt/vol), (0.16 mM) peptide	Non-integrin binding bicomponent hydrogel with the DGSR scrambled control dendrimer
Hyal	**Hyal-pa**, 2% (wt/vol), No peptide	Non-integrin binding bicomponent hydrogel control without grafted dendrimers

A LIVE/DEAD® cell viability assay was carried out to determine hMSC viability in the hydrogels at 7 and 21 days of culture in ODM or basal media (Fig. 19).

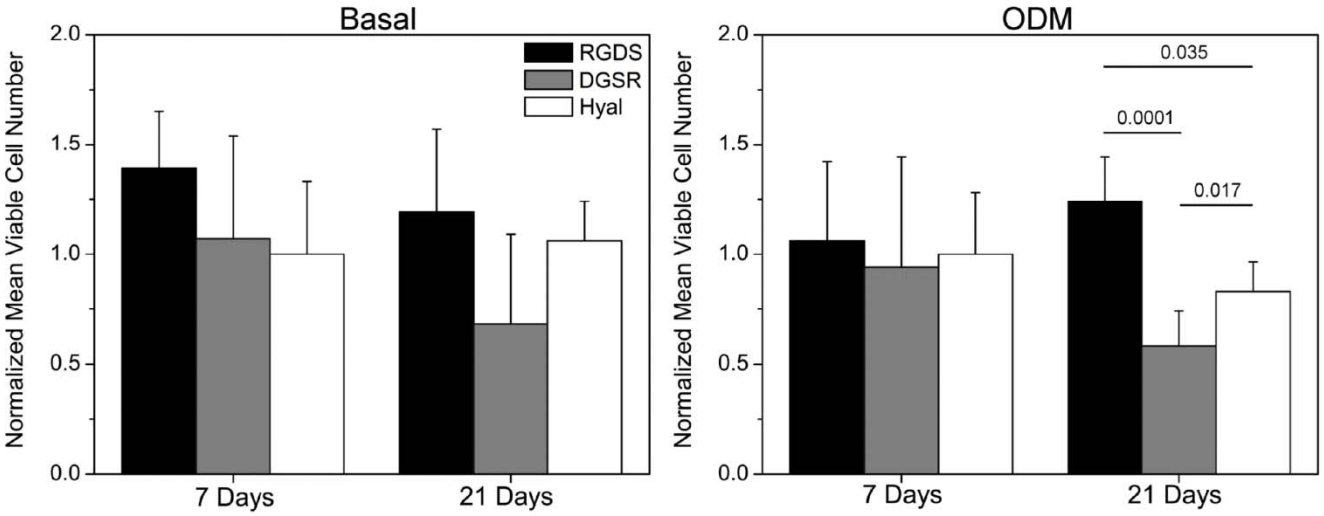

Fig. 19. Normalized mean viabilities of hMSCs encapsulated in RGDS, DGSR and Hyal hydrogels and cultured in osteogenic permissive (Basal) and differentiation (ODM) media over

21 days. Statistical significance was found in the day 21 ODM groups between RGDS and DGSR (p=0.0001), RGDS and Hyal (p=0.035), and DGSR and Hyal (p=0.017).

Table 15. Mean cell viabilities with standard deviations recorded at days 7 and 21 for hMSCs cultured in basal or differentiation medium in scaffolds combined with the one of the three type of hyaluronic acid synthesized in this study: RGDS, DGSR, or Hyal.

Day	Medium	RGDS	DGSR	Hyal
7	Basal	87% ±13%	67% ±19%	62% ±2%
7	ODM	67% ±16%	43% ±13%	74% ±23%
21	Basal	75%±23%	42%±6%	66%±6%
21	ODM	85%±12%	42%±17%	59%±12%

Cells collected from the hydrogel materials were suspended in media containing LIVE/DEAD® stain. The percentages of living cells were quantified from representative fluorescent images (data not shown). In order to minimize donor variation and measure the effects of the materials on viability, the results were normalized to the mean cell viabilities of the day 7 Hyal groups to the specific donor and type of medium. However, the actual mean cell viabilities were also reported (Table 15). In the tailored hyaluronan microenvironments, cell viability was maintained over the culture period in the Hyal and RGDS groups, whereas it declined with the culture time in the DGSR group (Fig. 19). Similar trends were also observed in osteogenic medium. Higher cell viability was observed at all time points in the RDGS group compared to the DGSR and Hyal groups in both media. Nonetheless, a statistically-significant difference was observed at day 21 in ODM (Kruskal-Wallis pairwise comparison: RGDS and DGSR (p=0.0001), RGDS and Hyal (p=0.035), and DGSR and Hyal (p=0.017)).

4.3.4 Assessment of hMSC morphology in the bicomponent hydrogels

A fluorescent membrane stain coupled with a DAPI counter-stain was placed on hydrogel cryosections to examine changes in hMSC morphology between the different materials and

culture media. Overall, the hMSCs maintained rounded morphologies, were approximately 10 μm in diameter, and remained homogenously dispersed throughout all the hydrogel compositions over the 21 day culture period, results which are exemplified in fluorescent micrographs taken after 7 days of culture (Fig. 20).

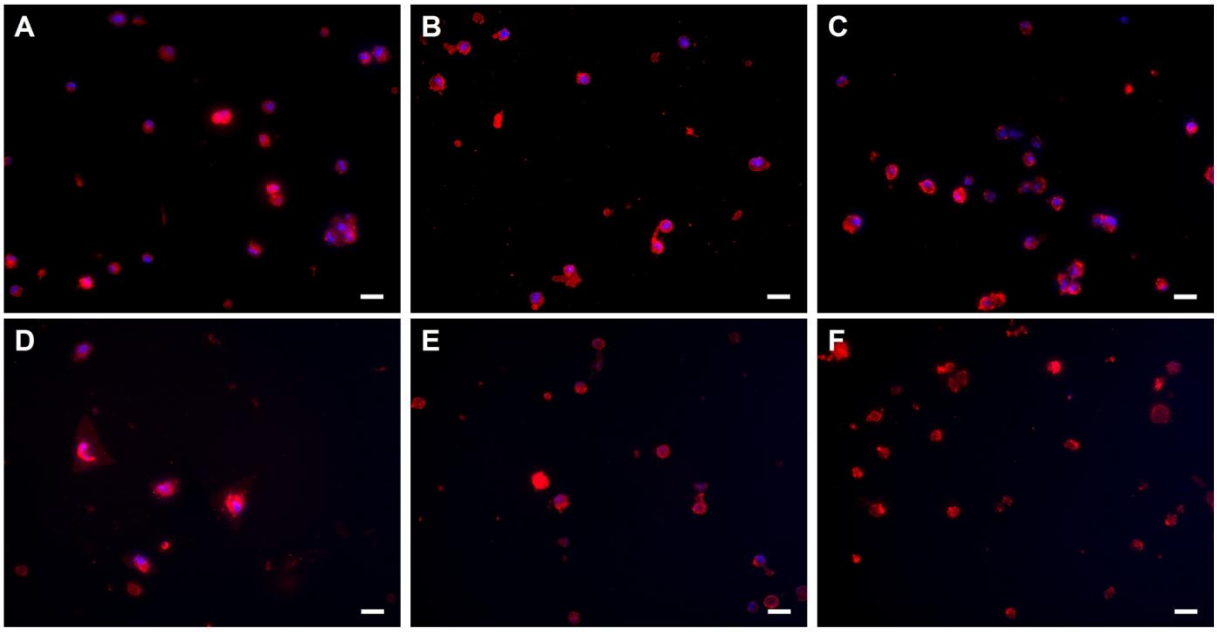

Fig. 20. Fluorescent micrographs of PKH26 labeled cryosections of hMSCs encapsulated in the (A and D) RGDS hydrogel, (B and E) DGSR hydrogel, and (C and F) Hyal hydrogel after (A, B, C) 7 and (D, E, F) 21 days of culture in ODM. Scale bar: 20 μm.

Toluidine blue stained cryosections were also prepared to identify cell distribution and morphology as well as matrix deposition in the cell-hydrogel constructs (Fig. 21). This staining confirmed the homogenous distribution throughout the hydrogel for the full culture period in all materials tested. There was no major deposition of pericellular matrix in any of the cell-material combinations.

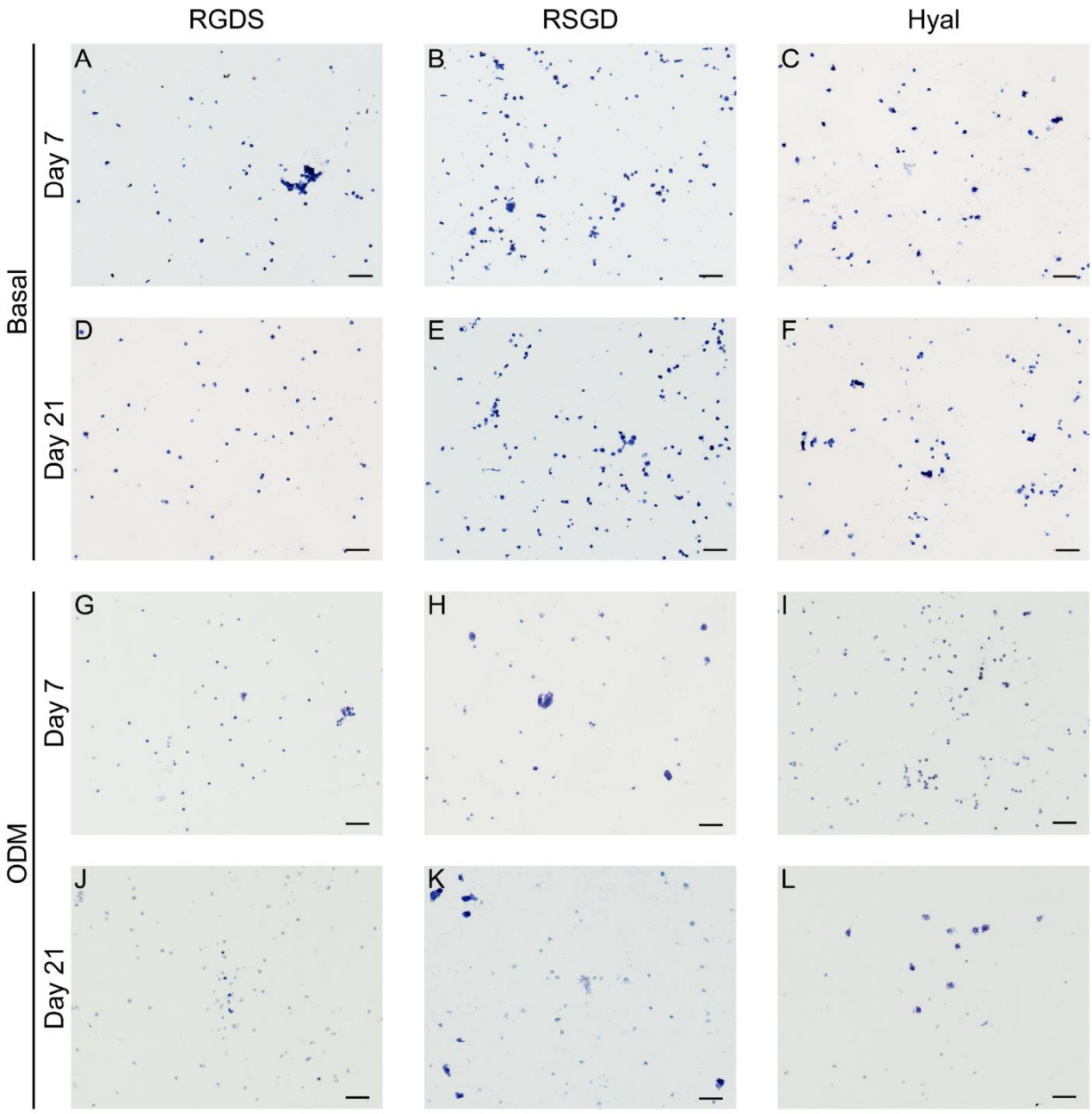

Fig. 21. Toluidine blue stained cryosections of hMSCs cultured in the bicomponent hydrogel at days 7 and 21 in basal medium and ODM. Scale bar: 100 μm.

4.3.5 Assessing the influence of RGDS dendrimers on the mRNA expression

Relative mRNA expression of sex determining region Y-box 9 (hSOX9) and human collagen type II-A1 (hCOL2), markers for chondrogenic differentiation, and runt related transcription

factor type 2 (hRUNx2) and alkaline phosphatase (hALP), markers for osteogenic differentiation, were determined using the ΔΔCT method normalized to hGAPDH endogenous control (Figs. 22 and 23).

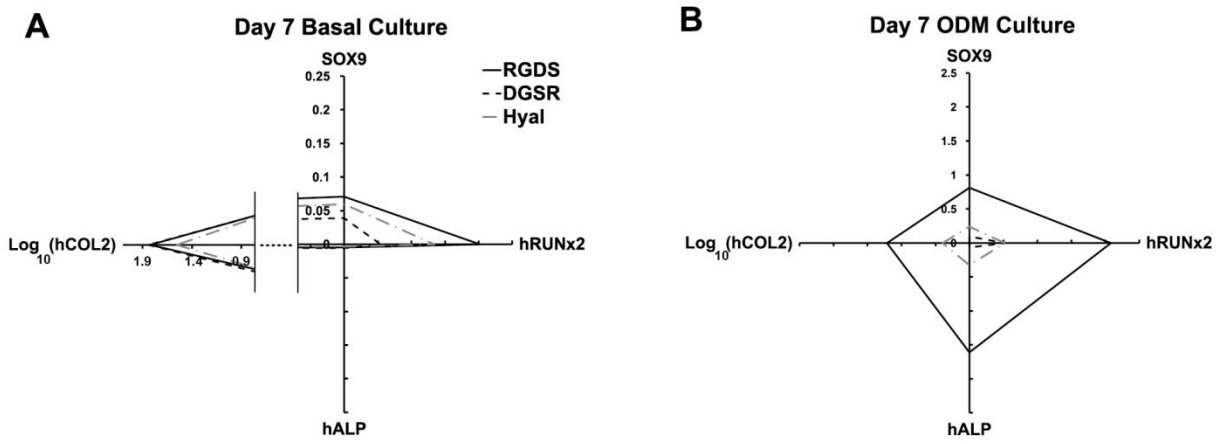

Fig. 22. Radar graphs comparing the relative mRNA expression of hSOX9, hRUNx2, hALP, and hCOL2 between encapsulated hMSCs at day 7 in basal media (A) and ODM (B). hCOL2 results are illustrated as $\log_{10}$(hCOL2) expression. The axis of the $\log_{10}$(hCOL2) expression was condensed to fit in the figure.

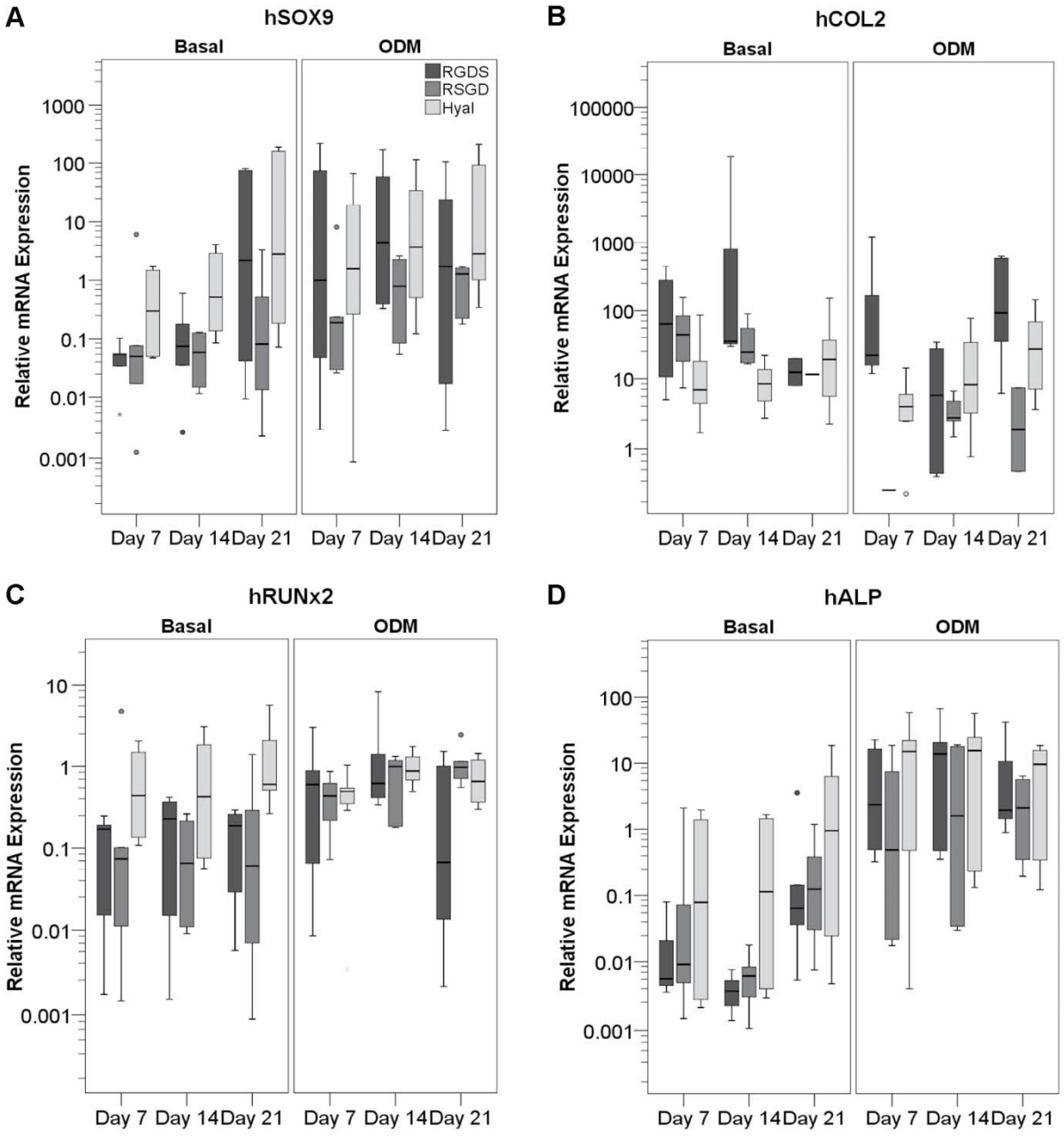

Fig. 23. qRT-PCR of (A) hSOX9, (B) hCOL2, (C) hRUNx2, and (D) hALP. Data was calculated as ΔΔCt by normalizing sample ΔCt values to the day 0 monolayer culture ΔCt values. The endogenous control employed was hGAPDH.

The hSOX9 gene expression for the RGDS group in basal media was lower at 7 days compared to the other hyaluronic acid compositions. This effect was not reproducible in osteogenic media. There was a strong upregulation of hCOL2 gene expression, between a 10 to 1000 fold increase, in all conditions. Furthermore, the response by the RGDS group at day 7 showed a statistically significant difference from the controls ($p<0.05$). Interestingly, hRUNx2 gene expression in ODM media was higher in the RGDS group at 7 days compared to the DGSR and Hyal groups, but was not different at day 21. There was a trend for higher hALP gene expression, up to a 10 fold increase, for the RGDS and Hyal groups in contrast to the DGSR dendrimer containing hydrogel in ODM, which can be expected due to the composition of the media (*i.e.* supplementing dexamethasone and glycerophosphate in ODM) with a maximum peak at 14 days.

4.4. Assessing the potential for de novo bone growth in a murine model: in vivo evaluation of BMP-2 and hMSC loaded Hyal-pN in a subcutaneous implant

4.4.1. Synthesis and characterization of Hyal-pN

Prior to the direct amidation synthesis which produces Hyal-pN, the hyaluronic acid and pN precursors were fully characterized by the MALDI-TOF technique (Table 16).

Table 16. Reported sizes in kg/mol of the precursors hyaluronic acid and pN quantified by MALDI-TOF analysis. The polydispersity value M_w/M_n is without units.

	M_p	M_n	M_w	M_z	M_w/M_n
Hyaluronan	244.6	157.5	293.5	469.1	1.9
pN	81.1	43.4	97.6	170.0	2.3

The Hyal-pN brush copolymer was synthesized with a direct amidation technique that was optimized for *in vivo* work [28, 29]. The benefit of this method was that it bypassed the need for

copper to produce the same polymer. Consequently, the step that modified the hyaluronan with propargylamine was no longer necessary. Hence, the properties of this Hyal-pN analog were slightly different. For instance, the signals for the propargylamine protons were present in the Hyal-pa (Fig. 24D, signals *b*) and the CuAAC reacted Hyal-pN (Fig. 24B) and were assigned at δ = 2.68 and 2.88 ppm. Furthermore, the absence of the propargylamine group in the CDI synthesized Hyal-pN is apparent in Fig. 24A.

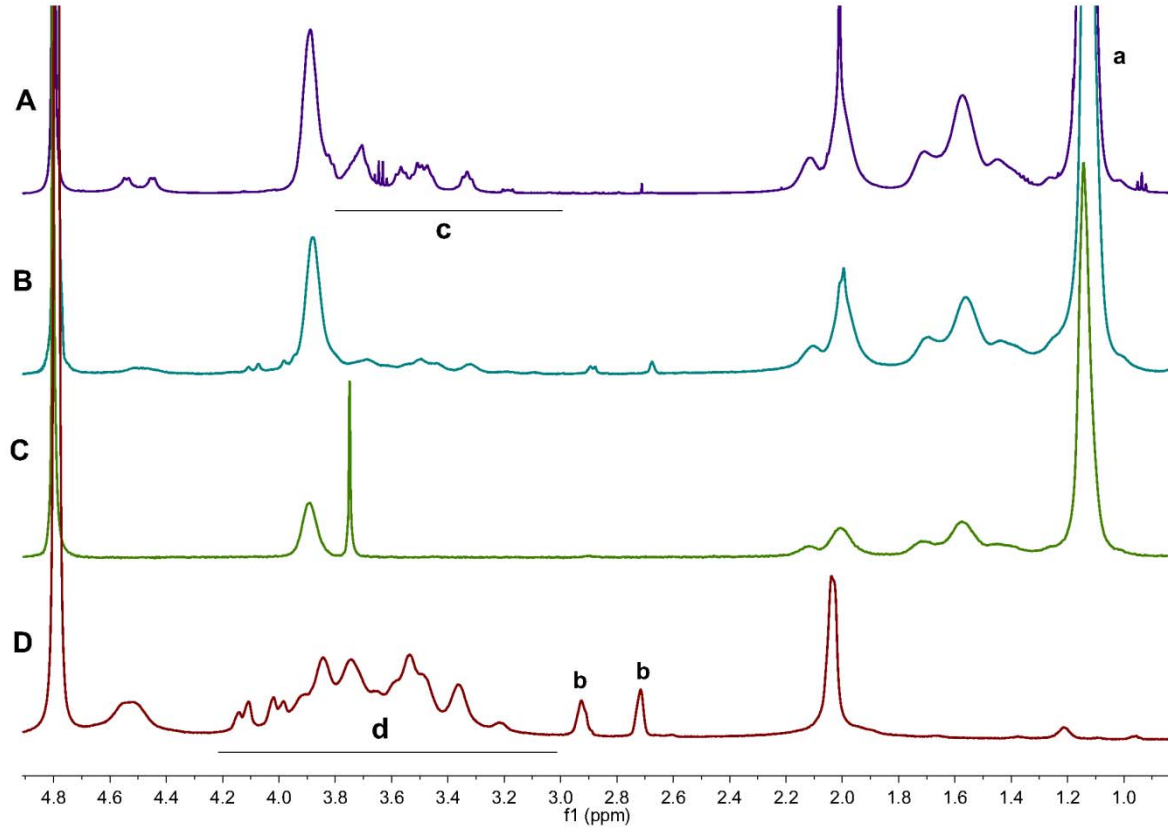

Fig. 24. ^{1}H NMR characterization of the Hyal-pN synthesized with (A) the direct amidation method compared to the (B) CuAAC method and (C) Hyal-pa and (D) N_3-pN (Mw = 28 kDa).

The calculated DG of the CDI synthesized Hyal-pN was 1.1 mol% corresponding to the molar ratio of the total NIPAM monomers to the total hyaluronan disaccharides. This method of

calculation was the same one used in the prior studies. Briefly, the signal intensity of the sp^2 hybridized methyl group protons of the NIPAM monomers were assigned at $\delta = 1.91$ ppm (Fig. 24A, signal *a*), and correlated with the integral taken in the range of $\delta = 3.8 – 3.0$ ppm associated with 9 protons of the disaccharide rings (Fig. 24A, signal *c*). This resulting proportion is the DG in molar percent of the pN grafted to the total disaccharide units. The unadulterated hyaluronic acid polysaccharide protons, $\delta = 3.0 – 4.2$ ppm, without overlap of a signal attributable to a pN chemical shift is further annotated (Fig 24D, signal *d*)

The direct amidation technique for the coupling of the poly(*N*-isorpopylacrylamide) onto hyaluronan does not require intermediate conjugation of the hyaluronan with propargylamine since it is performed in the absence of copper. Therefore, the absence of the hydrophobic propargylamide groups changes the rheological properties of the Hyal-pN (Fig. 25). Specifically, the material has a lower viscosity of 0.9 Pa at 20 ^{o}C compared to the CuAAC synthesized version that is 40.1 Pa (Table 17). Interestingly above the LSCT, the hydrogel synthesized by direct amidation revealed both elastic and viscous moduli almost an order of magnitude higher than the CuAAC reacted Hyal-pN. Yet this result could be because the size of the pN used in the CDI hydrogel was much larger, 97.6 kDa, with regard to the CuAAC reacted Hyal-pN, 16.3 kDa. However, what is clear is that the direct amidation synthesized hydrogel possessed a lower viscosity relative to its counterpart that was more suitable for injection.

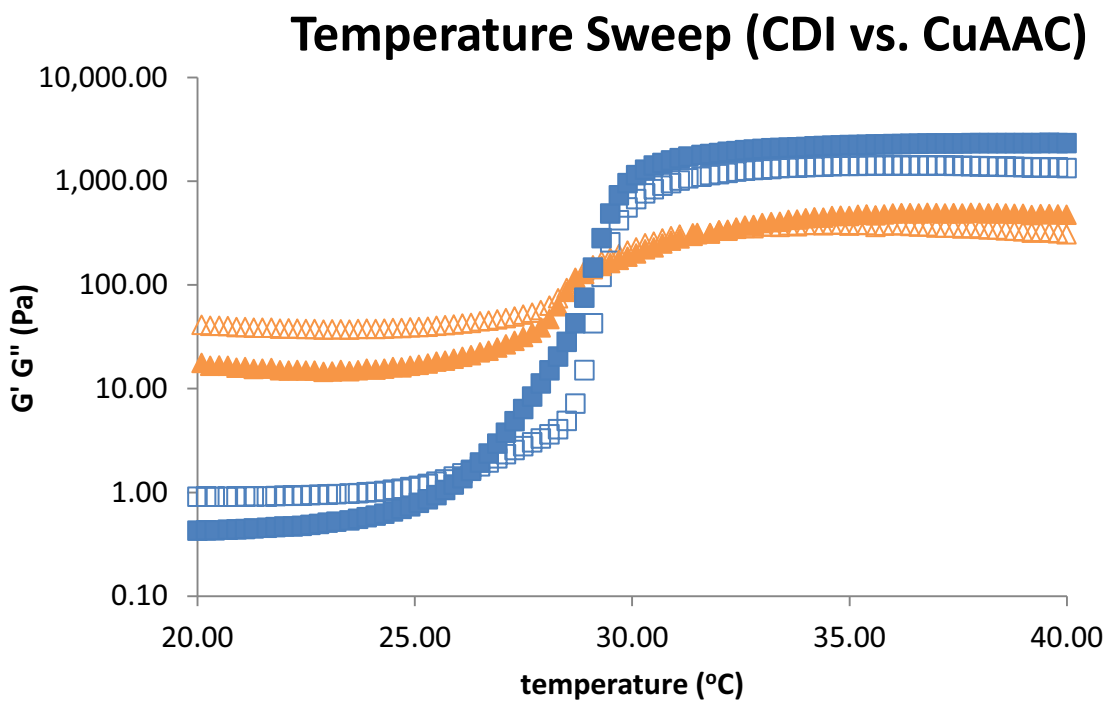

Fig. 25. Rheological characterization of the direct amidation synthesized Hyal-pN compared to the CuAAC version. The former batch is represented as blue squares with the G' illustrated as normal squares, and the G" as hollow squares. The latter is represented as orange triangles with G' is shown as the normal triangles and the G" as the hollow ones. The CuAAC synthesized hydrogel displayed had a pN M_w of 16.3 kg/mol whereas the hyaluronan a M_w of 1506 kg/mol.

Table 17. List of lower critical solution temperatures (LCST), elastic modulus (G') and viscous modulus (G") at 20 °C and 40 °C of the Hyal-pN synthesized by the direct amidation method versus the CuAAC method.

Synthesis method	LCST (°C)	G' (Pa) at 20 °C	G" (Pa) at 20 °C	G' (Pa) at 37 °C	G" (Pa) at 37 °C
CDI	26.5	0.43	0.9	2330.0	1330.0
CuAAC	32.0	17.7	41.2	474.0	307.0

4.4.2 Pre and post-operative observations

In the first set of *in vivo* experiments, lyophilized Hyal-pN polymer was weighted under a laminar flow hood in order to maintain sterility and reconstituted to a concentration of 20 % (wt/vol) in PBS with or without 10 μg/ml of BMP-2. Upon the day of surgery hMSCs were added to the polymer solutions at final concentrations of 5 x 10^6 cells/ml, 10 % (wt/vol) polymer, and 5 μg/ml of BMP-2. The acellular hydrogels were mixed with only DMEM to bring about the same final polymer concentration. Three nude mice (14042, 14043, and 14044) were implanted once on the left flank with 200 μl of the mixture of Hydrogel + BMP-2 and once on the right flank with 200 μl of the Hydrogel + BMP-2 + hMSCs for a total of two implants per mouse (Table 18).

For the second set of *in vivo* experiments, four nude mice (14061, 14062, and 14063) were implanted on the left flank with 200 μl of hydrogel without additional supplements. Each animal was also implanted on the right flank with 200 μl Hydrogel mixed with a suspension of hMSCs. The final polymer and cell concentrations were identical to the first series.

A third round of surgeries was carried out to repeat the first set of experiments. In this set four more mice (14065, 14066, 14067, and 14068) were injected in both flanks with the same composition of the carrier, drug, and cells as the first series.

Table 18. List of implanted samples in each nude mouse and major macroscopic observations at the implant site at the time of euthanasia. The identification numbers are used throughout the analyses to identify each individual. Furthermore the implant sites are specified by adding the prefix “L” corresponding to the left flank and “R” corresponding to the right flank implant (*e.g.* L14061 is the implant at the left flank of mouse 14061).

Mouse ID	Left flank	Right flank	Macroscopic Observations
14042	Hyal-pN+BMP-2	Hyal-pN+BMP-2 +hMSCs	No inflammation, normal aspect
14043	Hyal-pN+BMP-2	Hyal-pN+BMP-2 +hMSCs	No inflammation, normal aspect
14044	Hyal-pN+BMP-2	Hyal-pN+BMP-2+hMSCs	Left flank, abcess present; right flank, normal aspect
14061	Hyal-pN	Hyal-pN + hMSCs	Left flank, abcess present; right flank, normal aspect
14062	Hyal-pN	Hyal-pN + hMSCs	Left flank, minor closed wound; right flank, normal aspect
14063	Hyal-pN	Hyal-pN + hMSCs	No inflammation, normal appearance
14064	Hyal-pN	Hyal-pN + hMSCs	Left flank, normal aspect; right flank, redness present
14065	Hyal-pN+BMP-2	Hyal-pN+BMP-2 +hMSCs	No inflammation, normal appearance
14066	Hyal-pN+BMP-2	Hyal-pN+BMP-2 +hMSCs	Left flank, closed wound; right flank, abcess present
14067	Hyal-pN+BMP-2	Hyal-pN+BMP-2 +hMSCs	Excluded, experienced weight loss > 20%, not related to injection
14068	Hyal-pN+BMP-2	Hyal-pN+BMP-2 +hMSCs	Excluded, experienced weight loss > 20%, not related to injection

All animals gained weight after 4 weeks post operation except for two mice (14067 and 14068). Necropsy on those specimens was performed by a pathologist who concluded that food

blockage and infection not related to the injections were responsible for the reduced weight. Therefore, they were excluded from the study.

During macroscopic observations of the specimens, 12 of the 18 total implants sites had a normal appearance without any signs of redness or inflammation. In these individuals, 4 of the 9 total specimens did not experience an adverse reaction to the injections. At the location of implant L14062 there was some redness (Fig. 26). Closed wounds were observed at R14064 and L14066, whereas L14044, L14061, and R14066 were abscessed at the implant site. The size of the latter three implants also decreased over time. This was also the case for implants R14044, R14064, and L14066. The remaining 12 implants seemed to be the same or similar in size as the initial administered amount.

Two injections were made on the left flank of individual 14043 because an initial injection punctured through the skin. Upon collection of the implant and surrounding tissue in mouse 14062, the local region showed a reddish aspect from the subcutaneous viewpoint. There was a double bump on its right flank, with the 2 bumps being close to each other suggesting a two stage injection.

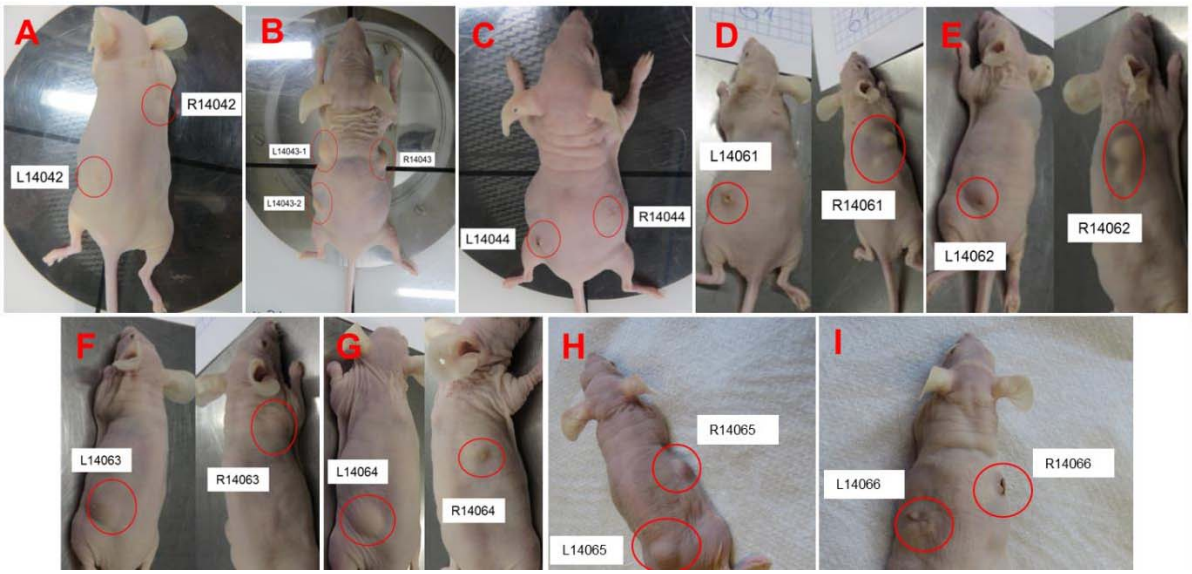

Fig. 26. Images of the specimens after euthanasia. Each mouse is identified with its ID as assigned in Table 18: (A) mouse 14042, (B) mouse 14043, (C) mouse 14044, (D) mouse 14061, (E) mouse 14062, (F) mouse 14063, (G) mouse 14064, (H) mouse 14065, and (I) mouse 14066. Implant locations are distinguished with the prefix "L" for left flank and "R" for right flank implant sites.

4.4.2 Verification of mineral formation via x-ray radiography

To examine radio dense tissue formation at the injection sites, x-ray radiographs were obtained for each specimen (Fig 27). In some of the mice, radio-opaque lumps were observed at the corresponding injection locations. In the case of Hyal-pN without additionally loaded BMP-2 or cells, no extra radio-opacity indicative of denser tissue or mineralization or both were measured. However, radio-opaque lumps were observed in 1/7 Hyal-pN + BMP-2 implants, 3/7 Hyal-pN + BMP-2 + hMSC and 3/4 Hyal-pN + hMSC were radio-opaque. Interestingly, observation of a wound at the injection site at 4 weeks correlates with the absence of radio-opaque lump in the radiographs for all mice. These suggest in addition to the macroscopic observations that in the absence of hMSCs most of the injected formulations are resorbed after 4 weeks, while the presence of hMSCs would lead to the conservation of the injected lump and formation of stable constructs at 4 weeks.

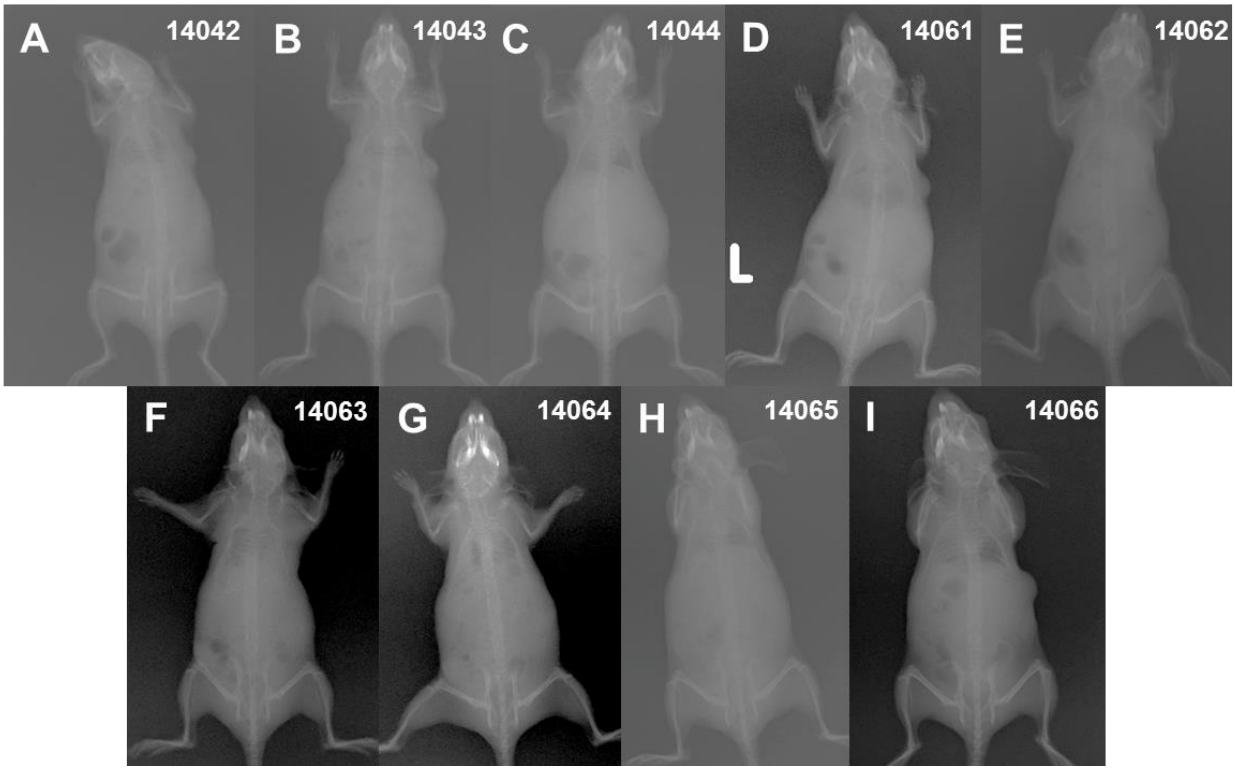

Fig. 27. X-ray radiographs of the euthanized mice. Each mouse is identified with its ID as assigned in Table 18: (A) mouse 14042, (B) mouse 14043, (C) mouse 14044, (D) mouse 14061, (E) mouse 14062, (F) mouse 14063, (G) mouse 14064, (H) mouse 14065, and (I) mouse 14066.

On close examination of the radiograph, only the right flank of the mice 14043 showed a significant radio-opacity (X-ray dense material) suggesting calcified material formation (Fig. 28).

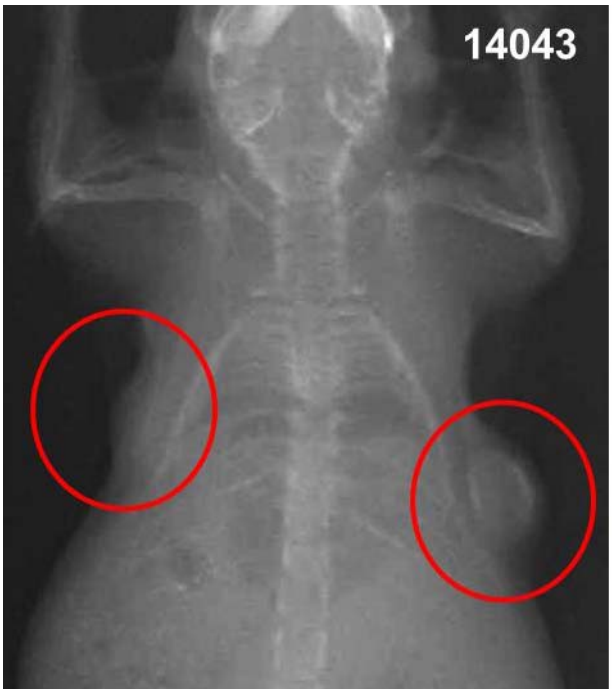

Fig. 28. Magnification of the radiograph image of specimen 14043 exhibiting a radio-opaque implant. In this case no open wounds were observed. Implant L14043 did reduce in volume. However, implant R14043 which contained cells did not. Furthermore this implant corresponding to the hydrogel containing both BMP-2 and hMSCs exhibited radio-opacity.

4.4.3 Implant excision and quantification of bone mineral density via μCT scanning

Every implant was excised with a scalpel from each mouse flank. The explants had well-defined spherical shapes and usually had a slightly yellowish and reddish aspect that easily differentiated it from the surrounding tissue (Fig. 29). For mouse 14044, upon manipulation, the material from the left side was extruded through the open wound on the skin.

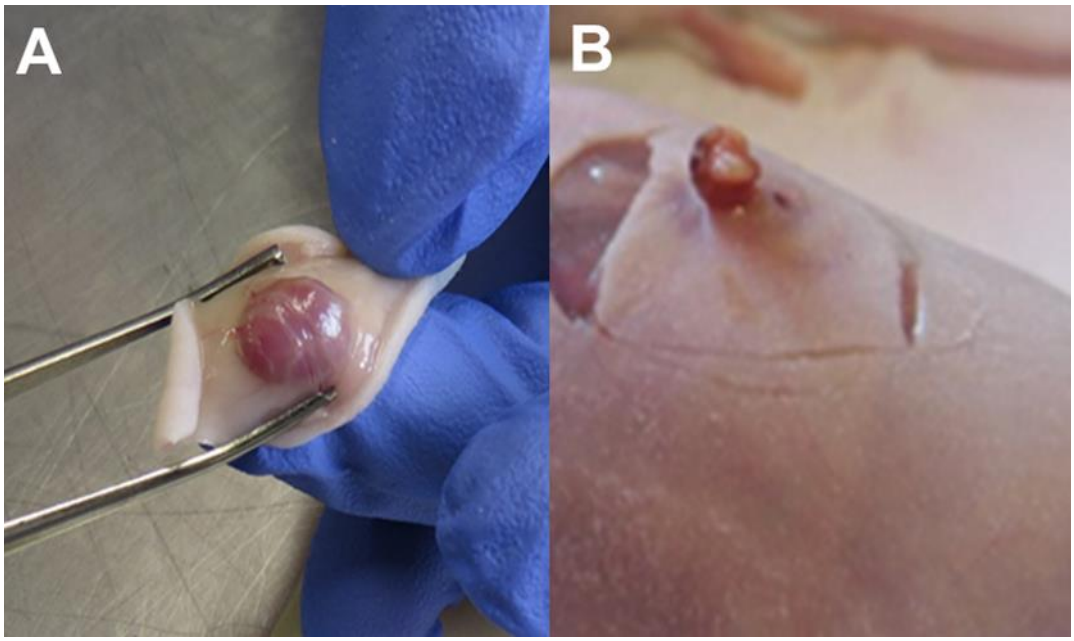

Fig. 29. Representative image of the excised implant and surrounding tissue from (A) the left flank of specimen 14062 viewed from the subcutaneous side of the dermis, and (B) material expelled through the open wound of the left implant of specimen 14044.

Excised samples usually looked well vascularized and were clearly differentiated from the surrounding tissue. After excision, the explants were put in a 4% formaledehyde solution. Representative explant cross-sections and 3D reconstructions were generated from individually scanned explants using a microtomograph (μCT 40, Scanco) with a threshold density set at 200 mg hydroxyapatite /cm^3 (Fig. 30).

All scanned tissue explants showed little to no mineralized tissue with a density above 200 mgHA/cm, except for mouse 14043 which showed a significant amount of dense material in both left (Hyal-pN + BMP-2) and right implants (Hyal-pN + BMP-2 + hMSCs). The most dense mineralization was primarily located at the periphery of the scaffold lumps. Mice 14042 showed more dense material on the right side than on the left side, but with relatively low density (<200 mgHA/cm). Mice 14043 showed significant amount of dense material on both side with a significant higher amount on the right flank (R14043). Mice 14044 contained some discretely

dense regions under the X-ray beam of the μCT, but this was not significant on either the left or right explants.

Left flank explants (-hMSCs)		*Right flank explants (+hMSCs)*	
Cross-section	**3D reconstruction**	**Cross-section**	**3D reconstruction**
Mouse 14042			
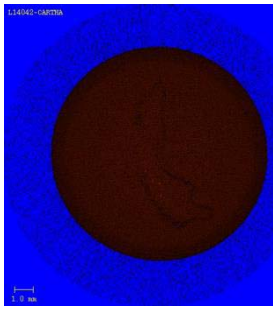	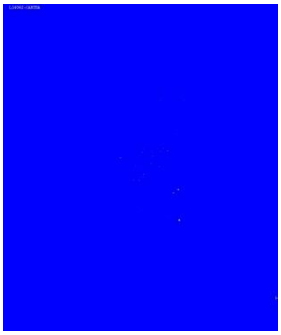	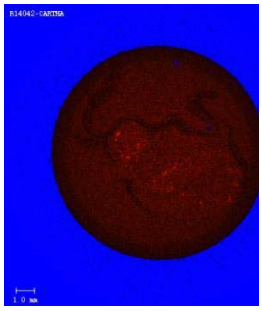	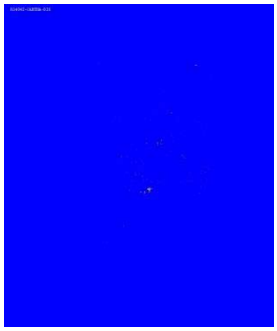
Mouse 14043			
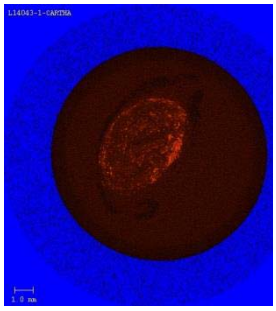	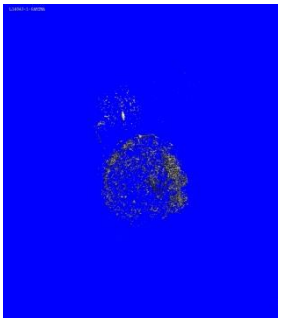	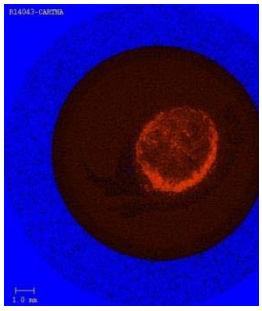	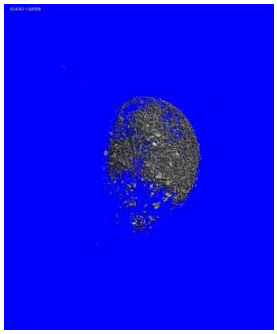
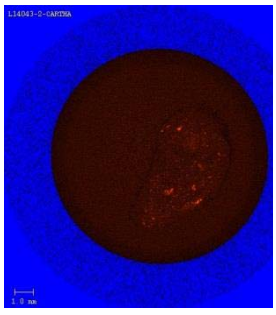	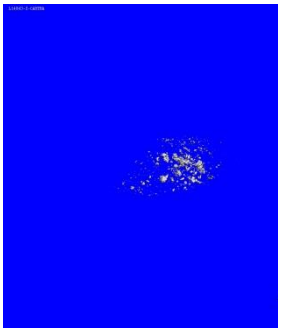		

Mouse 14044

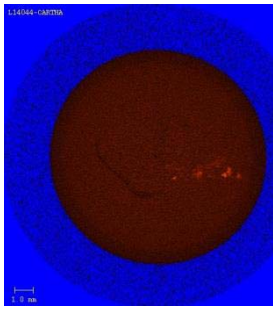

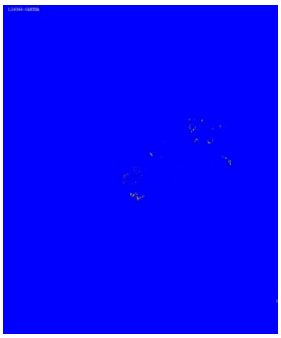

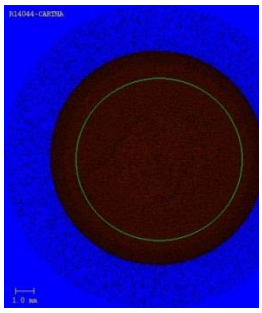

None. Calcium phosphate was not present.

Mouse 14061

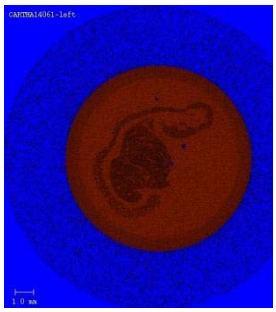

Not available.

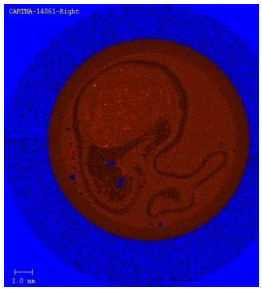

Not available.

Mouse 14063

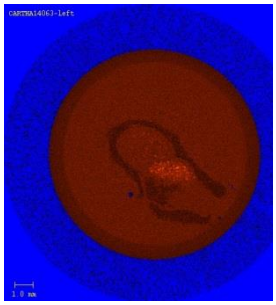

Not available. Not available. Not available.

Mouse 14064

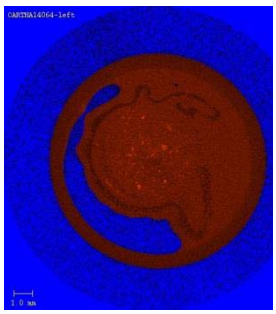

Not available. Not available. Not available.

Fig. 30. Representative μCT cross-sections and 3D reconstruction of the explants of mouse 14042, 14043, 14044, 14061, 14063, and 14064.

A color coded map of the results was compiled in order to see the efficacy of the materials to develop ectopic bone *in vivo* (Fig. 31).

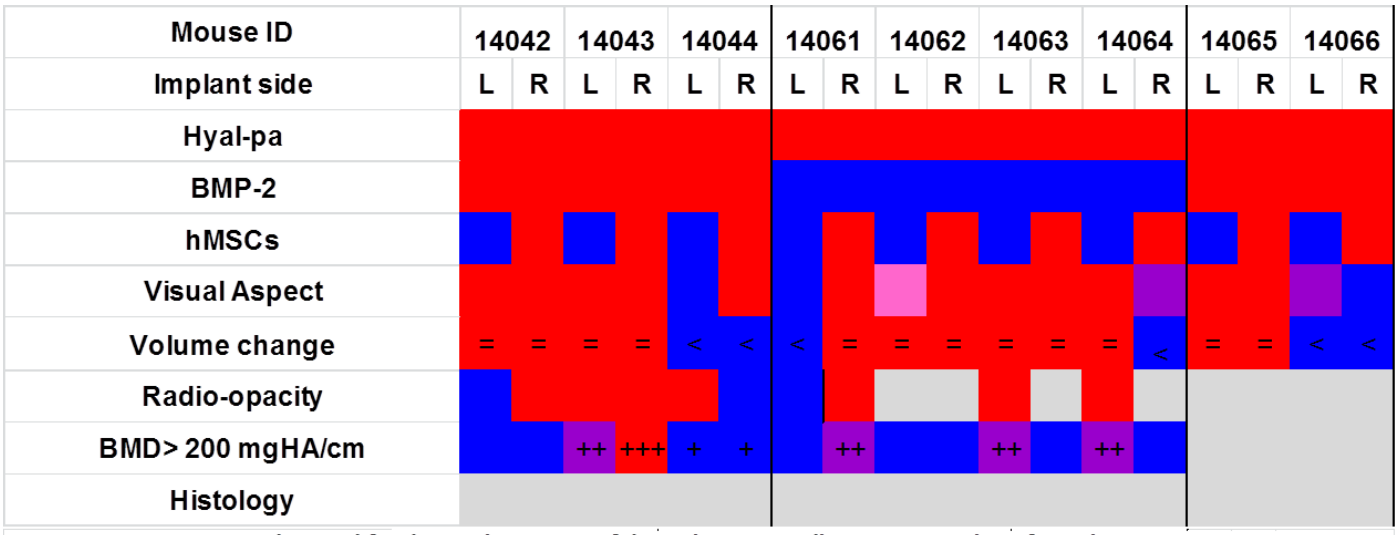

Legend for the assignments of the colors according to categories of results.	
Hyal-pa	Hyal-pa = Red, no Hyal-pa = Blue
BMP-2	BMP-2 = Red, No BMP-2 = Blue
hMSCs	Cells = Red, No cells = Blue
Visual Aspect	Abcess/Open Wound = Blue, Closed Wound = Purple, Redness = Pink, Normal = Red
Volume change	Equal = Red, Decrease = Blue, Increase = Orange
Radio-opacity	Radio-opaque = Red, Not radio-opaque = Blue
BMD> 200 mgHA/cm	BMP>200 mgHA/cm (significantly above) = Red, BMD=200 mgHA/cm = Purple, BMD<200/none observed = Blue
Histology	Organized bone = Red, Calcified bony-like = Purple, Adipose tissue/no bone = Blue

Fig. 31. Color coded map visualizing the results as a pattern of hues. The legend containing the assignments for the colors with respect to a defined category of results appears below the map. Generally speaking, red is the "positive" results; blue is the "negative" results; purple and pink symbolized mixed results. Gray filled boxes correspond to results that are pending. The black lines represent each series of experiments carried out.

Assessing the *de novo* ectopic bone growth with respect to the presence of Hyal-pN, BMP-2, and hMSCs, the combination of factors appears to be important in the development of new bone tissue. However, these preliminary results were graded from only 7 specimens. Without further evidence these preliminary results cannot be further corroborated. According to the color map

the preliminary results appear to be more influenced by the initial inflammatory response of the individual, indicated by the visual aspect at the implant sites, rather than the combination of the therapeutic agents (Fig. 31). For example, mouse 14043 which did not exhibit a negative reaction to the implant revealed the most mineralized tissue downstream. The animals with adverse reactions at the implant sites did not show formation of mineralized tissue within those implants. Furthermore, if the animal showed a normal aspect at one implant site and a closed wound at the other, then the bone mineral density (BMD) would be measured equal to or below 200 mg HA/cm. If the animal had a normal aspect and an abscess present, then minimal to no BMD would be measured in the implants (*i.e.* < 200 mg HA/cm). Therefore, it appears that if the animal had a depressed immune system as a result of an implant abscess or a healing wound then no significant mineralized tissue appeared on the radiographies.

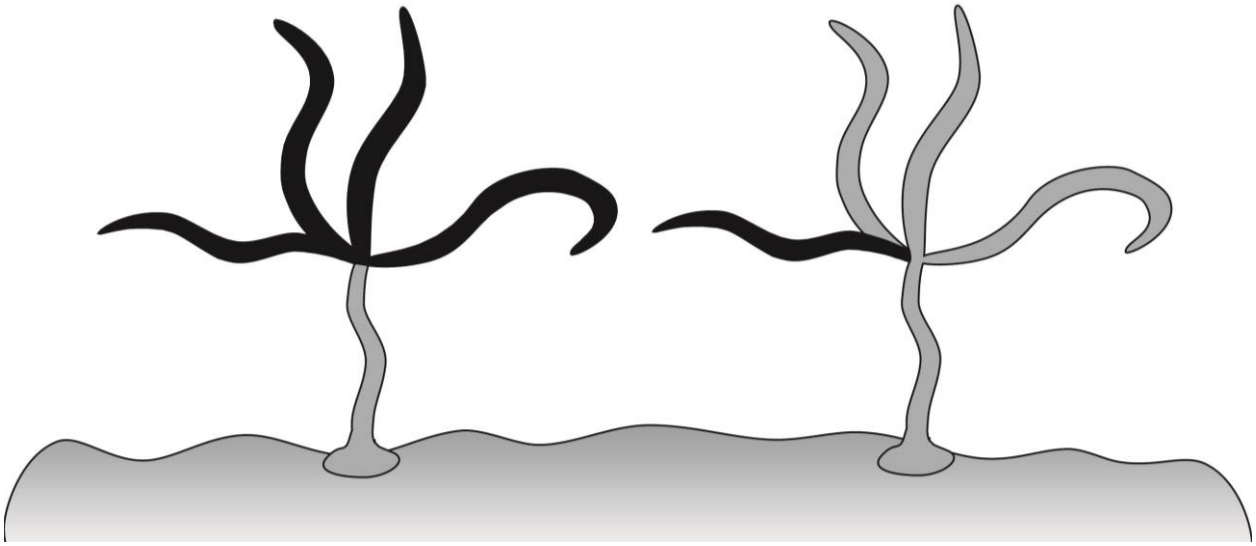

Chapter 5 – Discussion

5.1 Synthesis of the thermoresponsive injectable hydrogel

The CuAAC reaction performed with the pre-catalyst Cu^{+2}, $CuSO_4 \cdot 5H_2O$, and a reducing agent, ascorbic acid, in water closely resembled the hyaluronan oxidative degradation condition of the Weissberger's system, Cu^{+2} and ascorbic acid which could cause hyaluronan degradation in the presence of oxygen [35, 91]. For this reason, $CuBr(PPh_3)_3$ was chosen as a fast and effective alternative catalyst active at significantly lower concentrations than CuAsc [37]. Despite limited solubility in water, $CuBr(PPh_3)_3$ is more efficient in conjugating N_3-pN to HApa than the CuAsc, notably at a true catalyst concentration. Interestingly, an increase of copper content per weight of Hyal-pN was measured in the reaction using $CuBr(PPh_3)_3$. This counterintuitive rise can hypothetically be attributed to the low solubility of $CuBr(PPh_3)_3$ in the dialysis solutions and the

loss of unreacted Hyal-pa and N_3-pN, driving an apparent increase of copper in the dry sample. An improved copper extraction method is therefore needed for $CuBr(PPh_3)_3$. Additionally, the CuAAC reaction performed classically in the DMSO:water mixture using $CuBr(PPh_3)_3$ was not effective, possibly due to the poor solubility of N_3-pN in this solvent. The failure of conjugating N_3-pN to Hyal-pa in DMSO:water due to the insolubility of pN was confirmed by the absence of an LCST in the temperature sweep. In fact, this composition behaved similar to a pure Hyal-pa solution 15 % (wt/vol) which further supports the failure of the CuAAC reaction in this particular solvent mixture.

Comparison of the rheological profiles of the other two conjugation conditions, indicated that the solution of Hyal-pN prepared using $CuBr(PPh_3)_3$ presented a more pronounced temperature induced increase of storage modulus compared to the CuAsc. The difference of grafting density equal to 0.5 mol% could be the cause of this behavior; however this seems a rather minimal variance considering that a DG variation of 5 mol% has previously shown to have minimal effect of the storage modulus of HApN solutions [16]. Another hypothesis is that the degradation of the hyaluronan backbone occurs predominantly in the CuAsc catalyzed reaction as suggested by the lower % (wt) yield. The degraded Hyal-pN size and consequently shape in solution may differ to non-degraded Hyal-pN. The smaller brush macromolecules could interact more in solution than large globular macromolecules subsequently increasing the viscosity of the solution. This has not been observed previously, for a hyaluronic acid backbone of 1.6 MDa and 250 kDa [29]. This would suggest extensive degradation of the hyaluronan conjugate synthesized by CuAsc in line with reported findings [92]. The lack of methods permitting characterization of the Hyal-pN macromolecular structure needs to be addressed in order to confirm this hypothesis.

The CuAAC reaction is a versatile method to synthesize polymer-based biomaterials in addition to facilitating the grafting of bioactive macromolecules. Thus, this sophisticated synthesis framework was translated to the covalent conjugation of the disubstituted dendrimers containing one azide terminated branch to propargylamine modified hyaluronic acid. Furthermore, the CuAAC synthesis platform was the sole reaction sequence utilized in the creating of the hydrogels featured in this thesis because.

5.2. In vitro assessment of the dendrimer decorated drug releasing injectable hydrogel

In order to investigate the role of the density of the physical crosslinking network of Hyal-pN hydrogels, the biomaterials were synthesized with 9, 16, or 21 kDa sized pN with similar degrees of substitution across all batches. The pN chains typically undergo a transitional hydrophobic collapse upon increasing temperature above the LCST, in effect entangling the polymers into a cohesive material. The effective size of this polymer affects the stability and viscoelastic character of the polymers in PBS. Subsequently, HpN9 showed limited changes in G' and G" above 27.5 °C and experienced poor physical crosslinking as the G' values never crossed over the G" values. In solution HpN16 and HpN21 behaved as viscous liquids below their inflection temperatures, with similar G" values at 20 °C, akin to pristine hyaluronic acid. Whereas above this temperature, the G' supplanted the G" value indicative of stable hydrogel formation. Furthermore we observed that within the range of M_w of pN tested, the materials did not experience significant macroscopic shrinkage. The addition of dendrimers in Hyal-pN did not significantly influence the rheological features. The release profile of BMP-2 and TGF-β1 from the loaded hydrogels initially presented a burst of protein which peaked after 4 hours followed by an incremental release thereafter. No significant difference with respect to the size of pN was observed, except for a slight trend showing a diminished release of BMP-2 at 4h with an increase in size. Additionally, a significant amount of protein could not be measured in the media likely because they were bound to Hyal-pN even in PBS doped with BSA [49, 51]. This pattern was also true for the HpN9 even though it did not form a stable hydrogel.

The sustained release of drugs from hydrogels depots is governed by several factors including gradient diffusion, non-covalent binding (*i.e.* Lewis acid-base interactions), physical entrapment (*e.g.* crosslinking density), and the initial concentration loaded into the system [48, 51, 93]. Thus, the nature of the polymer scaffold is important [49, 94]. Kim and Valentini hypothesized that the release of BMP-2 from a hyaluronic acid-based hydrogel is attenuated by the electrostatic interaction of negatively charged carboxylic acid groups of the polysaccharide and the primary amine rich BMP-2, in other words an acid-base system [60]. In this case only 32% of the total loaded protein was retrieved whereas 88% was released from a collagen I sponge control. The full observed release of protein from the dendrimer conjugated hyaluronic acid based hydrogels never reached the amounts delivered from the control hydrogels. It is also

possible that the dendrimers delay the release of drugs [53] and would deliver a prolonged sustained released over an extended period of time dependent on the degradation of the hyaluronan conjugates. Nevertheless, the inevitable retention of protein within biomaterials has been shown to maintain bioactivity [50], improve cellular invasion, and increase the generation of tissue related markers within the depots [49, 60]. Even extremely low concentrations of BMP-2 localized within a hydrogel are sufficient to program the microenvironment towards guiding cellular differentiation [95]. In order to isolate the effects of the dendrimers, we developed a methodology inspired by Kolambkar *et al.* and Kimura *et al.* and loaded the hydrogels with BMP-2 or TGF- β1 supplemented with 0.1% BSA and 4 mM HCl in order to discourage non-specific binding with the biomaterial [50, 51]. The aforementioned peptide binding sequences were previously identified by phage display [53, 96, 97]. Furthermore the presentation of these binding sequences have been previously demonstrated to retain and attenuate the release of these cytokines [53, 96]. In our case, augmenting the molecular architecture of the drug delivery platform with peptide binding dendrimers also significantly affected the release of BMP-2 and TGF-β1. In accordance with results from the *in vitro* cell encapsulation study (Chapter 4, Section 3), the influence of dendrimers on the delivery of the cytokines in BSA supplemented PBS was compared with Hyal-pN containing Hyal-pa, the precursor of the Hyal-YPV and Hyal-LPL conjugates.

In this study, we demonstrated the ability of the peptide bearing dendrimers to attenuate the protein release from Hyal-pN depots, causing a sharp decrease in the burst phase as well as a lower final concentration at 7 days. The relatively high overall release of protein from the non-dendrimer containing depots compared to compositions modified with dendrimers can be clearly seen for HpN16 and HpN21. We checked the specificity of the synthesized peptide epitopes by performing analogous release studies by loading BMP-2 into depots containing Hyal-LPL (*i.e.* TGF-β1 binding hyaluronan) peptide, and vice versa. Interestingly in all scenarios, the dendrimers were at least similarly efficacious in retaining growth factors suggesting that the binding behavior of these peptides are not specific to BMP-2 and TGF-β1 or that the presentation of these peptides on the tip of the dendrimer branched structure render the peptides less specific. Hence, binding specificity may stem from the tertiary structure, as is the case with antigenic determinants in antibody recognition. Future studies could more closely examine the

peptide dendrimer binding affinity and specificity employing proteins outside of the TGF superfamily.

The dendrimer decorated hydrogel was capable of retaining loaded BMP-2 and TFG-β1 through affinity-based interactions of the functionalized peptide binding sequences and the GFs. These drug delivery platforms were proven to modulate the release profiles of these therapeutic agents, which is promising for future *in vitro* work aimed at guiding cells toward the regeneration of bone and cartilage. Another set of dendrimers that were able to bind with integrin were utilized in an *in vitro* study that encapsulated hMSCs into the hydrogel scaffold with the aim to induce the cells toward a direct ossification pathway.

5.3. In vitro evaluation of the dendrimer decorated hydrogels as a cell carrier-scaffold

The ability to precisely tailor microenvironments for stem cells is extremely important for both the understanding of their behavior in a simplified and controlled extracellular matrix and the development of clinically relevant stem cell based therapies such as the tissue engineering of bone [15, 68, 98]. In this section, we have developed a novel bicomponent, injectable hydrogel incorporating a thermoresponsive bioactive hyaluronan matrix and dendrimers that feature clustered presentations of a bioactive peptide. Singular, multivalent dendrimers functionalized with four RGDS peptides and one azide moiety were successfully synthesized and characterized. The grafting of these well-defined macromolecules upon a hyaluronic acid backbone presented clusters of binding epitopes with an exceptional degree of spatial control which when combined with the thermoreversible polymer produced a highly functionalized, injectable delivery system that formed a stable hydrogel platform upon an increase in temperature.

In a recent report by Lam *et al.,* RGD containing peptides were grafted in either a random or clustered fashion onto acrylated hyaluronan hydrogels over a concentration range of 0.01 to 1 mM peptide [81]. Utilizing encapsulated mouse MSCs, it was found in an in vitro study that the lowest concentration of RGD (10 μM) coupled with the highest density of peptide clustering (1.8 mmol RGD/mmol RGD grafted hyaluronan) promoted higher cellular spreading and integrin expression compared to the reciprocal parameters (0.1 mM RGD and 0.025 mmol RGD/mmol RGD grafted hyaluronan respectively, *i.e.* high concentration of RGD vs. low density of

clustering). One limitation to our study is that we did not explicitly explore this relationship within our experiments. Further work is therefore required to assess the clustering effect of the new multivalent dendrimers, explore the potential influence of higher generations of dendrimers and expand the repertoire of dendrimers to other biofunctionalities.

In the rheological results, the lack of hydrogel formation for the blend compared to the derivative poly(*N*-isopropylacrylamide) and hyaluronan could be attributed by the immiscibility of the phases at 37 ºC and weak physical entanglement of the polymers. The lower elastic modulus reached for the thermoresponsive hyaluronan was attributed to degradation of the hyaluronan during the CuAAC [92]. The biomaterial displayed a shear thinning property appropriate for cell encapsulation and injection (Fig. 18) which has also been previously shown [27]. The addition of OEG-based dendrimers bearing RGDS or DGSR peptides at the concentration used in this study did not influence significantly the examined rheological properties of the hyaluronan-based thermoresponsive hydrogels compared to the Hyal-pa containing hydrogel. Hence, the biological activities could be compared independently to the rheological properties.

The cell-hydrogel constructs were macroscopically stable for the duration of the study. We assumed that the polymer network stiffness remained relatively constant over the period of cell culture and therefore the viability was related to the presence of functional dendrimers. This data compares well with another study which showed an improved MSC viability in a poly(ethylene glycol) hydrogel grafted with 5 mM of a linear RGDS peptide sequence compared to the same hydrogel but without RGDS [86]. In addition, the results suggest that the molecular presentation of the RGDS peptides in a 3D hyaluronan-based hydrogel microenvironment is crucial for the efficacy of MSCs [80].

The spherical morphologies of the encapsulated cells were not significantly affected in any of the hydrogels after 7 or 21 days of culture, nor in basal or osteogenic media. This data correlated well with *in vivo* and *in vitro* studies using non-degradable hydrogels which impeded cell spreading [16, 27, 99].

The persistent cell dispersion and pericellular matrix deposition observed in the toluidine blue histology sections over time indicates that the thermoresponsive hydrogels were not degraded in the conditions used (Fig. 21). This finding corroborates another report that

determined photocrosslinked hyaluronan hydrogels with varying crosslinking density can actually inhibit ECM production and distribution throughout the polymer scaffold [13]. Furthermore, another report on a hyaluronan hydrogel incorporating a RGD peptide and a matrix metalloprotease (MMP) sensitive peptide permitted the spreading of cells via the enzymatic degradation of the MMP sensitive site [100]. Indeed, the presence of MMP degradable crosslinks in the reported acrylated hydrogel containing RGD, with storage moduli at 300 to 1300 Pa (for 10 kDa and 50 kDa hyaluronic acid chains respectively), permitted cell spreading in contrast to the hydrogel without a MMP sensitive peptide site. Therefore, we posit from our results that the lack of degradation of the Hyal-pN derivative *in vitro*, prevented substantial changes in cell morphology. Cell protrusions were observed to a larger degree for one hMSC donor encapsulated in the RGDS dendrimer containing hyaluronan hydrogel. However, this observation was not seen in the other hMSC donors.

In a previously reported degradable hyaluronan microenvironment, clustering of RGDS was reported to have no role in the differentiation of encapsulated mouse MSCs in basal media whereby CD105, a marker for stemness, decreased independently of the RGDS presentation [81]. In our experiment, mainly a strong up-regulation of hCOL2 was observed for all hydrogel compositions, media, and time points, notably in the presence of RGDS integrin binding epitopes after 7 days of osteogenic culture. These results correlate well with a similar study [101] and suggest that the hyaluronan matrix provides an environment that permits chondrogenesis. The lack of osteogenic response in ODM media, no up-regulation of hALP or hRUNx2, can possibly be attributed to the lack of degradation sensitive sites within the network [15] which subsequently restricted the cellular morphologies to maintain a rounded state. Exogenous hyaluronan in 2D culture has been reported to play a role in osteogenic differentiation of MSCs under osteoinductive conditions with hALP and hCOL1 gene expression being inhibited, hSOX9 being slightly increased at 7 days, while, interestingly, mineralization also increased by 21 days [102]. The initial trend of gene expression was similarly found in the thermoresponsive hyaluronan 3D environment, but the mineralization was not evidenced.

5.4. In vivo evaluation of the dendrimer decorated thermoresponsive hydrogel in a murine animal model

The thermoreversible hyaluronan based hydrogel was evaluated for its *in vivo* efficacy as an osteoinductive material when combined with BMP-2 and hMSCs. The reaction method employed in this study created a hydrogel that was a more suitable carrier for cells and drugs. The improved method eliminated the necessity of copper catalysts in the reaction. This change was biologically advantageous as copper is highly toxic to cells. Furthermore, the lower viscosity compared to the CuAAC formulation made it a better vehicle for delivering cells or proteins.

Postoperative observations of the mice found that there were mixed inflammatory responses at the implant sites. Three mice had no inflammation at any of the implant sites. Two mice showed minimal redness on at least one injection site, whereas four other mice had one abscess present. Of the mice with the latter adverse response three were located on the left flank (*i.e.* without cells) and one on the right (*i.e.* with cells). Furthermore it was observed that any mouse with an adverse response such as an abscess, no mineralization was observed via x-ray scanning. Mouse 14043 was injected with Hyal-pN, BMP-2, and hMSCs, had no adverse reaction to the injection of the implants, and subsequently showed significant mineralized tissue at the implant sites. Moreover, denser tissue was observed in the implant containing cells than the adjacent implant without. The mineral-dense tissue was concentrated at the periphery of the implant likely due to the proximity of the vascularization of the dermal tissue. However, most of the implants showed significantly less amount of radio-opaque materials. It is possible that the mixed inflammatory responses of the implant sites correlate with the depressed ectopic bone stimulation. In order to further understand the level of osteogenic response, histological analysis of the implant cross-sections are necessary. Furthermore, more repeats of the experiment are necessary in order to nullify the significance of the individual inflammatory response on the results. Future studies could also attempt to examine the vascularization of the implants.

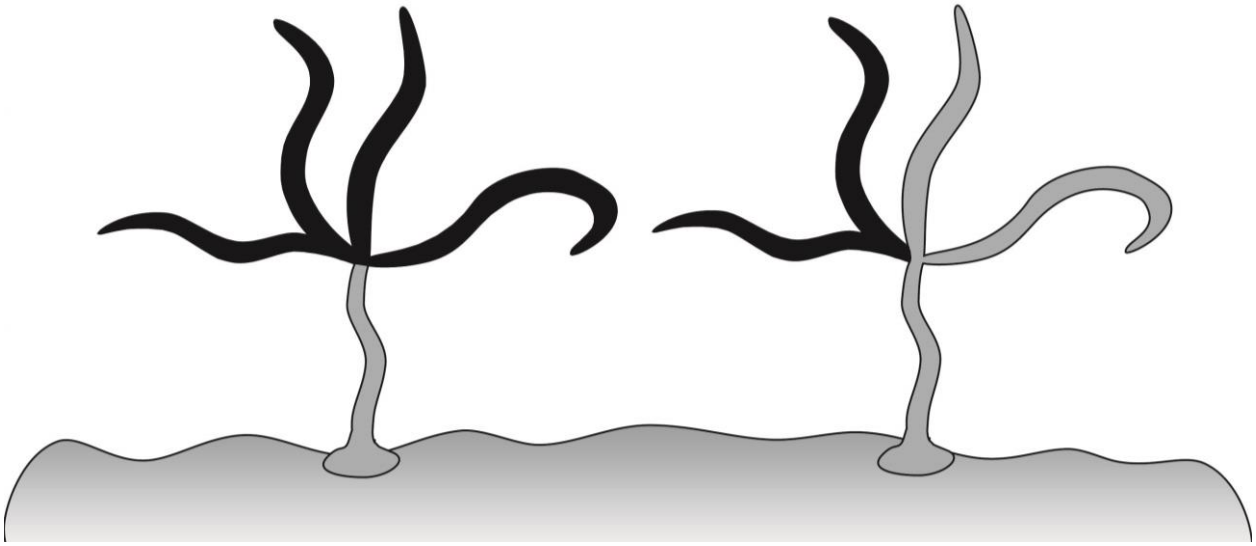

Chapter 6 – Conclusions

6.1 Synthesis of the thermoresponsive injectable hydrogel

The CuAAC reaction is a powerful method with the versatility to conjugate a milieu of biologically significant molecules to decorate polymer scaffolds. The CuAAC efficiency is typically near 100% for small molecules [32], but is lower in the case of the Hyal-pN reaction. Nevertheless, the $CuBr(PPh_3)_3$ is more efficient than the CuAsc catalyst system for the synthesis of poly(*N*-isopropylacrylamide) derivative of hyaluronan. Steric hindrance inherent in the larger macromolecular reaction is likely the culprit. This catalyst merits further examination for its ability to conjugate macromolecules and produce responsive hydrogels for drug delivery and tissue engineering applications. However, the sensitivity of hyaluronan to degrade in the presence of aqueous solutions of copper and ascorbic acid could pose problems for scaling up the

reaction. Furthermore, the trace amounts of the residual copper in the synthesized polymer could result in cytotoxicity during *in vitro* testing. Furthermore, hyaluronic acid is sensitive to degradation by copper and ascorbic acid. Therefore, newer methods such as the direct amidation of poly(*N*-isopropylacrylamide) to hyaluronic acid may be a viable copper-free alternative.

6.2 In vitro assessment of the dendrimer decorated drug releasing injectable hydrogel

We have designed, developed and characterized dendrimers which have been augmented with terminal peptide binding sequences and covalently grafted to an injectable hydrogel. The dendrimer decorated hydrogels attenuated the release BMP-2 and TFG-β1 through affinity-based interactions of the functionalized peptide binding sequences and the GFs. However, it is important for future studies to determine the reason for the non-specificity of the peptide sequences. One possibility is that heparin binding sequences are integrated into the primary structure of both cytokines, thus leading to the resultant non-specificity. The release studies highlight the potential of incorporating these unique types of dendrimers into a biomaterial platform with the goal to guide cells towards direct or endochondral ossification. Further experiments could examine the presentation of the terminal peptide sequences, changing the spacing of the bioactive molecules by altering the lengths of the branches. Moreover, the efficacy of the dendrimers could be tested in comparison to linear oglioethylene glycol molecules featuring the same terminal peptide sequences. Additional future *in vitro* work could test a cocktail of loaded agents such as BMP-2, TGF-β1, and antibiotics examining the individual sustained release profiles of each agent. For example, non-fouling polymers networks could be covalently modified with the peptide binding dendrimers to selectively bind and augment the release of BMP-2 or TGF-β1, or both, in order to add a dynamic or sustained release from a biomaterial scaffold.

6.3. In vitro evaluation of the dendrimer decorated hydrogels as a cell carrier-scaffold

In this study, we incorporated singular, multivalent dendrimers functionalized with integrin binding peptides which allowed us to strictly manipulate the spatial presentation of the biofunctionality inside our injectable hyaluronan-based hydrogel scaffolds. We fully

characterized the materials and carried out a three week in vitro osteogenic culture of encapsulated hMSCs examining the viability, morphology, and genetic and protein expression influenced by the RGDS dendrimer coupled hydrogels. We were able to show that this material maintains hMSC viability and remains stable over the culture period. The presence of the RGDS dendrimers showed promising trends for improved viability and expression of hSOX9 and hCOL2 which makes this dendrimer a promising tool to develop well-defined and controlled environments for cell-material interaction studies in decorated hydrogel platforms in vitro. Moreover, the potential of employing a molecular toolbox of peptide functionalized dendrimers in an injectable hydrogel to drive host tissue repair could be explored further for potential applications in the field of musculoskeletal repair. Additional future work could directly compare the influence of RGDS terminated linear oglioethylene glycol polymers versus dendrimers featuring various branch lengths which in essence affect the clustered presentation of the peptides to cells. Furthermore, the cellular viability and response to osteogenic factors could be improved by changing the Hyal-pN synthesis method, for example, by bypassing the copper-based CuAAC reaction and employing a direct amidation process.

6.4. In vivo evaluation of the thermoresponsive hydrogel in a murine animal model

Injected hyaluronic acid hydrogels with or without hMSCs did not form mineralized tissue in a subcutaneous mouse model after 4 weeks as assessed by μCT analysis. However, BMP-2 and BMP-2 + hMSCs loaded hyaluronic acid hydrogels did show ectopic bone formation after 4 weeks. Promising results were seen in one subject where radio-opaque material consistent with mineralized tissue was observed. Also, the amount of mineralization as assessed by μCT was relatively inconsistent and highly dependent on the animal. Histological results of all specimens are necessary in order to fully characterize the osteogenic capacity, tissue response to the biomaterial, hMSCs viability and biodegradation of the thermoresponsive hyaluronan.

6.5. General conclusions

Regenerative medicine is becoming more apt to the complicated task of healing musculoskeletal defects. The advent of smart biomaterials is giving medicine the medium to capably mimic the physical mechanics and biochemical signaling necessary to heal damaged

tissue. We have shown in this thesis that the hyaluronan hydrogel carrier augmented with dendrimers, with their capacity to present active peptide epitopes at a high density, can strongly influence molecular signaling of cells and modulate the release of loaded growth factors. The hydrogel alone is an excellent vehicle for the safe and local delivery of drugs and cells. Enhancing the molecular architecture of the biomaterial with peptide epitope modified dendrimers furthers the hand of control over how the presentation of specific peptides can drive biological outcomes. Thus, the next phase of musculoskeletal regeneration therapies that are clinically relevant should employ the nanotechnology-inspired molecular toolbox of dendrimers.

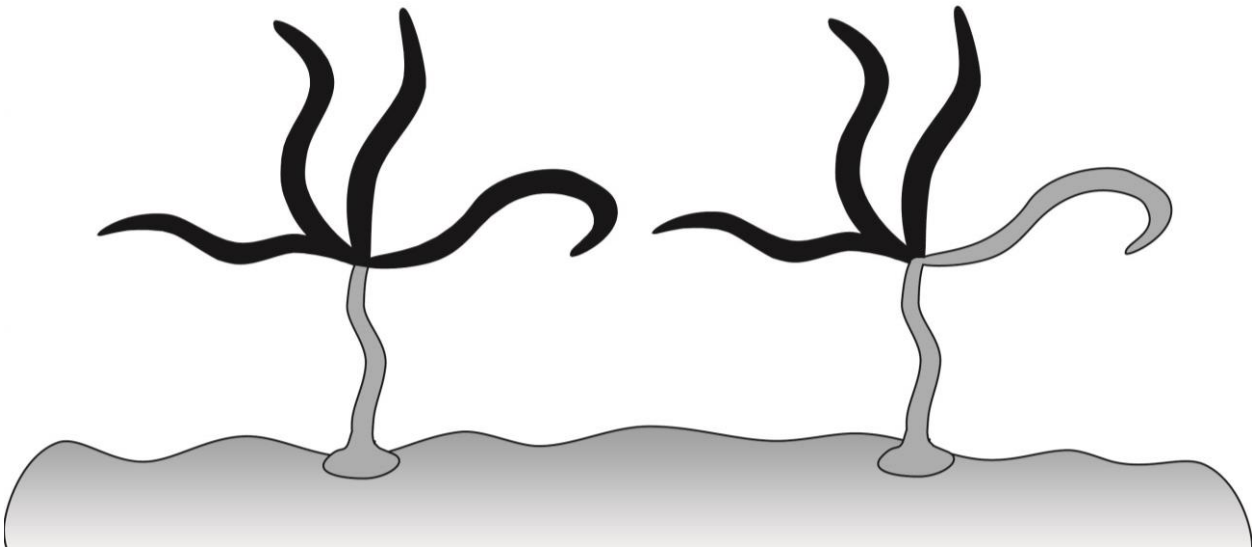

Appendix A: Resumen en castellano

A.1. Introducción

A.1.1.Biomateriales "inteligentes" para aplicaciones médicas regenerativas

El cuerpo por si solo no puede curar todas las heridas. Por ejemplo, fracturas no consolidadas u osteosarcomas que producen defectos óseos, requieren de una intervención quirúrgica para ayudar al cuerpo a curar esas heridas. Cada año millones de Estadounidenses padecen de una lesión musculo-esquelética, lo que comporta centeneras de billones de dólares en costes médicos, cirugías, rehabilitación física y pérdidas de salarios [1, 2]. Además, los pacientes de lesiones musculo-esqueléticas corren riesgos derivados de una cirugía como pueden ser una infección o

un rechazo a un implante. Ello comporta nuevas intervenciones y, en consecuencia, un aumento de la morbilidad del paciente. Por tanto, se está evidenciando cada vez más la necesidad de nuevos tratamientos médicos avanzados, clínicamente relevantes, en este sentido.

La medicina regenerativa utiliza distintos enfoques hacia procesos complejos de curación de lesiones: uno de ellos es la restauración de la función normal de tejidos mediante la combinación de biomateriales con células y fármacos [3].

Los Biomateriales son sistemas naturales o sintéticos inspirados en polímeros compuestos a base de cerámica u otros compuestos que ayudan al proceso de curación del cuerpo proveyendo un entorno adecuado para el crecimiento celular [4] del mismo. Los materiales a base de polímeros pueden hincharse en soluciones acuosas y reaccionar *in situ* para convertirse en hidrogeles.

Hablando de modo general, estos materiales aplicados al campo de la medicina regenerativa requieren de un proceso quirúrgico para su implantación. No obstante, una nueva clase de biomateriales puede introducirse mediante laparoscopia (con una inyección) en forma de líquido que cambiarán de estado al exponerse a un nuevo entorno. Es por esto que estos biomateriales pueden apodarse "inteligentes" puesto que tienen un gran potencial de adaptación y aplicaciones clínicas muy relevantes. Recientemente, se han encontrado polímeros naturales en el cuerpo humano lo que ha sido de gran inspiración para la creación de biomateriales que juegan un rol activo en los procesos de regeneración. Un polímero en concreto, el ácido hialurónico, está prácticamente omnipresente en las distintas funciones del cuerpo humano, y es un componente muy importante en el desarrollo de tejido y procesos de curación/cicatrización (superficial o profunda).

Pero si nos centramos en lo que ahora pueden hacer los biomateriales sabemos que son un material capaz de guiar tareas complejas en procesos de regeneración tisular. No obstante, la investigación en los laboratorios continua explorando este mundo inspirada por la búsqueda de soluciones para mejorar, todavía más, esta función de guía en el proceso de regeneración tisular. Hemos de ser capaces de controlar la entrega de agentes bioactivos en los microambientes que se encuentran a niveles en los que las células operan. Algunos investigadores han intentado aumentar la funcionalidad bioquímica de las estructuras de los polímeros, o "andamios" (en la literatura inglesa *scaffold*), mediante el control de la presentación espacial de moléculas

bioactivas jugando con clústeres de secuencias de péptidos, pero sin tener un alto control a escala nanoscópica. Ahora, para el problema sobre el control de la arquitectura molecular del microambiente de un biomaterial la nanotecnología tiene una solución. Se trata de los dendrímeros, moléculas sintéticas ramificadas, simétricas, monodispersas y con forma globular. Más importante todavía, su estructura inherente mantiene una presentación estricta de los grupos terminales. Hasta este momento, nunca antes se habían mezclado covalentemente dendrímeros con biomateriales para proporcionar un control estricto de la presentación de biomoléculas en el microambiente de "andamio". Esta nueva tecnología (la de los dendrímeros) coloca a los biomateriales en el nicho para la guía de la regeneración ósea.

El objetivo de estas tesis es contribuir al desarrollo de biomateriales inteligentes mediante la combinación de dendrímeros con afinidad por proteínas específicas en una plataforma de biomaterial termorreversible a base de ácido hialurónico. La meta: avanzar en el campo de la regeneración ósea.

A.1.2 Objetivos de la tesis

Los objetivos de esta tesis son:

e. Sintetizar y caracterizar un hidrogel portador de ácido hialurónico termorreversible modificado con dendrímeros multivalentes terminados con secuencias de péptidos.
f. Caracterizar *in vitro* la capacidad de este nuevo biomaterial inteligente para que funcione como un sistema de entrega/liberación de fármacos capaz de liberar a nivel local potentes bioactivos como por ejemplo: factores de crecimiento.
g. Caracterizar *in vitro* la capacidad "decorativa" del dendrímero sobre el biomaterial inteligente como sistema dual en el que pueda transportar células a la vez que provea a estas con un microambiente mejorado diseñado para guiar comportamientos que favorezcan la osteogénesis.
h. Llevar a cabo un estudio piloto que caracterice *in vivo* la eficacia del ácido hialurónico termorreversible como liberador de BMP-2 y células mesenquimales estromales humanas para la reparación ósea.

A.1.3 Contribuciones de esta tesis

Esta tesis se ha construido en base a cuatro publicaciones que ya se han publicado o que están siendo revisadas para su publicación.

e. La primera contribución ha sido elaborar una metodología clave para la síntesis de la plataforma de biomateriales inteligentes. Se testaron dos catalizadores a base de cobre por su eficiencia en una reacción de cicloadición azida-alquino, popularmente conocida como una reacción "click". Dentro de estos experimentos se ha caracterizado en un medio acuoso con distintos disolventes el injerto covalente de azida terminado poly(N-isopropylacrylamide (N_3-pN) a ácido hialurónico modificado con propargilamina. Esta serie de experimentos fueron publicados en un artículo titulado, *Copper catalyst efficiency for the CuAAC synthesis of a poly(N-isopropylacrylamide) conjugated hyaluronan* (*Seelbach et al. Clinical Hemorheology and Microcirculation. 2015.).*

f. La segunda contribución se ha centrado en la caracterización *in vitro* de la capacidad de este biomaterial como sistema de liberación de fármacos. La reacción de cicloadición azida-alquino catalizada por cobre (CuAAC) se tradujo en una síntesis de Hyal-pa covalente modificado con dendrímeros que fueron diseñados para unirse a proteínas morfogenéticas tipo 2 de hueso humano recombinadas (BMP-2) i factores de crecimiento humanos recombinados beta 1 (TGF-β1) los cuales fueron en consecuencia combinados con el hyaluronan copolímero (Hyal-pN). Dos estudios *in vitro* sobre la liberación de BMP-2 por un lado y TGF-β1 por el otro, fueron llevados a cabo durante una semana para así poder comprobar la mecánica de liberación del dendrímero modificado. Este trabajo se ha escrito en forma de artículo bajo el título *Peptide binding dendrimer decorated injectable hyaluronan hydrogels modulate the controlled release of BMP-2 and TGF-β1*, y se ha depositado para revisión en el Journal of Controlled Release.

g. La tercera contribución examina el potencial del Hyal-pN combinado con dendrímeros vinculantes afines a la integrina como andamios adecuados para el cultivo osteogénico *in vitro* de células madre humanas mesenquimatosas (hMSCs). Se analizaron los constructos de células-andamiaje para la viabilidad celular y la morfología, marcadores

de expresión osteogénica y desarrollo tisular. La capacidad del biomaterial para guiar la osetogénesis fue publicada en forma de artículo bajo el título *Multivalent Dendrimers Presenting Spatially Controlled Clusters of Binding Epitopes in Thermoresponsive Hyaluronan Hydrogels* [5].

h. La cuarta contribución examina la eficacia del biomaterial *in vivo* en un ratón como modelo animal. El biomaterial Hyal-pN, que fue sintetizado bajo un método mejorado para eliminar la necesidad utilizar el cobre como catalizador, fue cargado con hMSCs y BMP-2 y luego inyectado subcutáneamente en los pliegues de la piel de ratones. Las condiciones de los animales y los implantes fueron observados postoperatoriamente durante un período de un mes. Los implantes fueron extirpados después de sacrificar los animales y se midió la formación de hueso ectópico mediante rayos X. Esta compilación de experimentos está planeada para ser publicada este 2015.

A.2. Discusión

A.2.1 Síntesis de un hydrogel inyectable termosensible

La reacción CuAAC realizada con el pre-catalizador Cu^{+2}, $CuSO_4 \bullet 5H_2O$, y un agente reductor, ácido ascórbico, en agua, se parecía estrechamente al condición de degradación oxidativa hialuronana del sistema Weissberger, Cu^{+2} y ácido ascórbico podrían causar la degradación hialuronana en presencia de oxígeno [35, 91]. Por esta razón el $CuBr(PPh_3)_3$ fue escogido como una alternativa igual de rápida y efectiva como activo catalizador a concentraciones significativamente bajas como el CuAsc [37]. A pesar de la limitada solubilidad en el agua, el $CuBr(PPh_3)_3$ es más eficiente conjugando N_3-pN a Hyal-pa que el CuAsc, especialmente a una verdadera concentración para el catalizador. Curiosamente, se midió un aumento del contenido en cobre por peso de Hyal-pN en la reacción utilizando $CuBr(PPh_3)_3$.

Este aumento "contra-intuitivo" hipotéticamente se puede atribuir a la baja solubilidad del $CuBr(PPh_3)_3$ en las soluciones de diálisis y la pérdida de Hyal-pa (sin reaccionar) y N_3-pN, lo que parece conducir a un aumento aparente de cobre en la muestra seca . Por lo tanto, se necesita un método de extracción de cobre mejorado para $CuBr(PPh_3)_3$. Además, la reacción CuAAC realizada clásicamente en la mezcla DMSO:agua usando $CuBr(PPh_3)_3$ no fue eficaz,

posiblemente debido a la escasa solubilidad de N_3-pN en este disolvente. El fracaso de la conjugación de N_3-pN a Hyal-pa en DMSO:agua debido a la insolubilidad de pN se confirmó a causa de la ausencia de una LCST en el barrido de temperatura. De hecho, esta composición se comportó de manera similar a una solución pura de Hyal-pa 15% (wt/vol), lo que apoya aún más el fracaso de la reacción CuAAC en esta mezcla de disolventes en particular.

La comparación de los perfiles reológicos de las otras dos condiciones de conjugación, indicó que la solución de Hyal-pN preparada usando $CuBr(PPh_3)_3$ presentó un aumento más pronunciado de temperatura inducida de módulos de elasticidad en comparación con el CuAsc. La diferencia de la densidad de injerto igual a 0,5 mol% podría ser la causa de este comportamiento; sin embargo, esto parece una variación bastante escasa teniendo en cuenta que la DG de variación del 5 mol% previamente ha demostrado tener un efecto mínimo del módulo elasticidad de soluciones Hyal-pN [16]. Otra hipótesis es que la degradación de la cadena principal de ácido hialurónico se produce predominantemente en la reacción catalizada CuAsc según sugiere el menor % (wt) de rendimiento. El tamaño degradado de Hyal-pN y la consecuente forma en solución puede ser diferente para un no degradado Hyal-pN. Las macromoléculas cepillo de menor tamaño podrían interactuar más en la solución que grandes macromoléculas globulares y el consecuente aumento de la viscosidad de la solución. Esto no se había observado anteriormente para HA como cadena principal de 1,6 MDa y 250 kDa [29]. Esto sugeriría una extensa degradación del conjugado de ácido hialurónico sintetizado por CuAsc en la línea con los resultados reportados [92]. La falta de métodos que permiten la caracterización de la estructura macromolecular HA-pN deben ser abordados con el fin de confirmar esta hipótesis.

A.2.2. Evaluación in vitro del hidrogel del dendrímero "decorado" liberador de fármacos e inyectable

Hyal-pN fue sintetizado con tamaños de pN de 9, 16, o 21 kDa pN con similares grados de sustitución a través de todos los lotes. Las cadenas pN se sometieron a un colapso hidrofóbico transitorio con un aumento en la temperatura, "enredando" así los polímeros para convertirlos en un material cohesivo. El tamaño efectivo de este polímero afectó posteriormente el carácter estable y viscoelástico de los polímeros en PBS. Entonces, HpN9 mostró ligeros cambios en G' y G" por encima de 27,5 ºC y experimentó una reticulación física pobre por valores de G' que nunca se cruzaron en los valores G". En la solución, HpN16 y HpN21 se comportaron como

líquidos viscosos debajo de sus temperaturas de inflexión, con valores similares de G" a 20 ºC, comportamiento similar al ácido hialurónico no adulterado. Mientras tanto, por encima de esta temperatura, el G' suplantó el valor G" lo que indicaba la formación del hidrogel estable. Además se observó que en el intervalo de M_w de pN probado, los materiales no experimentaron una contracción macroscópica significativa. La adición de dendrímeros a Hyal-pN no influyó significativamente en las características reológicas. El perfil de liberación de BMP-2 y TGF-β1 de los hidrogeles cargados presentaron inicialmente una explosión de proteína que alcanzó su punto máximo después de 4 horas, seguido de una liberación gradual después. No se observó ninguna diferencia significativa con respecto al tamaño de pN, a excepción de una ligera tendencia que muestra una liberación disminuida de BMP-2 en 4 h con un aumento de tamaño. Además, una cantidad significativa de proteínas no se puedo medir en el medio probablemente porque estaban ligados al Hyal-pN incluso al PBS dopado con BSA [49, 51]. Este patrón también era cierto para HpN9 a pesar de que no se formó un hidrogel estable.

La liberación sostenida de fármacos a partir de depósitos de hidrogeles se rige por varios factores, incluyendo la difusión de gradiente, la unión no covalente (es decir, relaciones de Lewis ácido-base), atrapamiento físico (por ejemplo, la densidad de reticulación), y la concentración inicial cargada en el sistema [48, 51, 93]. Así, la naturaleza de "andamio" del polímero es importante [49, 94]. Kim y Valentini hipotetizaron que la liberación de BMP-2 a partir de un hidrogel a base de ácido hialurónico es atenuada por la interacción electrostática de los grupos de ácidos carboxílicos cargados negativamente del polisacárido y la amina primaria rica BMP-2 , en otras palabras, el sistema ácido - base de Lewis [60]. En este caso se recuperó sólo el 32% de la proteína total cargada, mientras que el 88% fue liberada de una esponja de colágeno I control. La observación completa de la liberación de proteínas a partir hidrogeles de ácido hialurónico acido base conjugados con dendrímeros nunca llegó a las cantidades entregadas a partir de los hidrogeles de control. También es posible que los dendrímeros puedan retrasar la liberación de los fármacos [53] y se entregue una liberación prolongada y sostenida durante un período prolongado dependiendo del tiempo de degradación del ácido hialurónico conjugado. Sin embargo, la retención inevitable de la proteína dentro de los biomateriales se ha demostrado relevante para mantener la bioactividad [50], mejorar la invasión celular, y aumentar la generación de marcadores relacionados con los tejidos dentro de los depósitos [49, 60]. Incluso concentraciones extremadamente bajas de BMP-2 localizadas dentro de un hidrogel son suficientes para

programar el microambiente como guía hacia la diferenciación celular [95]. Con el fin de aislar los efectos de los dendrímeros, hemos desarrollado una metodología inspirada en Kolambkar *et al*. y Kimura *et al*. y hemos cargado los hidrogeles con BMP-2 o TGF-β1 suplementados con 0,1% de BSA y 4 mM de HCl con el fin de desalentar la unión no específica con el biomaterial [50, 51]. Las secuencias de unión de péptidos antes mencionadas [53, 96, 97], fueron identificadas previamente por presentación de fagos. Además la presentación de estas secuencias de unión previamente han demostrado retener y atenuar la liberación de estas citoquinas [53, 96]. En nuestro caso, aumentando la arquitectura molecular de la plataforma de liberación de fármacos con dendrímeros de unión de péptidos también afectó significativamente la liberación de BMP-2 y TGF-β1. De acuerdo con los resultados anteriores [5], la influencia de los dendrímeros en la entrega de las citocinas en PBS suplementado con BSA se comparó con Hyal -PN que contenía Hyal -pa, el precursor de los conjugados Hyal-YPV y Hyal-LPL.

En este estudio, hemos demostrado la capacidad del péptido que porta dendrímeros para atenuar la liberación de proteínas desde los almacenes de Hyal-pN, causando una fuerte disminución en la fase de explosión, así como una concentración final inferior a 7 días. La relativamente alta liberación global de la proteína de los depósitos sin dendrímero en comparación con composiciones modificadas con dendrímeros se puede ver claramente para HpN16 y HpN21. Se verificó la especificidad de los epítopos de péptidos sintetizados mediante la realización de estudios de liberación análogos mediante la carga de BMP-2 en depósitos que contienen Hyal-LPL (es decir, hialuronano de unión a TGF-β1) péptido, y viceversa. Curiosamente en todos los escenarios, los dendrímeros eran al menos eficaces en la retención de los factores de crecimiento lo que sugiere que el comportamiento de unión de estos péptidos no es específico a BMP-2 y TGF-β1 o que la presentación de estos péptidos en la punta de la estructura del dendrímero ramificado hace que la de los péptidos menos específica. Teniendo en cuenta que ambos péptidos están diseñados para tratar los sitios de unión a heparina y que ambas proteínas son miembros de la superfamilia TGF de proteínas, la primera hipótesis es más probable. En estudios futuros se podría examinar más de cerca la unión dendrímero-péptido así como su especificidad empleando proteínas fuera de la superfamilia TGF vinculante. Además, los polímeros no incrustantes tales como PEG se pueden aumentar para unirse selectivamente sólo a las proteínas deseadas con la incorporación de un dendrímero de unión de epítopo de

péptido modificado para aumentar la liberación del fármaco que quiera añadir una liberación dinámica o sostenida en un biomaterial de "andamio" cargado.

A.2.3. Evaluación in vitro del hidrogel de dendrímero "decorado" como célula portadora-andamio

La capacidad de microambientes diseñados con precisión a medida para células madre es extremadamente importante tanto para la comprensión de su comportamiento en una matriz extracelular simplificada y controlada como para el desarrollo de terapias basadas en células madre clínicamente relevantes tales como la ingeniería de tejidos del hueso [15, 68, 98]. En esta parte del trabajo, hemos desarrollado un biocomponente novel, un hidrogel inyectable que incorpore una matriz de hialuronano bioactivo termosensible y dendrímeros que cuentan con presentaciones en clúster de un péptido bioactivo. Dendrímeros singulares (como únicos), polivalentes funcionalizados con cuatro péptidos RGDS y un resto azida fueron sintetizados y caracterizados con éxito. El injerto de estas macromoléculas bien definidas sobre una cadena principal de ácido hialurónico presentó grupos de epítopos de unión con un grado excepcional de control espacial que cuando se combinó con el polímero termorreversible produjo un sistema de entrega altamente funcionalizado, un sistema inyectable que formó una plataforma de hidrogel estable tras un aumento de la temperatura.

En un informe reciente de Lam *et al.*, péptidos que contenían RGD se injertaron a modo random o agrupados en hidrogeles de ácido hialurónico acrilados en un intervalo de concentración de 0,01 a 1 mM péptido [81]. Utilizando MSCs de ratón encapsuladas, se encontró en un estudio *in vitro* que la concentración más baja de RGD (10 μM), se aparejó con la mayor densidad de clúster péptido (1,8 mmol RGD / mmol RGD hialuronano injertado) promoviendo una difusión celular superior así como expresión de la integrina en comparación con los parámetros recíprocos (0,1 mM RGD y 0,025 mmol RGD / mmol RGD ácido hialurónico injertado, respectivamente, es decir, alta concentración de RGD vs. baja densidad de agrupación). Una limitación de nuestro estudio es que no exploramos explícitamente esta relación dentro de nuestros experimentos. Por lo tanto, se requiere trabajo adicional para evaluar el efecto del agrupamiento de los nuevos dendrímeros polivalentes, explorar la influencia potencial de mayores generaciones de dendrímeros y ampliar el repertorio de dendrímeros a otras biofuncionalidades.

En los resultados de reología, la falta de formación de hidrogel en la mezcla en comparación con el derivado de poly(*N*-isopropylacrylamide) y hialuronano puede ser atribuido por la inmiscibilidad de las fases a 37 ºC y el débil "enredo" físico de los polímeros. El módulo elástico inferior alcanzado por el hialuronano termosensible se atribuyó a la degradación del ácido hialurónico durante la CuAAC [92]. El biomaterial muestra una propiedad reductora del corte apropiada para la encapsulación de células y la inyección (Fig. 18), que también se ha demostrado previamente [27]. La adición de los dendrímeros de OEG que llevan RGDS o péptidos DGSR a la concentración utilizada en este estudio no influyó significativamente en las propiedades reológicas examinadas en los hidrogeles termosensibles a base de ácido hialurónico en comparación con el Hyal-pa que contiene hidrogel. Por lo tanto, las actividades biológicas podrían ser comparadas de forma independiente a las propiedades reológicas.

Los constructos de células de hidrogel eran macroscópicamente estables durante la duración del estudio. Asumimos que la rigidez de la red del polímero se mantuvo relativamente constante durante el período de cultivo de células y por lo tanto la viabilidad estaba relacionada con la presencia de dendrímeros funcionales. Estos datos se pueden comparar con otro estudio que mostró una viabilidad mejorada MSC en un hidrogel de poly(ethylene glycol) injertado con 5 mM de una secuencia de péptido lineal RGDS en comparación con el mismo hidrogel pero sin RGDS [86]. Además, los resultados sugieren que la presentación molecular de los péptidos RGDS en un microambiente 3D de hidrogel a base de hialuronano es crucial para la eficacia de las MSC [80].

La morfología esférica de las células encapsuladas no se vio afectada significativamente en ninguno de los hidrogeles después de 7 ó 21 días de cultivo, ni en medios basales o osteogénicos. Estos datos se correlacionan bien con el *in vivo* y con estudios *in vitro* utilizando hidrogeles no degradables que impiden la propagación de células [16, 27, 99].

La dispersión celular persistente y deposición de matriz pericelular observadas en la histología de toluidina azul a lo largo del tiempo indica que los hidrogeles termosensibles no se degradan en las condiciones utilizadas (Fig. 21). Este hallazgo corrobora otro informe que determinó que hidrogeles de ácido hialurónico fotoentrecruzado con diferentes densidades de reticulación en realidad podrían inhibir la producción y distribución de ECM en todo el "andamio" de polímero [13]. Además, otro informe sobre un hidrogel hialuronano que incorporaba

un péptido RGD y una matriz de metaloproteasa (MMP) sensible al péptido, permitió la propagación de las células a través de la degradación enzimática del sitio sensible del MMP [100]. De hecho , la presencia de reticulaciones degradables de MMP en el hidrogel acrilado reportado que contiene RGD, con módulos de almacenamiento a 300-1300 Pa (de 10 kDa y 50 kDa cadenas de ácido hialurónico, respectivamente), permitió la propagación de células en contraste con el hidrogel sin un sitio péptido-sensible para MMP. Por lo tanto, postulamos de nuestros resultados que la falta de degradación del derivado de Hyal-pN *in vitro*, impidió cambios sustanciales en la morfología celular. Salientes (como protrusiones) de las células se observaron en un grado más grande para un donante de hMSC encapsulado en el dendrímero RGDS que contenía hidrogel hialuronano. Sin embargo, esta observación no se observó en los otros donantes de hMSC .

Anteriormente, en un microambiente hialuronano degradable, se informó de que la clústeres de RGDS no tenían ningún papel en la diferenciación de las MSCs de ratón encapsuladas en medios basales con lo que CD105, un marcador para la capacidad de diferenciarse, disminuyó de forma independiente de la presentación del RGDS [81]. En nuestro experimento, se observó principalmente una fuerte sobre regulación de hCOL2 para todas las composiciones, los medios y los puntos de tiempo del hidrogel, especialmente en presencia de epítopos de unión RGDS de integrina después de 7 días de cultivo osteogénico. Estos resultados se correlacionan bien con un estudio similar [101] y sugieren que la matriz de hialuronano proporciona un entorno que permite la condrogénesis. La falta de respuesta osteogénica en medios ODM, no sobre regulación de hALP o hRUNx2, posiblemente podría ser atribuida a la falta de degradación de los sitios sensibles dentro de la red [15], que limita posteriormente las morfologías celulares para mantener un estado redondeado. Hialuronano exógeno en cultivo 2D fue reportado como capaz de desempeñar un papel en la diferenciación osteogénica de las MSC en condiciones osteoinductoras con HALP y hCOL1 con expresión génica inhibida, hSOX9 aumentó ligeramente a los 7 días, mientras que, curiosamente, la mineralización también aumentó en 21 días [102]. La tendencia inicial de la expresión de genes se encontró de manera similar en el entorno 3D hialuronano termosensible, pero la mineralización no se evidenció.

A.2.4. Evaluación in vivo *del hidrogel termosensible en un ratón como modelo animal.*

El hidrogel hialuronano termorreversible se evaluó por su eficacia *in vivo* como un material osteoinductivo cuando se combina con BMP- 2 y hMSC. El método de reacción empleado en este estudio creó un hidrogel que era un portador más adecuado para las células y fármacos. Ese método mejorado elimina la necesidad de catalizadores de cobre en la reacción. Este cambio era biológicamente ventajoso ya que el cobre es altamente tóxico para las células. Además, la viscosidad más baja en comparación con la formulación CuAAC hizo de mejor vehículo para la entrega de las células o proteínas.

Observaciones postoperatorias de los ratones revelaron que había respuestas inflamatorias mixtas en los lugares del implante. Tres ratones no tenían ninguna inflamación en ninguno de los sitios de implante. Dos ratones mostraron un mínimo enrojecimiento en al menos un lugar de introducción de la inyección, mientras que otros cuatro ratones tenían un absceso presente. De los ratones con la última respuesta adversa, tres se encuentran en el flanco izquierdo (es decir, sin células) y una a la derecha (es decir, con las células). Además se observó que en cualquier ratón con una respuesta adversa tal como un absceso, no fue observada una mineralización a través de la exploración de rayos x. Al ratón 14043 le fue inyectado Hyal-pN, BMP-2, y hMSCs, y no tuvo ninguna reacción adversa a la inyección de los implantes, y posteriormente mostró tejido mineralizado significativo en los sitios de implante. Por otra parte, el tejido más denso se observó más en el implante que contenía células que en el implante adyacente sin células. El tejido denso mineral, se concentró en la periferia del implante probablemente debido a la proximidad de la vascularización del tejido dérmico. Sin embargo, la mayoría de los implantes mostraron significativamente menos cantidad de materiales radio-opacos. Es posible que las respuestas inflamatorias mixtas de los sitios de implante se correlacionan con la estimulación de hueso ectópico deprimido. Para entender aún más el nivel de respuesta osteogénica, el análisis histológico de las secciones transversales de implantes son necesarios. Además, más repeticiones del experimento son necesarias con el fin de eliminar la respuesta inflamatoria individual de los resultados. Los estudios futuros también podrían examinar la vascularización de los implantes.

A.3. Conclusiones

A.3.1. Síntesis de un hidrogel termosensible inyectable.

La reacción CuAAC es un poderoso método que goza de la versatilidad para conjugar un medio de moléculas biológicamente significativas para "decorar" andamios (en la literatura inglesa *scaffolds*) de polímeros. La eficiencia CuAAC está típicamente cerca del 100 % para las moléculas pequeñas [32], pero es inferior en el caso de la reacción Hyal-pN. Sin embargo, el $CuBr(PPh_3)_3$ es más eficiente que el sistema catalizador CuAsc para la síntesis de poly(*N*-isopropylacrylamide) derivado de hialuronano. El impedimento estérico inherente en la reacción macromolecular más grande es probable que sea el culpable. Este catalizador merece un examen más detenido por su capacidad de conjugar macromoléculas y producir hidrogeles que liberen fármacos y su aplicación en ingeniería tisular. Sin embargo, la sensibilidad del hialuronano para degradarse en presencia de soluciones acuosas de cobre y ácido ascórbico podría plantear problemas para la ampliación de la reacción. Además, las trazas de cobre residual en el polímero sintetizado podrían resultar en citotoxicidad durante las pruebas *in vitro*. Además, el ácido hialurónico es sensible a la degradación por cobre y ácido ascórbico. Por lo tanto, los nuevos métodos como la amidación directa de poly(*N*-isopropylacrylamide) a ácido hialurónico pueden ser una alternativa libre de cobre viable.

A.3.2. Evaluación In vitro del hidrogel de dendrímero "decorado" liberador de fármacos e inyectable

Hemos diseñado, desarrollado y caracterizado herramientas únicas a nanoescala llamadas dendrímeros que han sido aumentadas con secuencias de unión de péptidos terminales. Estas macromoléculas tienen un fuerte control sobre la presentación espacial de péptidos de unión basados en afinidad que se presentan en los extremos terminales de las ramas. Encontramos que los dendrímeros de unión a péptidos atenúan la liberación de los GFs. Sin embargo, es un dato importante para futuros estudios para determinar el motivo de la no especificidad de las secuencias de péptidos. Una posibilidad es que las secuencias de unión a heparina se integren en la estructura primaria de ambas citocinas, que conduce a la no especificidad resultante. Los estudios de liberación subrayan el potencial de la incorporación de estos tipos singulares de dendrímeros en una plataforma de biomaterial con el objetivo de controlar la funcionalidad de

"andamio" con precisión nanométrica. Otros experimentos podrían examinar la presentación de las secuencias de péptidos terminales, cambiando la separación de las moléculas bioactivas mediante la alteración de las longitudes de las ramas. Por otra parte, la eficacia de los dendrímeros puede ser probada en comparación a moléculas de oglioethyleno lineal que ofrecen las mismas secuencias de péptidos terminales. Futuros trabajos adicionales *in vitro* podrían probar un cóctel de agentes cargados como BMP-2, TGF-β1, y antibióticos que examinen los perfiles de liberación sostenida individuales de cada agente.

A.3.3. Evaluación in vitro de hidrogeles de dendrímero "decorado" como célula portadora-andamio

En este estudio hemos incorporado dendrímeros singulares, polivalentes funcionalizados con péptidos de unión de integrina lo que nos ha permitido manipular estrictamente la presentación espacial de la biofuncionalidad dentro de nuestros "andamios" a base de hidrogel de ácido hialurónico inyectable. Hemos caracterizado completamente los materiales y durante tres semanas hemos hecho un cultivo osteogénico in vitro de hMSC encapsuladas para examinar la expresión de viabilidad la morfología y genética y la proteína influenciada por los hidrogeles RGDS dendrímero-acoplados. Hemos sido capaces de demostrar que este material mantiene la viabilidad hMSC y permanece estable durante el período de cultivo. La presencia de los dendrímeros RGDS mostró tendencias prometedoras para mejorar la viabilidad y la expresión de hSOX9 y hCOL2 que hace que este dendrímero sea una herramienta prometedora para desarrollar ambientes bien definidos y controlados para estudios de interacción de células de material en plataformas de hidrogel "decoradas" *in vitro*. Por otra parte, el potencial de empleo de una caja de herramientas moleculares de dendrímeros de péptidos funcionalizados en un hidrogel inyectable para impulsar la reparación del tejido anfitrión podría estudiarse más a fondo para posibles aplicaciones en el campo de la reparación musculoesquelética. Trabajos futuros adicionales podrían comparar directamente la influencia de polímeros de RGDS terminados lineales de oglioethylene glicol frente dendrímeros que ofrecen las diversas longitudes de rama que en esencia afectan la presentación de clústeres de los péptidos a las células. Además, la viabilidad celular y respuesta a factores osteogénicos podrían mejorarse cambiando el método de síntesis Hyal-pN, por ejemplo, sin pasar por la reacción CuAAC a base de cobre y empleando un procedimiento de amidación directa.

A.3.4. Evaluación in vivo *del hidrogel termosensible en un ratón como modelo animal.*

Los hidrogeles de ácido hialurónico inyectados con o sin hMSC no formaron tejido mineralizado en un modelo de ratón a nivel subcutáneo después de 4 semanas según la evaluación de análisis μCT. Sin embargo, BMP-2 y BMP-2 + hMSCs que cargaron hidrogeles de ácido hialurónico sí mostraron la formación de hueso ectópico después de 4 semanas. Se vieron resultados prometedores en un tema en el que se observó material radio-opaco consistente con tejido mineralizado. Además, la cantidad de mineralización según la evaluación de μCT era relativamente inconsistente y altamente dependiente del animal. Los resultados histológicos de todos los especímenes son necesarios con el fin de caracterizar completamente la capacidad osteogénica, la respuesta del tejido al biomaterial, la viabilidad hMSC y la biodegradación del hialuronano termosensible.

A.3.5. Conclusiones generales

La medicina regenerativa está cada vez más capacitada para resolver la complicada tarea de sanar defectos musculo-esqueléticos. El advenimiento de los biomateriales inteligentes está dando a la medicina el medio para imitar hábilmente los mecanismos físicos y señalización bioquímica necesarios para curar el tejido dañado. Hemos demostrado en esta tesis que el soporte de hidrogel hialuronano aumentado con dendrímeros, con su capacidad de presentar epítopos de péptidos activos a una densidad alta, puede influir fuertemente en la señalización molecular de las células y modular la liberación de factores de crecimiento cargados. El hidrogel en si mismo es un excelente vehículo para la entrega segura y local de fármacos y células. Ayudando a mejorar la arquitectura molecular del biomaterial con dendrímeros de epítopos de péptidos modificados fomentamos el que podamos tomar el control sobre cómo la presentación de péptidos específicos puede impulsar resultados biológicos. Por lo tanto, en la siguiente fase en terapias de regeneración musculo-esqueléticas clínicamente relevantes deberán emplear “la caja de herramientas moleculares” inspirada en la nanotecnología de dendrímeros.

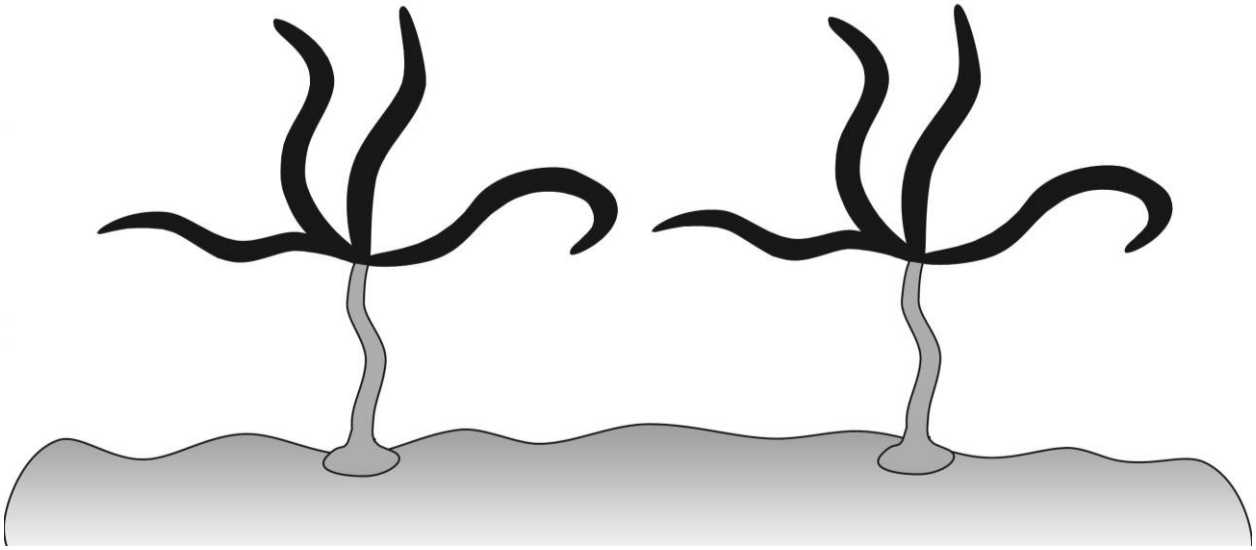

Appendix B: SEM imaging of the Hyal-pN ultrastructure in samples prepared by cryofixation and cryofracture

B.1. Introduction

The preparation of soft heterogenous samples such as tissues for scanning electron microscopy (SEM) is not a straightforward task. Critical point drying (CPD) is a common method to prepare samples for SEM visualization. However, this technique requires the sample to be first dehydrated which alters the structure of the cells and extracellular matrix. Therefore, a process that preserves the ultrastructure of delicate specimens is necessary. Cryofixation is a process by which delicate samples can be preserved via snap-freezing at liquid nitrogen

temperatures (-196 ^{o}C). This process is supposed to freeze the sample before ice crystals can form effectively preserving the fragile micro and nanoscale architecture. Once the samples are frozen, they are then fractured under vacuum, dehydrated, and coated with platinum and carbon. The thermoreversible hydrogel platform that was a focus of this thesis is comprised of hyaluronic acid; this technique could be possibly translated to this biomaterial. Within this study, the Hyal-pN samples dissolved at 15% (wt/vol) in PBS were subjected to three sample preparation methods: hexamethyldisilizane (HMDS), CPD, and cryofixation. The samples were then visualized with the SEM to assess the appropriate strategy for visualizing the unmolested ultrastructure of the hydrogel. Samples prepared by cryofixation were further optimized by manipulating the thickness of the metal-organic composite coating in order to identify the best method to accurately visualize the fine microstructure of the hydrogel.

B.2. Methods

B.2.1. Synthesis of Hyal-pN

Hyal-pN was synthesized via the CuAAC reaction as described in the thesis section 3.3.5. The average molecular weight of the N_3-pN was 27.5 kDa. Polymers were purified by dialysis in 12-14 kDa MWCO membranes for 5 days followed by lyophilization until dry. Additionally Hyal-pN incorporated with RGDS modified dendrimers was synthesized by CuAAC as following the protocol in section 3.3.6 of the thesis.

B.2.2. Dehydration of the Hyal-pN samples for HMDS and CPD preparation

Polymer solutions of Hyal-pN at 15% (wt/vol) were dehydrated stepwise in solutions of 50% - 95% EtOH in water. The replacement of water was finished in 99% EtOH for SEM Preparation (Sigma Aldrich). During the dehydration process, the Hyal-pN hydrogels began to dissolve above 70% EtOH. Therefore, these samples were not further examined for study.

B.2.3 Cryofixation, cryofracture, and visualization of the Hyal-pN sample

The protocols for cryofixation and cryofracture were carried out following an established protocol [103]. Prepared polymer solutions of Hyal-pN at 15% (wt/vol), or Hyal-pN + Hyal-RGDS at 13% (wt/vol) and 2% (wt/vol) respectively, were placed with a spatula on a petri dish and floated on hot water bath to activate the thermally responsive sol-gel transition. Once the

hydrogels were formed the materials were quickly transferred to a copper sandwich with a prewarmed spatula. Then the copper sandwich was plunged into liquid propane followed by quickly transferring the sample to liquid nitrogen. The samples were stored in liquid nitrogen until further use.

The frozen samples were placed in a custom mount and loaded into a BAL-TEC BAF 060 Freeze Fracture & Freeze Etch System (Leica Microsystems GmbH, Germany). The samples were subsequently fractured at -150^{o} C at 10^{-8} bar after which the machine internal temperature was raised to -90^{o} C and maintained for 5 hours to allow the water to sublime. The samples were coated in 2 nm Pt evaporated at 45^{o} followed by 10 nm C evaporated at 90^{o}. All prepared samples were analyzed with a NOVA NanoSEM 230 (FEI Company, USA).

B.3. Results

B.3.1. Dehydration of the Hyal-pN samples for HMDS and CPD preparation

The hydrogels were dehydrated stepwise with EtOH in order to prepare them for HMDS and CPD processing. However above 70% EtOH the Hyal-pN began to dissolve away. In order to verify the disassociation of the hydrogel did not occur because of sudden lowered solvent temperatures, the dehydration process was carried out on a hot plate to no avail.

B.3.2. SEM imaging of the cryofractured hydrogels

Preliminary results of the cryofractured samples did not show a uniformly fractured sample as can be seen from Fig. B1 where the hydrogel took on a hexagonal form. The gold film grids that were also used in the copper sandwich apparatus possessed holes that were hexagonal in shape. Furthermore, the aspect of the sample was smooth as if it was covered by a blanket. Further examination of a clearly fractured portion of the sample showed a more porous structure (Fig. B2). Moreover, it became quickly apparent that there were structurally different elements of the cryofractured samples, especially in regions where the sample was not fractured (Fig. B3).

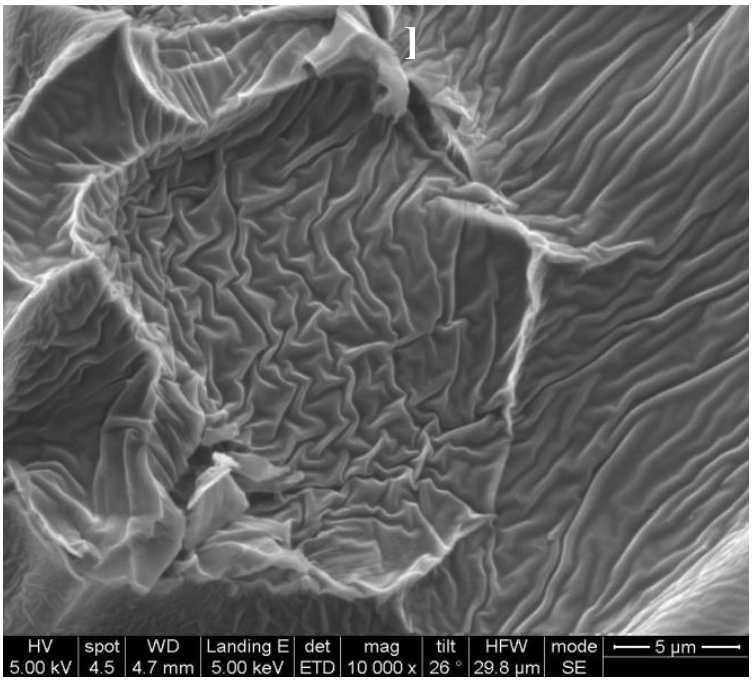

Fig. B1. Preliminary results of the Hyal-pN showing a non-uniform fracture of the sample.

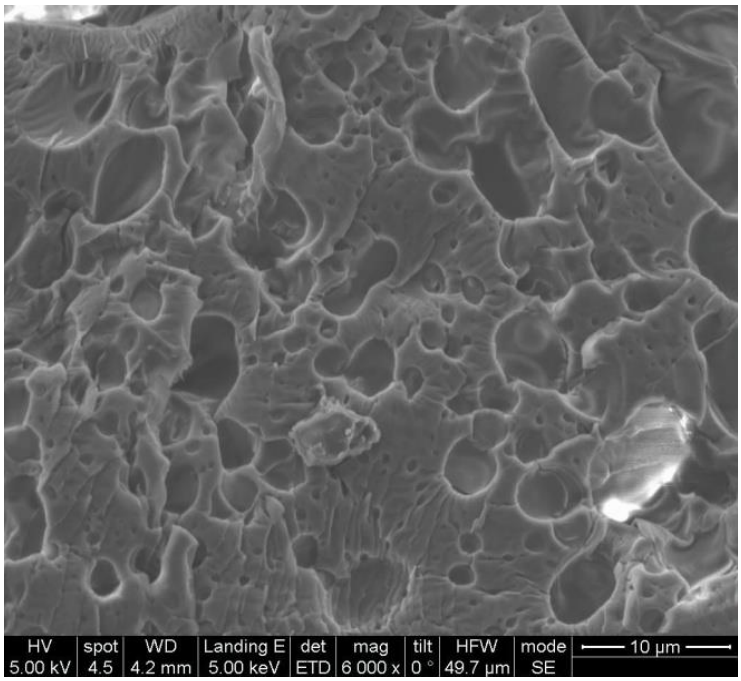

Fig. B2. Preliminary results of the Hyal-pN showing a fractured portion of the sample. Here the hydrogel appears smooth with empty micron sized vacuoles that likely contained water.

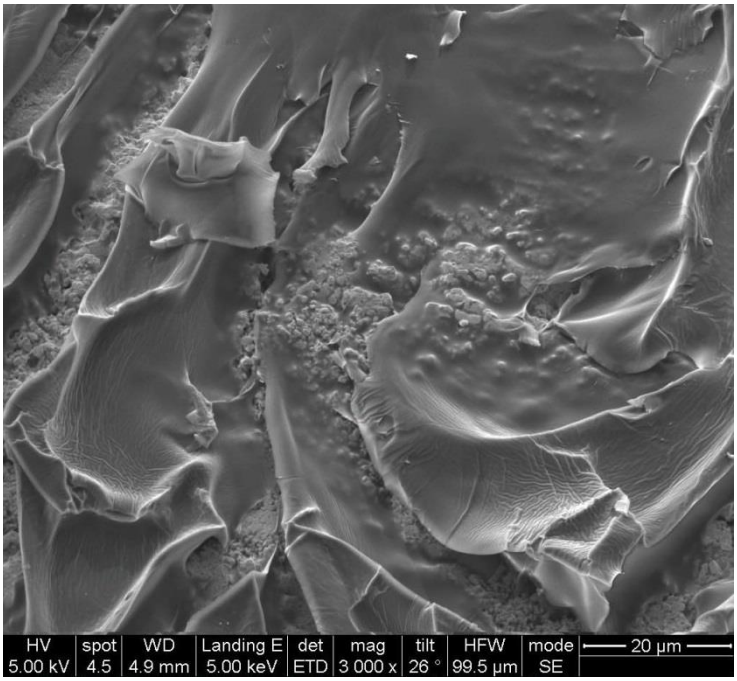

Fig. B3. Further examination of the sample showed that the hydrogel possessed structural elements that were starkly different from one region to the next.

The hydrogel samples were heterogenous in structure. Some areas possesses smooth layers (Figs. B1 and B2) whereas compact clusters were present in others (Fig. B3). Furthermore from Fig. B3, appeared to cover the actual hydrogel as if a blanket were covering the actual sample. An examination of a Hyal-pN sample possessing RGDS modified dendrimers, revealed that the smooth surfaces may have been hiding a more fibrous network underneath (Fig. B4).

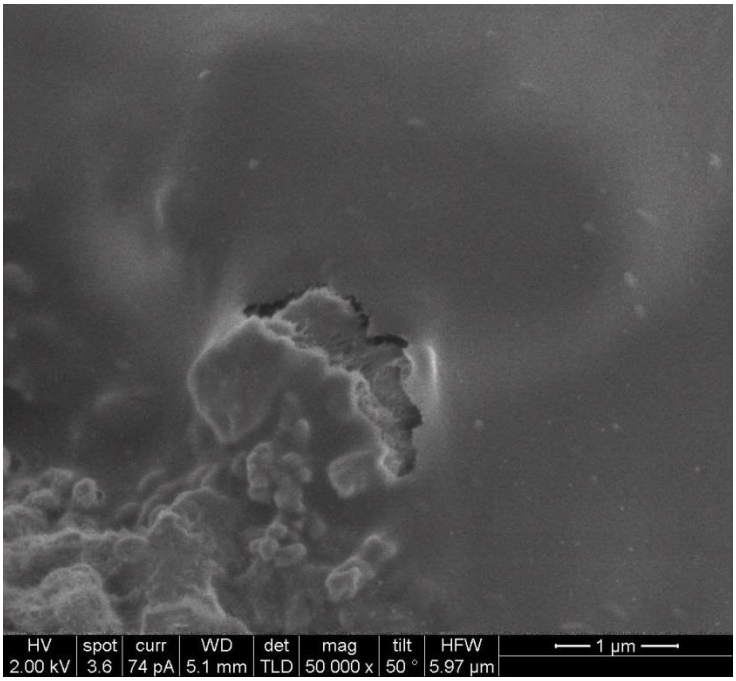

Fig. B4. SEM micrographs of Hyal-pN containing RGDS dendrimers containing a fibrous network beneath a smooth coating.

More samples revealed regions where the smooth layer was ruptured, and a fibrous network was clearly visible below (Figs. B5 and B6).

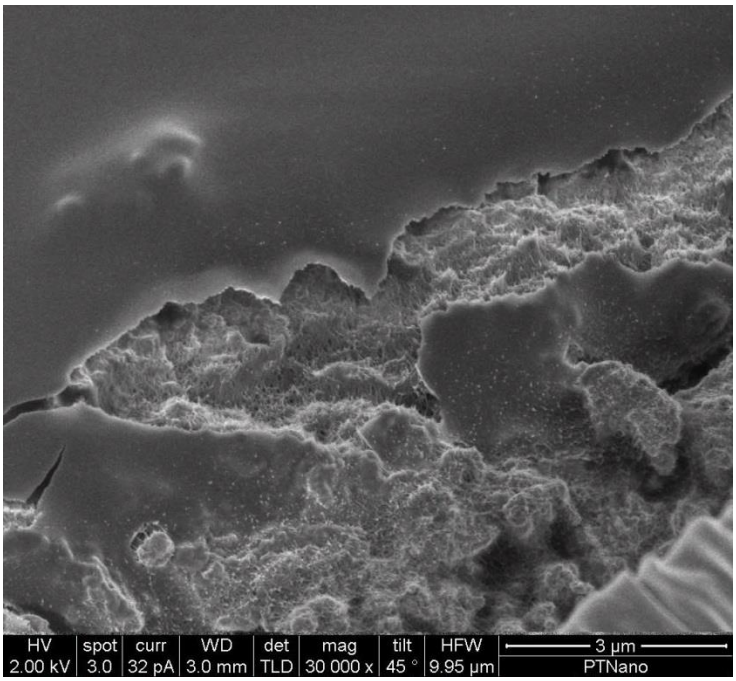

Fig. B5. SEM micrographs of a cryofractured Hyal-pN sample revealing a fibrous network underneath the smooth coating.

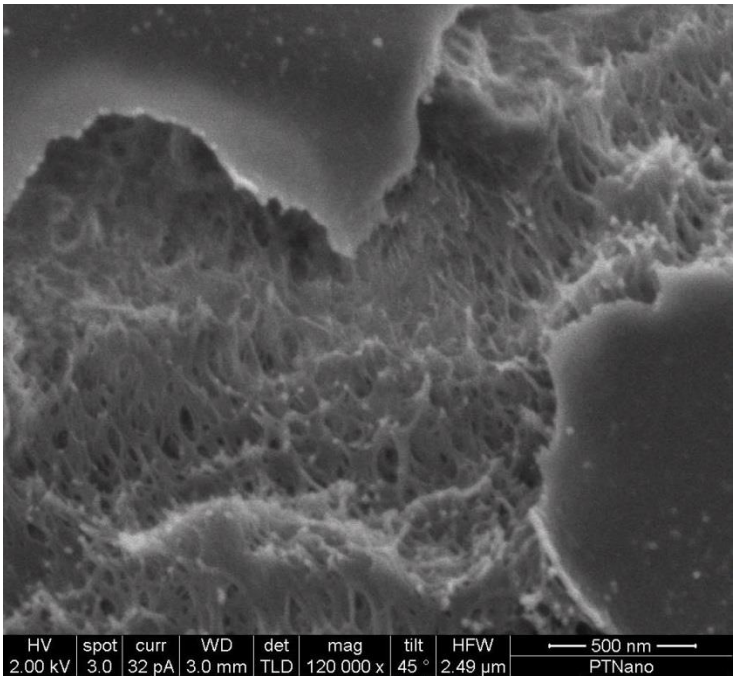

Fig. B6. Higher resolution SEM micrograph of Fig. B5 exhibiting a polymer network possessing nanoscale porosity.

It was unclear whether the smooth layer was the result of an artifact introduced by the process of evaporating the Pt and C metal-organic composite coating, incomplete dehydration of the biomaterial, or something else. However, it became more evident that the smooth areas were less relevant and that more accurate representions of the hydrogel could be observed in areas that clearly fractured and were well dehydrated (Figs. B7, B8, and B9).

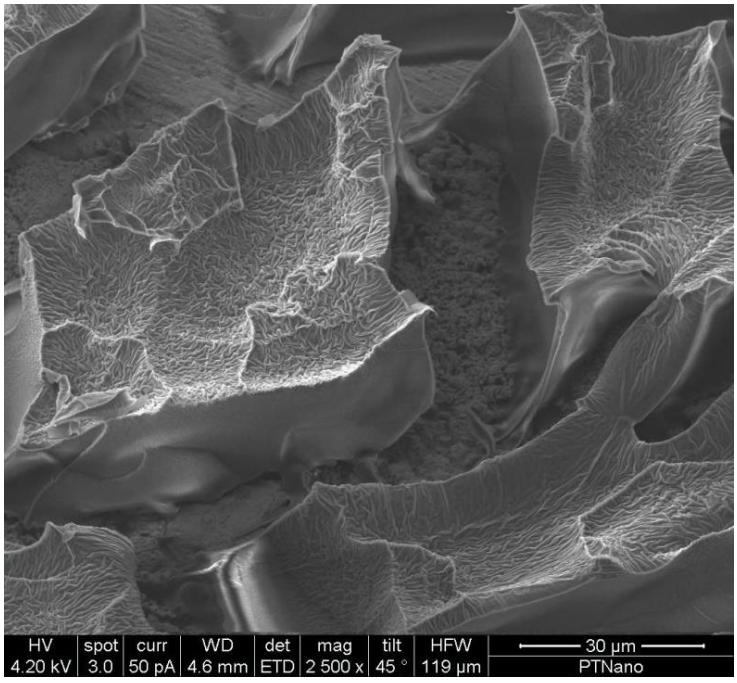

Fig. B7. SEM micrograph of both fractured and unfractured regions of the sample.

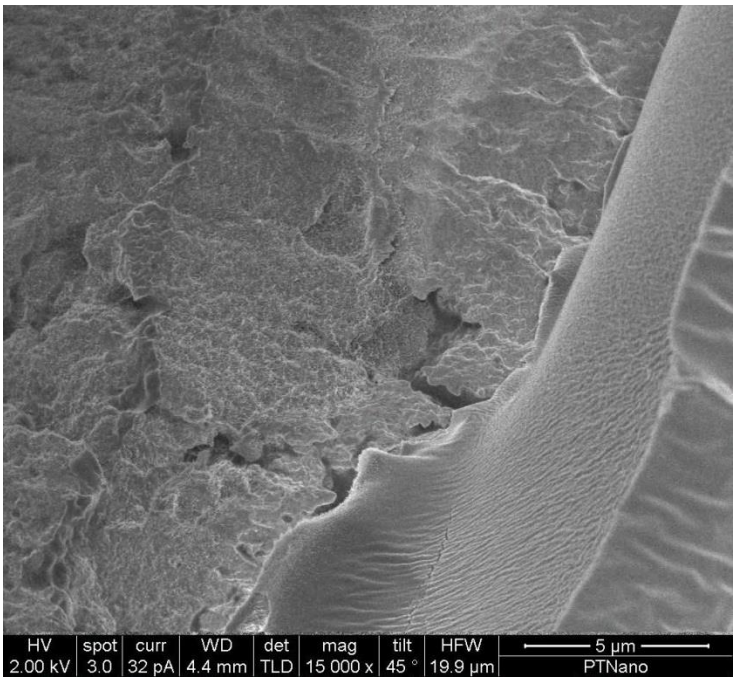

Fig. B8. Higher resolution SEM micrograph of Fig. B7 where the microscope was zoomed into the valley of the fractured sample to focus upon the porous network below.

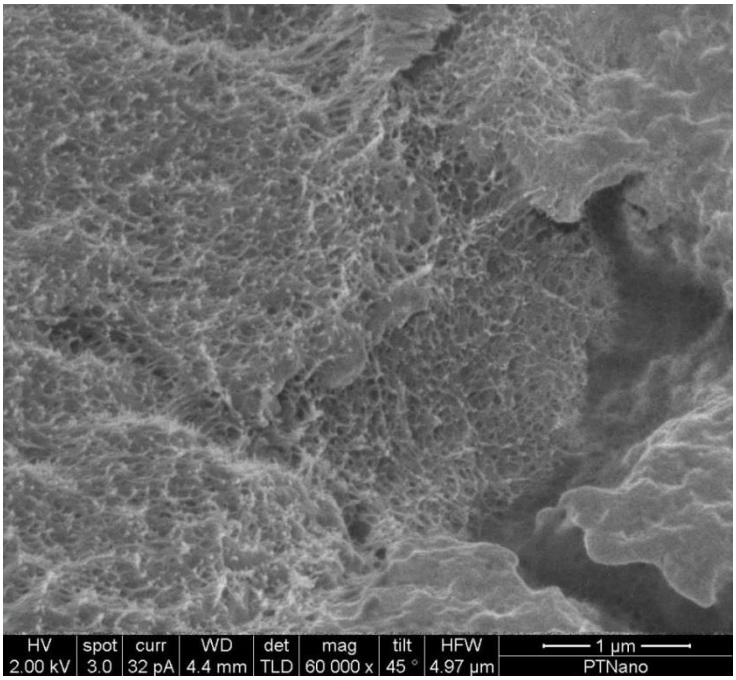

Fig. B9. SEM micrograph of a region shown in Figs. B7 and B8 that was zoomed in to more clearly show the porous structure of the fractured material.

Another sample was observed that clearly showed a portion of the sample that exemplified the high energy involved in the fracture process (Fig. B10). In Fig. B10, the sample was broken into many pieces that were illusory to the rubble of a destroyed building. Here the porous structure was easily discernable because the fracture process and the dehydration of the sample were both highly successful. Furthermore, a smooth surface on the left side of the larger piece that runs into the foreground seems to show that this area might be a layer of collapsed hydrogel or the interface between the hydrogel and atmosphere. Furthermore, this micrograph seems to show that the smooth layer must have been present before the Pt and C coating process. Hence, the hydrogel-atmosphere interface was likely responsible for producing that artifact.

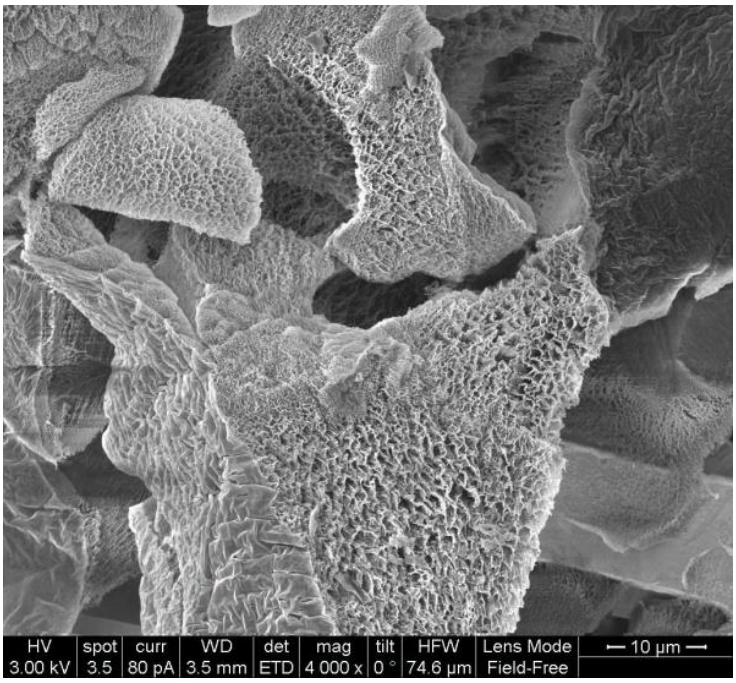

Fig. B10. SEM micrograph of a portion of sample that had been fractured elucidating a highly porous biomaterial. Additionally on the left side of the larger piece that runs into the foreground, the smooth layer. This artifact is likely the interface between the hydrogel and the atmosphere.

Given the chance to view a cross-section of the hydrogel perpendicular to the smooth interface, the sample stage was rotated 90^{o} clockwise, and viewed (Fig. B11). Imagining that the smooth layer represented the hydrogel-atmosphere interface, this image was taken along the z-plane of the hydrogel. The porosity is larger 5-10 microns from the surface, but becomes smaller and more compact deeper inside the biomaterial. Here there is a clear range of microscale pores in this portion of the hydrogel. A higher resolution image of Fig. B11 showed the ultrastructure of the hydrogel (Fig. B12). Walls of polymer were dotted with nanoscale pores and featured fibers protruding from the surfaces and entangling together. Additionally globular agglomerates were present along the fibers and within the polymer walls that framed out the pores. These structures can also be more clearly seen in a separate region (Fig. B13).

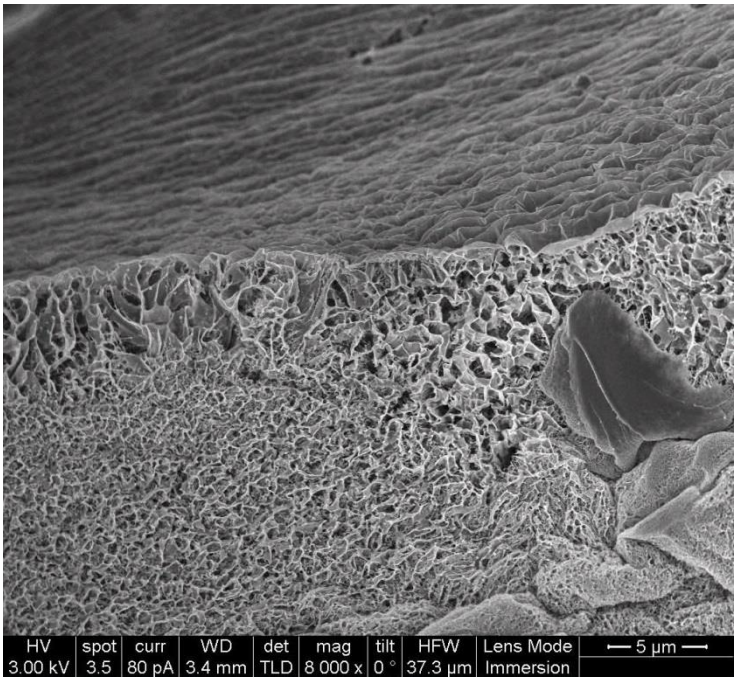

Fig. B11. SEM micrograph of a cross-section of the cryofractured hydrogel. This view is looking along the z-plane of the hydrogel. The smooth surface as the top half of the image represents the interface of the hydrogel with the atmosphere.

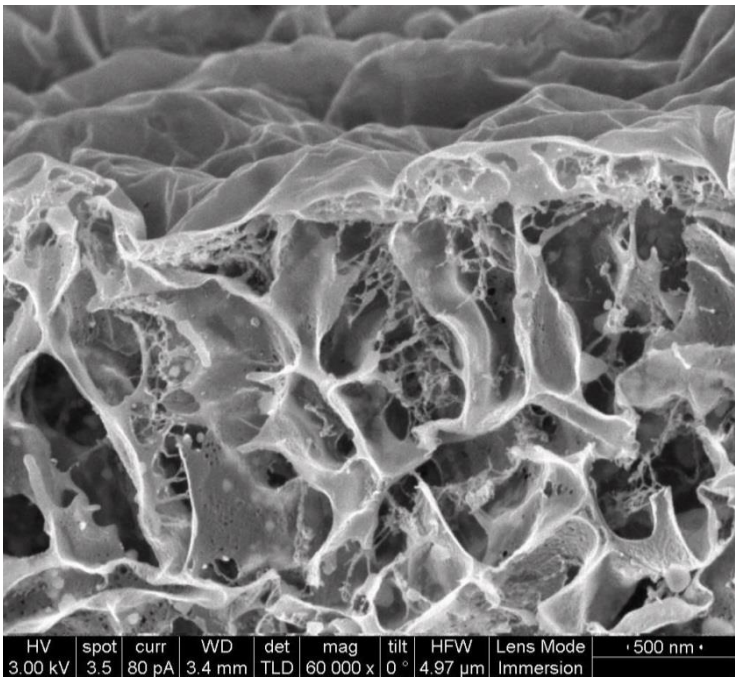

Fig. B12. Zoomed in SEM micrograph of a Fig. B11 featuring a cross-section of the cryofractured hydrogel. This view is looking along the z-plane of the hydrogel. The smooth surface on the top half of the image likely represents the hydrogel-atmosphere interface. The ultrastructure of the hydrogel can be clearly seen. Microscale pores are framed by walls of polymers. These polymer walls feature nanoscale pores and globular agglomerates. Fibers protruding from the framework also appear entangled with other fibers from adjacent walls. These structures could be exhibiting the physical crosslinking characteristic of Hyal-pN.

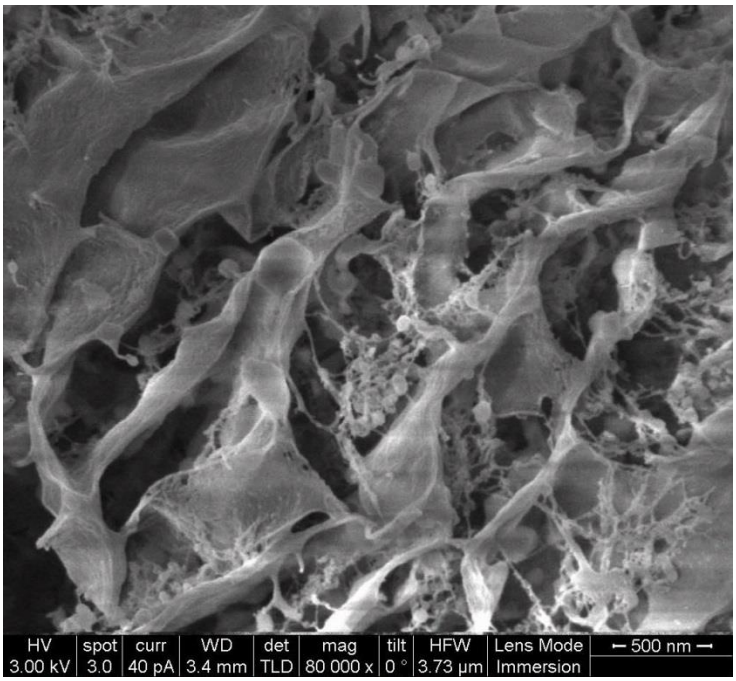

Fig. B13. SEM micrograph of the ultrastructure of the hydrogel. This image was taken near the region illustrated in Fig. B12. Here microscale pores are evident as well as the entangled fibers and globular agglomerates illustrating a rich polymer architecture.

Finally, another area of the hydrogel surface appeared to dehydrate very well in the cryofracture process and the smooth layer characteristic of the material-atmosphere interface was replaced by a highly porous network (Figs. B14 and B15).

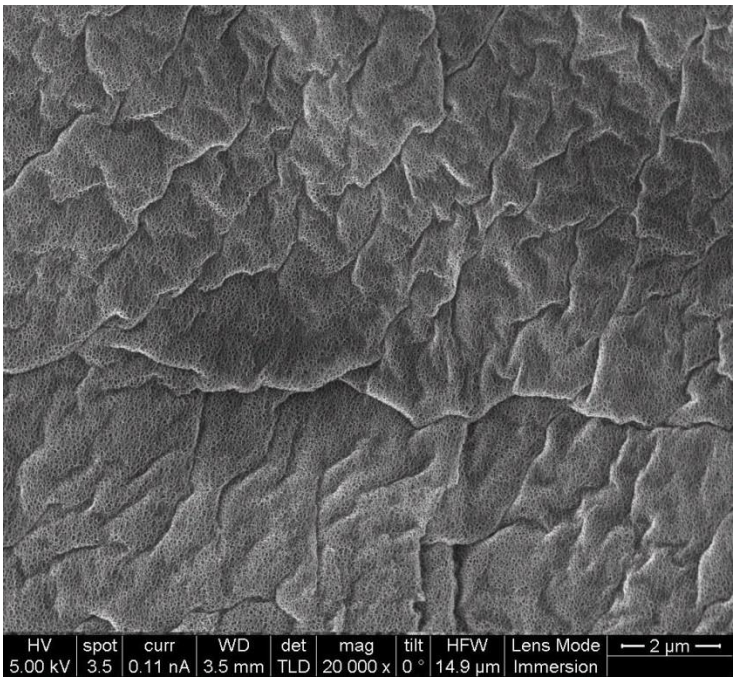

Fig. B14. SEM micrograph of an area that appeared to be a well dehydrated portion of the hydrogel surface.

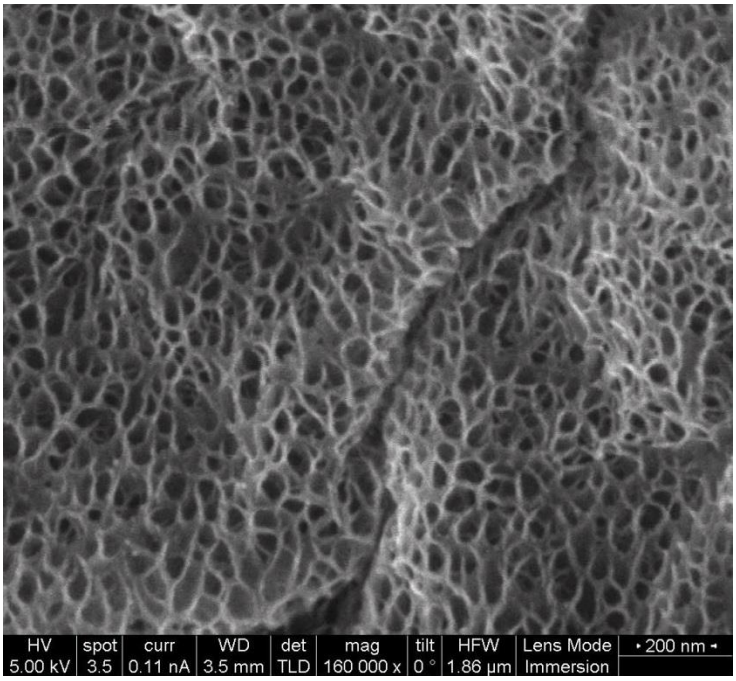

Fig. B15. Higher resolution SEM micrograph of Fig. B14 clearly illustrating a fine nanoporous structure at the hydrogel surface that is only clear if the cryofracture processing can absolutely dehydrate the sample.

B.4. Discussion

The HMDS and CPD sample preparations required the hydrogel to be dehydrated before proceeding further. However it was observed that the solution properties of the Hyal-pN are different than that of hyaluronic acid in the presence of EtOH. Whereas hyaluronic acid will typically collapse in a solution of EtOH greater than 50%, the Hyal-pN began to dissolved away. It is likely that in another solvent other than water the hydrophobic effect, that is responsible for the collapse of the thermos-sensitive polymer, does not occur. Therefore, it was clear from the beginning of the study that in the case of this hydrogel, the appropriate method of sample preparation is cryofixation followed by cryofracture.

Initial observations of the Hyal-pN prepared by cryofixation and cryofracture showed a hydrogel material that was not completely fractured and heterogenous structures from smooth surfaces to compact clusters were present. The unfractured portions of the sample appeared smooth on the surface. Furthermore, the samples were not porous indicating that the sample processing may not have completely liberated the water held within the biomaterial. Another possibility for the lack of apparent porosity or the existence of a polymeric network was that the Pt and C coating process yielded a smooth layer blanketing the surface of the biomaterial. However, it was still not clear if these regions were simply the result of the incomplete dehydration of samples. Thus the third possibility was that the smooth areas were simply the hydrogel-atmosphere interface.

Further examination revealed that a thin superficial layer covered the hydrogel. Ruptured portions of this blanket revealed a porous structure was visible underneath. Once it was clear that a representative polymer network was below the smooth blanket layer, observations were focused primarily around fractured regions of the sample. One specific sample region in Fig. B10 illustrated the high energy involved in the cryofracture process resulting in pieces of the hydrogel that looked like rubble from a destroyed building. On the left side of the larger piece the smooth layer was observed, whereas on the perpendicular surface a highly porous structure was clearly seen. This evidence was the key to understanding that the blanket was most likely the hydrogel-atmosphere interface. This layer likely was either incompletely dehydrated, collapsed network, or existed because of the inherent surface tension of the biomaterial. Therefore, the blanket was

not an artifact of the evaporation of the metal-organic composite. Furthermore, the cross-section revealed a beautiful hydrogel ultrastructure.

Fine details into the architecture of the polymer network became clear. The micrographs captured the architecture of the polymer network illustrating walls of polymer that framed the pores. The high resolution image of Fig. B12 showed an intricate network of walls of polymer that were speckled with nanodiameter pores possibly aiding in the diffusion of solutes and smaller molecules. Furthermore, this framework could be the hyaluronan portion of the copolymer associating itself into the portions that appear as walls and frame the porous structure. Entangled fibers and globular agglomerates were also apparent which could actually be evidence of the pN forming physical crosslinks. The other possibility is that these fibers could be a mixture of the copolymers that could have woven together through affinity-based interactions. Stronger interacting polymers, for example collapsed entangled pN, could have formed the globular agglomerates.

B.5 Conclusion

In conclusion, the process of cryofixation and fracture is a good method to visualize the ultrastructure of a soft biomaterial such as Hyal-pN. High resolutions images can be obtained revealing a rich polymeric network with a highly interconnected network of microscale and nanoscale pores. In order to obtain these images, it was important to focus on the fractured regions of the hydrogel. Furthermore, the sample must be well dehydrated for high quality visualition of the intricate polymeric network. To visualize the porous network at the material-atmosphere interface, the dehydration forces must overcome surface tension. Otherwise the surface will show a smooth blanket-like layer.

Acknowledgements

The authors would like to thank Dr. Carmen Lopez Iglesias and Gemma Martinez Ruiz of the Centres Científics i Tecnològics, Universitat de Barcelona for their expertise and assistance with the cryofixation and fracture processing. Additional gratitude is owed to Judith Linacero Blanco of the Institute for Bioengineering of Catalonia and Yolanda Atienza García of the Serveis Científics Comuns of the Barcelona Science Park for their assistance with SEM imaging.

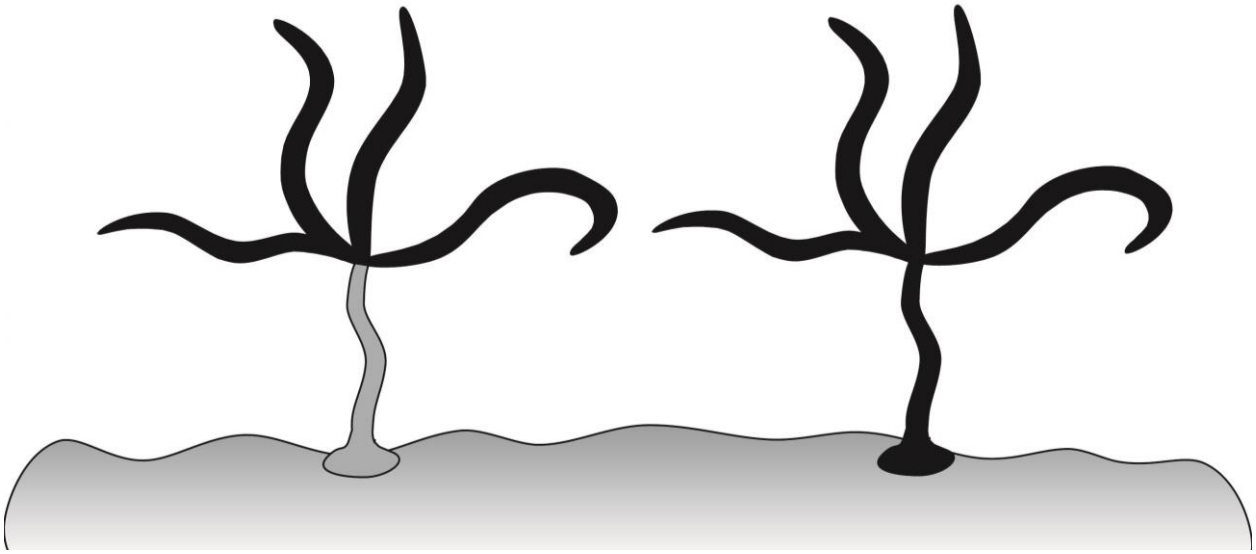

Annex C: Publications and Conferences Attended

C.1. Publications

1.) **Seelbach RJ**, *et al.* Multivalent dendrimers presenting spatially controlled clusters of binding epitopes in thermoresponsive hyaluronan hydrogels. *Acta Biomaterialia*. 2014;10(10):4340-50. doi: 10.1016/j.actbio.2014.06.028. (Impact factor: 5.684, Q1)

2.) **Seelbach RJ**, *et al.* Copper catalyst efficiency for the CuAAC synthesis of a poly(*N*-isopropylacrylamide) conjugated hyaluronan. *Clinical Hemorheology and Microcirculation*. 2015. (*In Press*, Impact factor: 2.215, Q3)

3.) **Seelbach RJ**, *et al.* Injectable hyaluronan hydrogels with peptide binding dendrimers modulate the controlled release of BMP-2 and TGF-β1. *Advanced Healthcare Materials*. (*Submitted article*, Impact Factor: 4.880, Q1)

C.2. Conferences Attended

C.2.1 Oral Presentations

1.) **Seelbach R**, Peroglio M, Fransen P, Albericio F, Royo M, Alini M, Eglin D, Mata A. "Modulating the biochemical environment of a hyaluronan-based thermo-reversible hydrogel with integrin binding dendrimers" (*Oral Presentation*) European Society of Biomaterials, September 2013, Madrid, Spain.

2.) **Seelbach R**, Peroglio M, Mata A, Alini M, Eglin D. "Bio-functional hyaluronan hydrogel for cell and drug delivery." (*Oral Presentation*) Graubünden forscht - Young Scientists in Contest, August 25, 2010, Chur, Switzerland.

C.2.2. Poster Presentations

3.) **Seelbach R**, Peroglio M, Mata A, Alini M, Eglin D. "Designing a Multifunctional, Thermoreversible Hyaluronan-Based Hydrogel for Tissue Regeneration" (*Poster Presentation)* European Society of Biomaterials, August 2011, Dublin, Ireland.

4.) **Seelbach R**, Peroglio M, Mata A, Alini M, Eglin D. "Designing a Multifunctional, Thermoreversible Hyaluronan-Based Hydrogel for Tissue Regeneration" (*Poster Presentation)* Tissue Engineering and Regenerative Medicine International Society (TERMIS), 6-9 June 2011, Granada, Spain.

5.) **Seelbach R**, Peroglio M, Mata A, Alini M, Eglin D. "Designing a Multifunctional, Thermoreversible Hyaluronan-Based Hydrogel for Tissue Regeneration" (*Poster Presentation)* Swiss Society of Biomaterials, May 2011, Switzerland.

C.2.3. Conferences Attended

6.) eCM XI: Cartilage & Disc: Repair and Regeneration *(Attendee)* eCells & Materials Conference, 28-30 June 2010, Davos, Switzerland.

7.) 18th European Conference on Orthopaedics *(Attendee)* European Orthopaedic Research Society, July 2010, Davos, Switzerland.

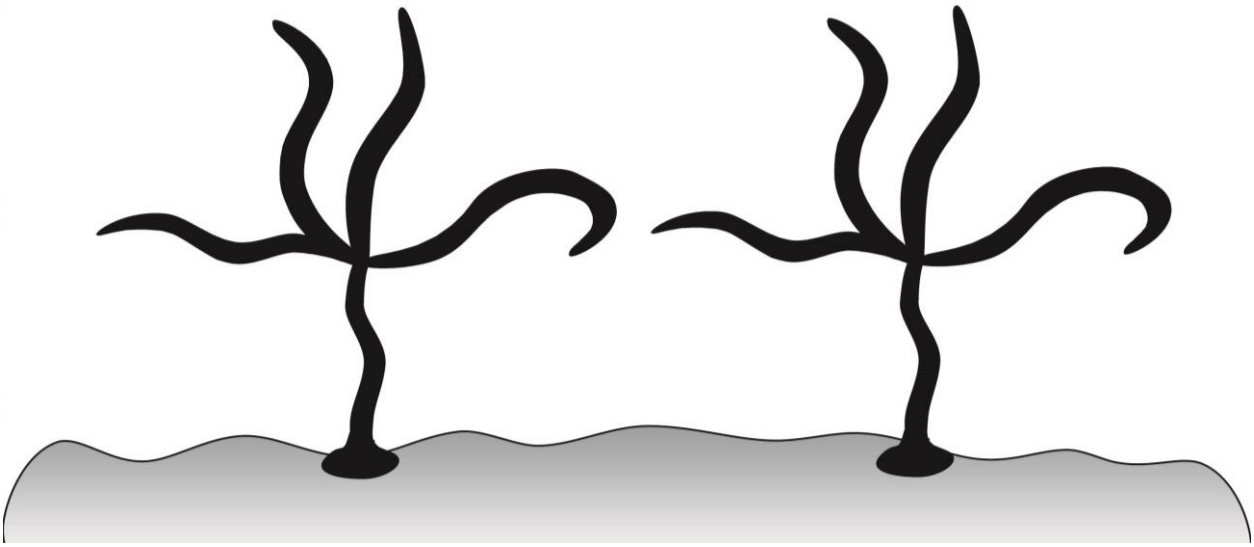

References

1. Weinstein, S.L. 2000-2010: the bone and joint decade. *The Journal of bone and joint surgery. American volume* **82**, 1-3 (2000).
2. Lee, K., Silva, E.A. & Mooney, D.J. Growth factor delivery-based tissue engineering: general approaches and a review of recent developments. *Journal of the Royal Society, Interface / the Royal Society* **8**, 153-170 (2011).
3. Prestwich, G.D. Hyaluronic acid-based clinical biomaterials derived for cell and molecule delivery in regenerative medicine. *J Control Release* **155**, 193-199 (2011).
4. Burdick, J.A. & Prestwich, G.D. Hyaluronic acid hydrogels for biomedical applications. *Adv.Mater.* **23**, H41-H56 (2011).
5. Seelbach, R.J. et al. Multivalent dendrimers presenting spatially controlled clusters of binding epitopes in thermoresponsive hyaluronan hydrogels. *Acta Biomater* **10**, 4340-4350 (2014).

6. Kopeček, J. & Yang, J. Hydrogels as smart biomaterials. *Polymer International* **56**, 1078-1098 (2007).
7. Discher, D.E., Mooney, D.J. & Zandstra, P.W. Growth Factors, Matrices, and Forces Combine and Control Stem Cells. *Science* **324**, 1673-1677 (2009).
8. Stuart, M.A. et al. Emerging applications of stimuli-responsive polymer materials. *Nature materials* **9**, 101-113 (2010).
9. Farnsworth, N.L., Mead, B.E., Antunez, L.R., Palmer, A.E. & Bryant, S.J. Ionic osmolytes and intracellular calcium regulate tissue production in chondrocytes cultured in a 3D charged hydrogel. *Matrix biology : journal of the International Society for Matrix Biology* **40**, 17-26 (2014).
10. Yan, C. & Pochan, D.J. Rheological properties of peptide-based hydrogels for biomedical and other applications. *Chemical Society reviews* **39**, 3528-3540 (2010).
11. Morra, M. Engineering of biomaterials surfaces by hyaluronan. *Biomacromolecules.* **6**, 1205-1223 (2005).
12. Laurent, T.C. & Fraser, J.R. Hyaluronan. *FASEB J* **6**, 2397-2404 (1992).
13. Bian, L. et al. The influence of hyaluronic acid hydrogel crosslinking density and macromolecular diffusivity on human MSC chondrogenesis and hypertrophy. *Biomaterials* **34**, 413-421 (2013).
14. Chaterji, S., Kwon, I.K. & Park, K. Smart Polymeric Gels: Redefining the Limits of Biomedical Devices. *Progress in polymer science* **32**, 1083-1122 (2007).
15. Engler, A.J., Sen, S., Sweeney, H.L. & Discher, D.E. Matrix Elasticity Directs Stem Cell Lineage Specification. *Cell* **126**, 677-689 (2006).
16. Mortisen, D., Peroglio, M., Alini, M. & Eglin, D. Tailoring thermoreversible hyaluronan hydrogels by "click" chemistry and RAFT polymerization for cell and drug therapy. *Biomacromolecules.* **11**, 1261-1272 (2010).
17. McCormick, C.L., Sumerlin, B.S., Lokitz, B.S. & Stempka, J.E. RAFT-synthesized diblock and triblock copolymers: thermally-induced supramolecular assembly in aqueous media. *Soft Matter* **4**, 1760-1773 (2008).
18. Lapcik, L., Jr., Lapcik, L., De Smedt, S., Demeester, J. & Chabrecek, P. Hyaluronan: Preparation, Structure, Properties, and Applications. *Chemical reviews* **98**, 2663-2684 (1998).
19. Garg, H.G. & Hales, C.A. (eds.) Chemistry and Biology of Hyaluronan, Edn. First. (Elsevier Science, Ltd., Oxford; 2004).
20. Bulpitt, P. & Aeschlimann, D. New strategy for chemical modification of hyaluronic acid: preparation of functionalized derivatives and their use in the formation of novel biocompatible hydrogels. *Journal of biomedical materials research* **47**, 152-169 (1999).
21. Pereira, C.L. et al. The effect of hyaluronan-based delivery of stromal cell-derived factor-1 on the recruitment of MSCs in degenerating intervertebral discs. *Biomaterials* **35**, 8144-8153 (2014).
22. Mazumder, M.A.J., Fitzpatrick, S.D., Muirhead, B. & Sheardown, H. Cell-adhesive thermogelling PNIPAAm/hyaluronic acid cell delivery hydrogels for potential application as minimally invasive retinal therapeutics. *Journal of Biomedical Materials Research Part A* **100A**, 1877-1887 (2012).
23. Tan, H. et al. Thermosensitive injectable hyaluronic acid hydrogel for adipose tissue engineering. *Biomaterials* **30**, 6844-6853 (2009).

24. Ohya, S., Sonoda, H., Nakayama, Y. & Matsuda, T. The potential of poly(N-isopropylacrylamide) (PNIPAM)-grafted hyaluronan and PNIPAM-grafted gelatin in the control of post-surgical tissue adhesions. *Biomaterials* **26**, 655-659 (2005).
25. Naito, H. et al. Three-dimensional cardiac tissue engineering using a thermoresponsive artificial extracellular matrix. *ASAIO journal* **50**, 344-348 (2004).
26. Peroglio, M., Eglin, D., Benneker, L.M., Alini, M. & Grad, S. Thermoreversible hyaluronan-based hydrogel supports in vitro and ex vivo disc-like differentiation of human mesenchymal stem cells. *Spine J.* **13**, 1627-1639 (2013).
27. Peroglio, M. et al. Injectable thermoreversible hyaluronan-based hydrogels for nucleus pulposus cell encapsulation. *Eur.Spine J.* **21 Suppl 6**, S839-S849 (2012).
28. D'Este, M., Eglin, D. & Alini, M. A systematic analysis of DMTMM vs EDC/NHS for ligation of amines to hyaluronan in water. *Carbohydrate polymers* **108**, 239-246 (2014).
29. D'Este, M., Alini, M. & Eglin, D. Single step synthesis and characterization of thermoresponsive hyaluronan hydrogels. *Carbohydr.Polym.* **90**, 1378-1385 (2012).
30. Pitarresi, G., Fiorica, C., Licciardi, M., Palumbo, F.S. & Giammona, G. New hyaluronic acid based brush copolymers synthesized by atom transfer radical polymerization. *Carbohydrate polymers* **92**, 1054-1063 (2013).
31. Liang, L.Y. & Astruc, D. The copper(I)-catalyzed alkyne-azide cycloaddition (CuAAC) "click" reaction and its applications. An overview. *Coordin Chem Rev* **255**, 2933-2945 (2011).
32. Kolb, H.C., Finn, M.G. & Sharpless, K.B. Click Chemistry: Diverse Chemical Function from a Few Good Reactions. *Angewandte Chemie International Edition* **40**, 2004-2021 (2001).
33. Hale, C.W. Studies on diffusing factors: 4. The action of reducing agents on hyaluronic acid and other polysaccharides. *Biochemical Journal* **38**, 362-368 (1944).
34. Uchida, K. & Kawakishi, S. Oxidative Depolymerization of Polysaccharides Induced by the Ascorbic Acid-Copper Ion Systems. *Agricultural and Biological Chemistry* **50**, 2579-2583 (1986).
35. Soltés, L. et al. Degradation of High-Molar-Mass Hyaluronan and Characterization of Fragments. *Biomacromolecules* **8**, 2697-2705 (2007).
36. Elshahawy, W.M., Watanabe, I. & Kramer, P. In vitro cytotoxicity evaluation of elemental ions released from different prosthodontic materials. *Dental materials : official publication of the Academy of Dental Materials* **25**, 1551-1555 (2009).
37. Lal, S. & Diéz-Gonzaléz, S. in The Journal of Organic Chemistry, Vol. 76 2367-2373 (American Chemical Society, 2011).
38. Kyllönen, L., D'Este, M., Alini, M. & Eglin, D. Local drug delivery for enhancing fracture healing in osteoporotic bone. *Acta Biomaterialia* **11**, 412-434 (2015).
39. D'Este, M. & Eglin, D. Hydrogels in calcium phosphate moldable and injectable bone substitutes: Sticky excipients or advanced 3-D carriers? *Acta Biomaterialia* **9**, 5421-5430 (2013).
40. Bibbo, C., Nelson, J., Ehrlich, D. & Rougeux, B. Bone morphogenetic proteins: indications and uses. *Clinics in podiatric medicine and surgery* **32**, 35-43 (2015).
41. Kubiczkova, L., Sedlarikova, L., Hajek, R. & Sevcikova, S. TGF-beta - an excellent servant but a bad master. *Journal of translational medicine* **10**, 183 (2012).
42. Carragee, E.J., Hurwitz, E.L. & Weiner, B.K. A critical review of recombinant human bone morphogenetic protein-2 trials in spinal surgery: emerging safety concerns and

lessons learned. *The spine journal : official journal of the North American Spine Society* **11**, 471-491 (2011).
43. Kelly, M.P. et al. Cancer Risk from Bone Morphogenetic Protein Exposure in Spinal Arthrodesis, Vol. 96. (2014).
44. Varga, J. & Pasche, B. Transforming growth factor beta as a therapeutic target in systemic sclerosis. *Nature reviews. Rheumatology* **5**, 200-206 (2009).
45. Buijs, J.T., Stayrook, K.R. & Guise, T.A. TGF-beta in the Bone Microenvironment: Role in Breast Cancer Metastases. *Cancer microenvironment : official journal of the International Cancer Microenvironment Society* **4**, 261-281 (2011).
46. Censi, R., Di Martino, P., Vermonden, T. & Hennink, W.E. Hydrogels for protein delivery in tissue engineering. *J Control Release* **161**, 680-692 (2012).
47. Bianchera, A. et al. Chitosan hydrogels for chondroitin sulphate controlled release: an analytical characterization. *Journal of analytical methods in chemistry* **2014**, 808703 (2014).
48. Chen, F.-M. et al. Periodontal regeneration using novel glycidyl methacrylated dextran (Dex-GMA)/gelatin scaffolds containing microspheres loaded with bone morphogenetic proteins. *Journal of Controlled Release* **121**, 81-90 (2007).
49. Luca, L., Rougemont, A.-L., Walpoth, B.H., Gurny, R. & Jordan, O. The effects of carrier nature and pH on rhBMP-2-induced ectopic bone formation. *Journal of Controlled Release* **147**, 38-44 (2010).
50. Kimura, Y. et al. Controlled release of bone morphogenetic protein-2 enhances recruitment of osteogenic progenitor cells for de novo generation of bone tissue. *Tissue Eng Part A* **16**, 1263-1270 (2010).
51. Kolambkar, Y.M. et al. An alginate-based hybrid system for growth factor delivery in the functional repair of large bone defects. *Biomaterials* **32**, 65-74 (2011).
52. Gorgieva, S. & Kokol, V. Processing of gelatin-based cryogels with improved thermomechanical resistance, pore size gradient, and high potential for sustainable protein drug release. *Journal of biomedical materials research. Part A* **103**, 1119-1130 (2015).
53. Shah, R.N. et al. Supramolecular design of self-assembling nanofibers for cartilage regeneration. *Proceedings of the National Academy of Sciences of the United States of America* **107**, 3293-3298 (2010).
54. Hosseinkhani, H., Hosseinkhani, M., Khademhosseini, A. & Kobayashi, H. Bone regeneration through controlled release of bone morphogenetic protein-2 from 3-D tissue engineered nano-scaffold. *Journal of Controlled Release* **117**, 380-386 (2007).
55. Rahimi, S., Sarraf, E.H., Wong, G.K. & Takahata, K. Implantable drug delivery device using frequency-controlled wireless hydrogel microvalves. *Biomedical microdevices* **13**, 267-277 (2011).
56. Geever, L.M. et al. Characterisation and controlled drug release from novel drug-loaded hydrogels. *European journal of pharmaceutics and biopharmaceutics : official journal of Arbeitsgemeinschaft fur Pharmazeutische Verfahrenstechnik e.V* **69**, 1147-1159 (2008).
57. Sershen, S.R., Westcott, S.L., Halas, N.J. & West, J.L. Temperature-sensitive polymer–nanoshell composites for photothermally modulated drug delivery. *Journal of biomedical materials research* **51**, 293-298 (2000).

58. Chen, H., Gu, Y., Hub, Y. & Qian, Z. Characterization of pH- and temperature-sensitive hydrogel nanoparticles for controlled drug release. *PDA journal of pharmaceutical science and technology / PDA* **61**, 303-313 (2007).
59. Jeon, O., Powell, C., Solorio, L.D., Krebs, M.D. & Alsberg, E. Affinity-based growth factor delivery using biodegradable, photocrosslinked heparin-alginate hydrogels. *Journal of Controlled Release* **154**, 258-266 (2011).
60. Kim, H.D. & Valentini, R.F. Retention and activity of BMP-2 in hyaluronic acid-based scaffolds in vitro. *Journal of biomedical materials research* **59**, 573-584 (2002).
61. Maxwell, D.J., Hicks, B.C., Parsons, S. & Sakiyama-Elbert, S.E. Development of rationally designed affinity-based drug delivery systems. *Acta Biomaterialia* **1**, 101-113 (2005).
62. Simon-Gracia, L. et al. Biocompatible, multifunctional, and well-defined OEG-based dendritic platforms for biomedical applications. *Org.Biomol.Chem.* **11**, 4109-4121 (2013).
63. Yabbarov, N.G., Posypanova, G.A., Vorontsov, E.A., Obydenny, S.I. & Severin, E.S. A new system for targeted delivery of doxorubicin into tumor cells. *J Control Release* **168**, 135-141 (2013).
64. Pla, D. et al. in Bioconjugate Chemistry, Vol. 20 1112-1121 (American Chemical Society, 2009).
65. Pulido, D., Albericio, F. & Royo, M. Controlling Multivalency and Multimodality: Up to Pentamodal Dendritic Platforms Based on Diethylenetriaminepentaacetic Acid Cores. *Org Lett* **16**, 1318-1321 (2014).
66. Burdick, J.A. & Vunjak-Novakovic, G. Engineered microenvironments for controlled stem cell differentiation. *Tissue Eng Part A* **15**, 205-219 (2009).
67. Lutolf, M.P., Raeber, G.P., Zisch, A.H., Tirelli, N. & Hubbell, J.A. Cell-Responsive Synthetic Hydrogels. *Advanced Materials* **15**, 888-892 (2003).
68. Mata, A. et al. Bone regeneration mediated by biomimetic mineralization of a nanofiber matrix. *Biomaterials* **31**, 6004-6012 (2010).
69. Crespo, L. et al. in Chemical Reviews, Vol. 105 1663-1682 (American Chemical Society, 2005).
70. Lee, C.C., MacKay, J.A., Frechet, J.M.J. & Szoka, F.C. Designing dendrimers for biological applications. *Nat Biotech* **23**, 1517-1526 (2005).
71. Tansey, W. et al. Synthesis and characterization of branched poly(L-glutamic acid) as a biodegradable drug carrier. *J Control Release* **94**, 39-51 (2004).
72. van der Poll, D.G. et al. Design, Synthesis, and Biological Evaluation of a Robust, Biodegradable Dendrimer. *Bioconjugate Chemistry* **21**, 764-773 (2010).
73. Joshi, N. & Grinstaff, M. Applications of dendrimers in tissue engineering. *Curr.Top.Med Chem.* **8**, 1225-1236 (2008).
74. Santos, J.L., Oramas, E., Pego, A.P., Granja, P.L. & Tomas, H. Osteogenic differentiation of mesenchymal stem cells using PAMAM dendrimers as gene delivery vectors. *J Control Release* **134**, 141-148 (2009).
75. Oliveira, J.M. et al. The osteogenic differentiation of rat bone marrow stromal cells cultured with dexamethasone-loaded carboxymethylchitosan/poly(amidoamine) dendrimer nanoparticles. *Biomaterials* **30**, 804-813 (2009).
76. Gerecht, S. et al. Hyaluronic acid hydrogel for controlled self-renewal and differentiation of human embryonic stem cells. *Proc.Natl.Acad.Sci.U.S.A* **104**, 11298-11303 (2007).

77. Tokatlian, T., Cam, C. & Segura, T. Non-viral DNA delivery from porous hyaluronic acid hydrogels in mice. *Biomaterials* **35**, 825-835 (2014).
78. Bhakta, G. et al. The influence of collagen and hyaluronan matrices on the delivery and bioactivity of bone morphogenetic protein-2 and ectopic bone formation. *Acta Biomaterialia* **9**, 9098-9106 (2013).
79. Liang, Y., Walczak, P. & Bulte, J.W.M. The survival of engrafted neural stem cells within hyaluronic acid hydrogels. *Biomaterials* **34**, 5521-5529 (2013).
80. Park, Y.D., Tirelli, N. & Hubbell, J.A. Photopolymerized hyaluronic acid-based hydrogels and interpenetrating networks. *Biomaterials* **24**, 893-900 (2003).
81. Lam, J. & Segura, T. The modulation of MSC integrin expression by RGD presentation. *Biomaterials* **34**, 3938-3947 (2013).
82. Kim, J. et al. Bone regeneration using hyaluronic acid-based hydrogel with bone morphogenic protein-2 and human mesenchymal stem cells. *Biomaterials* **28**, 1830-1837 (2007).
83. Crescenzi, V., Cornelio, L., Di Meo, C., Nardecchia, S. & Lamanna, R. Novel hydrogels via click chemistry: synthesis and potential biomedical applications. *Biomacromolecules* **8**, 1844-1850 (2007).
84. Lai, J.T., Filla, D. & Shea, R. Functional polymers from novel carboxyl-terminated trithiocarbonates as highly efficient RAFT agents. *Macromolecules* **35**, 6754-6756 (2002).
85. Gondi, S.R., Vogt, A.P. & Sumerlin, B.S. Versatile Pathway to Functional Telechelics via RAFT Polymerization and Click Chemistry. *Macromolecules* **40**, 474-481 (2007).
86. Li, M., De, P., Gondi, S.R. & Sumerlin, B.S. Responsive Polymer-Protein Bioconjugates Prepared by RAFT Polymerization and Copper-Catalyzed Azide-Alkyne Click Chemistry. *Macromolecular Rapid Communication* **29**, 1172-1176 (2008).
87. Oudshoom, M.H.M., Rissmann, R., Bouwstra, J.A. & Hennink, W.E. Synthesis of methacrylated hyaluronic acid with tailored degree of substitution. *Polymer* **48**, 1915-1920 (2007).
88. Burdick, J.A. & Anseth, K.S. Photoencapsulation of osteoblasts in injectable RGD-modified PEG hydrogels for bone tissue engineering. *Biomaterials* **23**, 4315-4323 (2002).
89. Livak, K.J. & Schmittgen, T.D. Analysis of Relative Gene Expression Data Using Real-Time Quantitative PCR and the 2−ΔΔCT Method. *Methods* **25**, 402-408 (2001).
90. Mayo, S.L., Olafson, B.D. & Goddard, W.A. DREIDING: a generic force field for molecular simulations. *The Journal of Physical Chemistry* **94**, 8897-8909 (1990).
91. Stern, R., Kogan, G., Jedrzejas, M.J. & Soltes, L. The many ways to cleave hyaluronan. *Biotechnology advances* **25**, 537-557 (2007).
92. Lallana, E., Riguera, R. & Fernandez-Megia, E. Reliable and Efficient Procedures for the Conjugation of Biomolecules through Huisgen Azide–Alkyne Cycloadditions. *Angewandte Chemie International Edition* **50**, 8794-8804 (2011).
93. Wen, B. et al. An evaluation of BMP-2 delivery from scaffolds with miniaturized dental implants in a novel rat mandible model. *Journal of Biomedical Materials Research Part B: Applied Biomaterials* **97B**, 315-326 (2011).
94. Xie, H.-G. et al. Effect of surface wettability and charge on protein adsorption onto implantable alginate-chitosan-alginate microcapsule surfaces. *Journal of Biomedical Materials Research Part A* **92A**, 1357-1365 (2010).

95. Xu, J., Li, X., Lian, J.B., Ayers, D.C. & Song, J. Sustained and localized in vitro release of BMP-2/7, RANKL, and tetracycline from Flexbone, an elastomeric osteoconductive bone substitute. *Journal of Orthopaedic Research* **27**, 1306-1311 (2009).
96. Boontheekul, T. & Mooney, D.J. Protein-based signaling systems in tissue engineering. *Current Opinion in Biotechnology* **14**, 559-565 (2003).
97. Behanna, H.A., Donners, J.J.J.M., Gordon, A.C. & Stupp, S.I. Coassembly of Amphiphiles with Opposite Peptide Polarities into Nanofibers. *Journal of the American Chemical Society* **127**, 1193-1200 (2005).
98. Rowlands, A.S., George, P.A. & Cooper-White, J.J. Directing osteogenic and myogenic differentiation of MSCs: interplay of stiffness and adhesive ligand presentation. *Am.J.Physiol Cell Physiol* **295**, C1037-C1044 (2008).
99. Khetan, S. & Burdick, J.A. Patterning network structure to spatially control cellular remodeling and stem cell fate within 3-dimensional hydrogels. *Biomaterials* **31**, 8228-8234 (2010).
100. Kim, J. et al. Synthesis and characterization of matrix metalloprotease sensitive-low molecular weight hyaluronic acid based hydrogels. *Journal of Materials Science: Materials in Medicine* **19**, 3311-3318 (2008).
101. Chung, C. & Burdick, J.A. Influence of three-dimensional hyaluronic acid microenvironments on mesenchymal stem cell chondrogenesis. *Tissue Eng Part A* **15**, 243-254 (2009).
102. Zou, L. et al. Effect of hyaluronan on osteogenic differentiation of porcine bone marrow stromal cells in vitro. *J.Orthop Res* **26**, 713-720 (2008).
103. Lopez, O. et al. Influence of chemical and freezing fixation methods in the freeze-fracture of stratum corneum. *Journal of structural biology* **146**, 302-309 (2004).